

Alma Mater Studiorum – Università di Bologna

DOTTORATO DI RICERCA IN
SCIENZE CHIMICHE

Ciclo XXIV ciclo

Settore Concorsuale di afferenza: 03/A1 - Chimica Analitica

CHEMICAL PRODUCTION AND
MICROELECTRONIC APPLICATIONS
OF GRAPHENE AND NANO-GRAPHENE DERIVATIVES

Presentata da: Emanuele Treossi

Coordinatore Dottorato

Prof. Adriana Bigi

Relatore

Dr. Loris Giorgini

Correlatore

Dr Vincenzo Palermo

Esame finale anno 2012

Alla mia famiglia

Vorrei ringraziare

Vincenzo Palermo per avermi sopportato durante questi anni, per l'ottimo lavoro fatto a livello scientifico e l'autorevolezza con cui gestisce il gruppo di ricerca

Paolo Samorì per essersi interessato al mio "secondo tempo" nel campo della ricerca e per la competenza scientifica dimostrata in questo periodo

Andrea Liscio per il suo aiuto e la sua compagnia durante questi anni

Loris Giorgini per la capacità e competenza dimostratami

Manuela Melucci, Giulio Paolo Veronese, Emanuele Orgiu, Jeffrey M. Mativetsky, Luca Ortolani, Vittorio Morandi, Rita Rizzoli, Cinzia Casiraghi, Giuliano Giambastiani, Massimo Gazzano, Francesco Suriano, Francesco Rossella, Vittorio Bellani, Alberto Zanelli, Philipp Klar per il buon lavoro svolto e i bei momenti passati

Tutti hanno contribuito al lavoro fatto in questi anni e in modo diverso hanno realizzato quello che forse è ancora più importante dei risultati cioè un Team .

Un grazie a tutte quelle persone che semplicemente con la loro compagnia, hanno allietato le mie giornate al CNR e in particolare all'ISOF

Il ringraziamento più grande va infine ai miei genitori, che mi hanno sempre sostenuto e incoraggiato durante tutti questi anni.

ABSTRACT

Graphene is a single layer of carbon atoms arranged in a honeycomb, all-aromatic structure obtained by exfoliation of graphite. Its discovery dates back to 2004 when its outstanding physical and electronic properties were revealed to the scientific community worldwide leading to the Nobel Prize in physics in 2010. In the last few years the number of papers and patents on graphene increases exponentially and graphene and graphenic derivatives have rapidly emerged as an extremely promising materials for electronic, optical, thermal, and mechanical applications.¹⁻²

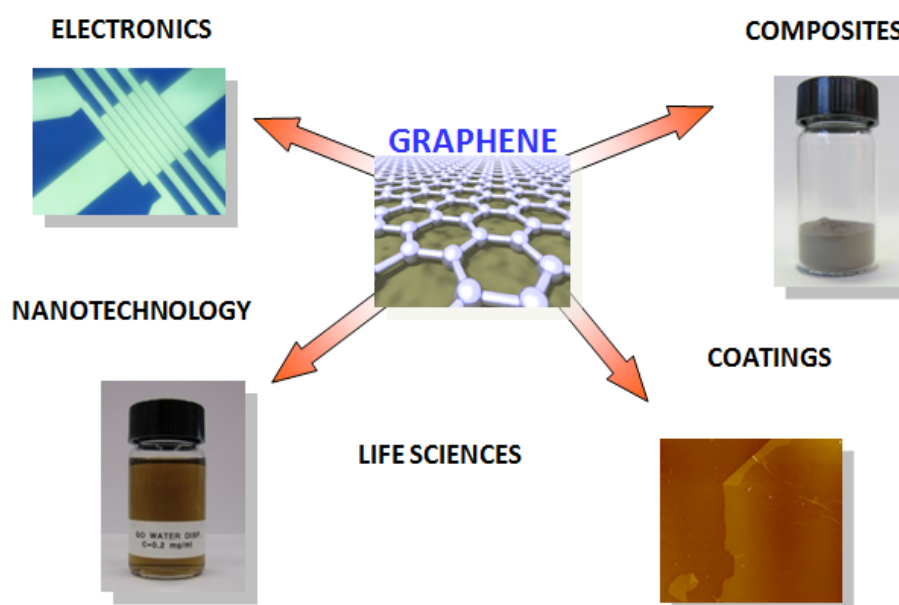


Figure 1. Fields of interest in graphene research.

Several approaches have been developed to produce these materials (i.e. scotch tape, CVD, chemical and solvent exfoliation). In our work we used a chemical approach to produce graphene by reducing graphene oxide (GO) via thermal or electrical/electrochemical methods. Graphene oxide, synthesized from oxidation of graphite by modified Hummer methods,²⁻³ is soluble in water due to the polar groups (i.e. hydroxyl and carboxyl) present on its surface and can be deposited as single sheets or continuous film on different substrates.

Graphene oxide is an intrinsically insulating material because composed of isolated aromatic carbon domains connected to oxidized carbon. The GO reduction, restoring the conducting network (increasing and connecting the previously isolated aromatic domains), is usually performed by chemical or thermal treatment. We have shown that it is possible to use the tip of a scanning probe microscope or the electric field between nano- and micro-electrodes to induce the electrochemical reduction of GO; the process can be used to pattern conductive patterns into an insulating, mono-atomic sheet of GO. In the future this kind of approach could be exploited to paint electric circuit on graphene oxide or realize mass production of graphene devices.^{5,7}

Moreover, we studied the interaction between graphene derivatives and organic molecules focusing on the following aspects:

- Improvement of optical contrast of graphene on different substrates for rapid monolayer identification. Graphene is atomically thick and is pretty hard to detect optically on different substrates; usually graphene and graphene derivatives could be optically localized and studied only on silicon oxide substrates 300 or 90 nm thick, thanks to a weak contrast due to light interference. We developed a new technique to visualize graphene on different substrates based on fluorescence quenching. We functionalized different substrates with a fluorescent self-assembled monolayer and we used the fluorescence of this layer to visualize single sheets of graphene oxide deposited on the substrates. In this way is possible to localize and study graphene and graphene derivative with better contrast and over a much wider range of surfaces than is currently possible.³

- We use graphene oxide sheets as two dimensional platforms to covalently tether on their surface thousands of optically active quaterthiophene molecules, acting as optical antennas. This new material shows high interaction between quaterthiophene and graphene derivative, better solubility in apolar solvent than graphene oxide and can be interesting in the electronic and optoelectronic field.⁴

- Graphene-based transistors show high charge mobility, but low ION/IOFF (ability to switch on or off the device), organic semiconductors show high ION/IOFF but low charge mobility. We realized hybrid systems based on blend of these two

classes of compounds to tune the property of devices. In our work⁶ we realized transistor devices with different amounts of reduced graphene oxide (RGO) and polythiophene (P3HT) polymer. The hybrid devices show better charge mobility of P3HT or RGO alone and the possibility to tune performance and characteristics changing the coverage of graphene derivative on the device.

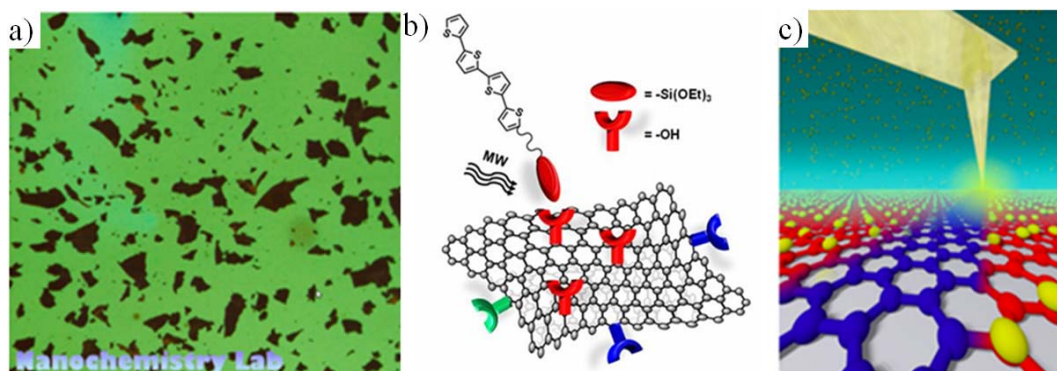


Figure 2. a) fluorescence image of GO single sheets on a fluorescent self-assembled monolayer,³ b) Sketch of one-step chemical functionalization of graphene,⁴ c) cartoon depicting local GO electrochemical reduction with a scanning probe tip.⁵

Overall, we think that graphene chemistry can potentially allow seamless integration of graphene technology in organic electronics devices to improve device performance and develop new applications for graphene-based materials.⁸

BIBLIOGRAPHY

1. Y. Zhu, S. Murali, W. Cai, X. Li, J. W. Suk, J. R. Potts, and R. S. Ruoff, *Adv. Mater.*, 2010, 22, 3906.
2. K. P. Loh, Q. Bao, G. Eda, and M. Chhowalla, *Nat. Chem.* 2010, 2, 1015.
3. E. Treossi, M. Melucci, A. Liscio, M. Gazzano, P. Samorì, and V. Palermo, *J. Am. Chem. Soc.*, 2009, 131, 15576.
4. M. Melucci, E. Treossi, L. Ortolani, G. Giambastiani, V. Morandi, P. Klar, C. Casiraghi, P. Samorì, and V. Palermo, *J. Mater. Chem.*, 2010, 20, 9052.
5. J.M. Mativetsky, E. Treossi, E. Orgiu, M. Melucci, G.P. Veronese, P. Samorì, and V. Palermo, *J. Am. Chem. Soc.*, 2010, 132, 14130.

6. A. Liscio, G.P. Veronese, E. Treossi, F. Suriano, F. Rossella, V. Bellani, R. Rizzoli, P. Samorì and V. Palermo, *J. Mater. Chem.*, 2011, 21, 2924.
7. J.M. Mativetsky, A. Liscio, E. Treossi, E. Orgiu, A. Zanelli, P. Samorì , V. Palermo, *J. Am. Chem. Soc.*, 2011, 133, 14320.
8. Chemical production and applications of graphene based materials. Emanuele Treossi. Accepted for publication on *La Chimica e l'Industria*.

CONTENTS

ABSTRACT	7
INDEX	11
CHAPTER 1: INTRODUCTION	13
1.1 ORGANIC ELECTRONICS	13
1.2 ORGANIC SEMICONDUCTORS SELF-ASSEMBLY AND SUPRAMOLECULAR CHEMISTRY	15
1.3 NANO-GRAPHENES	20
1.4 GRAPHENE	25
1.4.1 CARBON ALLOTROPES	25
1.4.2 GRAPHENE, PRODUCTION AND APPLICATIONS	26
1.5 BIBLIOGRAPHY	30
CHAPTER 2: COVALENT AND SUPRAMOLECULAR INTERACTION BETWEEN GRAPHENE OXIDE AND ORGANIC MOLECULES	33
2.1 GRAPHENE OXIDE	33
2.2 VISUALIZING GRAPHENE SHEETS BY FLUORESCENCE QUENCHING	37
2.3 COVALENT FUNCTIONALIZATION OF GRAPHENE SHEETS WITH OPTICALLY ACTIVE OLIGOTHIOPHENES.	43
2.4 BIBLIOGRAPHY	54
CHAPTER 3: ELECTROCHEMICAL REDUCTION AND PATTERNING OF GRAPHENE OXIDE	57
3.1 REDUCED GRAPHENE OXIDE	57
3.2 TIP-INDUCED REDUCTION OF GRAPHENE OXIDE.	65
3.3 THIN-FILM TRANSISTORS BASED ELECTROCHEMICAL REDUCED GRAPHENE OXIDE.	70
3.4 BIBLIOGRAPHY	73

CHAPTER 4: TUNING THE TRANSPORT PROPERTIES OF GRAPHENE BY NONCOVALENT FUNCTIONALIZATION	75
4.1 TAKING THE BEST OF TWO MATERIALS	75
4.2 INTERACTION BETWEEN RGO AND P3HT	77
4.3 INTERACTION BETWEEN RGO AND NANO-GRAPHENE DERIVATIVES	96
4.4 BIBLIOGRAPHY	99
PUBLICATIONS AND AWARDS	101

CHAPTER 1

INTRODUCTION

1.1 ORGANIC ELECTRONICS

In the next years organics electronics will play an important role in our lives, offering new solutions for different technological areas such as energy, environment, communication, mobility entertainment and health.

Organic electronics is a branch of electronics dealing with carbon-based compounds; it includes not only organic semiconductors, but also organic dielectrics, conductors and light emitters.

Flexible Displays, Solid State Lighting, Solar Cells, Integrated Smart Systems and Sensors are some of the most important application of this promising technology.

Organic electronics is also a strategic market, public e private organization are investing significant amounts of money, manpower, and resources in this field; the worldwide sales of organic and printed electronics is expected to grow to almost 60 billion US\$ by 2019.

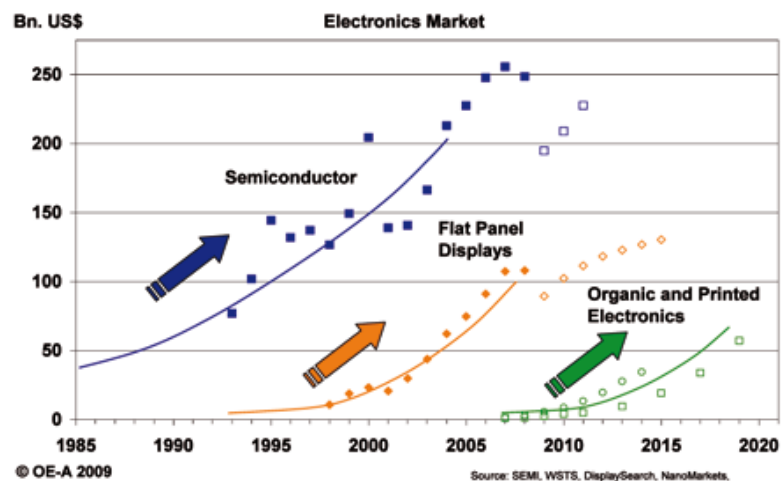


Figure 1.1 Market Forecast for Organic and Printed Electronics. The Market development of semiconductors and Flat Panel Displays are shown for comparison: (Data: WSTS, Display- Search, SIA von Custer, NanoMarkets, IDTechEx; Graph OE-A).¹

This technology is based on the new class of materials, molecules and polymers whose chemical structure can be tailored for specific electronic or optical properties.

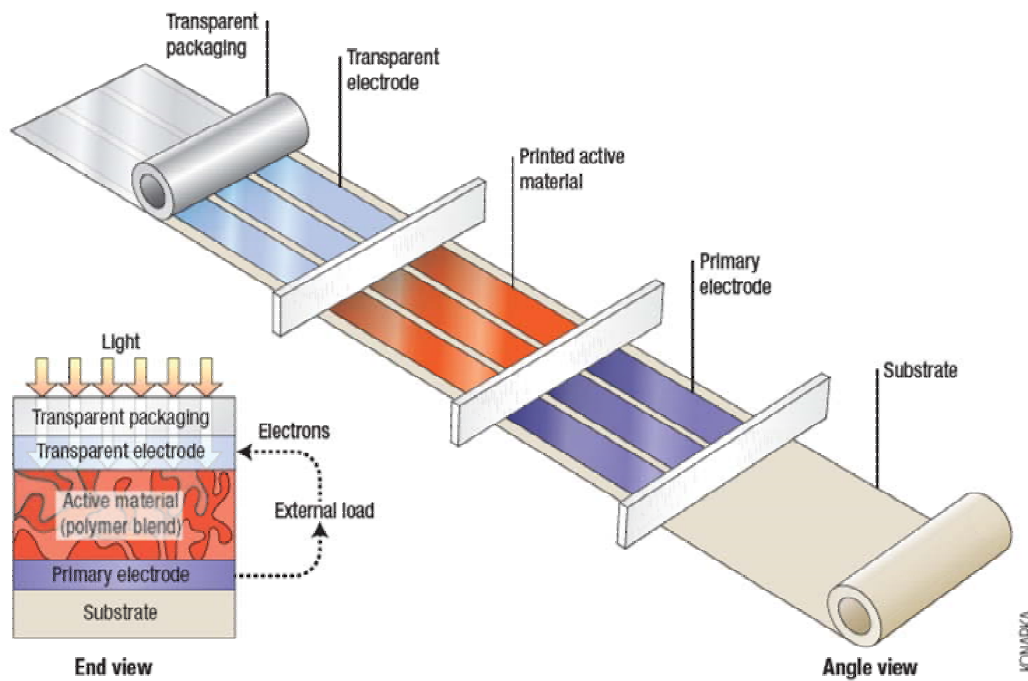


Figure 1.2 Polymer-based photovoltaic cells can be manufactured using standard printing processes.²

Moreover this technology can potentially avoid expensive vacuum or high temperature process steps, which are instead needed for conventional semiconductors such as silicon.

It is cheap, sustainable, compatible with flexible or transparent substrates and suitable for large area processes i.e. roll-to-roll printing.

1.2 ORGANIC SEMICONDUCTORS SELF-ASSEMBLY AND SUPRAMOLECULAR CHEMISTRY

Organic semiconductors are classified in function of nature of majority charge carriers: in p-type there are more holes than electrons and they are the main current carriers while for n-type it is the opposite. These molecules can also be divided in the main classes of polymers and small molecules in reason of the structure.

In conjugated system, the extended π -orbitals' network formed by conjugated p_z orbitals (unhybridized sp^2) confers semiconducting properties and drives through π - π interaction the self assembly in ordered superstructures, i.e. crystallites for polymer or columnar for disk-like molecular shape.

Charge transport is fast along the π - π stacking direction while is slower in the alkyl stacking direction in P3HT crystallites (see fig. 1.3); conductivity along the columns in the columnar mesophases is higher than in perpendicular direction, see fig. 1.3.

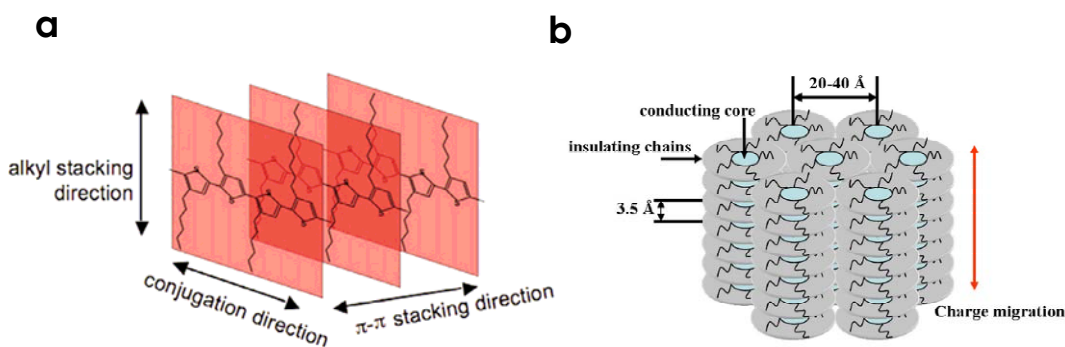


Figure 1.3 Supramolecular assembly in a) poly(3-hexyl-thiophene) crystallite and b) discotic liquid crystal in columnar phase.³⁻⁴

These materials show a large anisotropy in carrier transport properties therefore texture, relative orientation and interconnection of crystallites change dramatically the electrical property and the use in different device.

In OFET (Organic Field-Effect Transistors) hole and electron move between source and drain at the interface of the dielectric substrate, therefore edge-on orientation of molecules facilitates the charge transport.

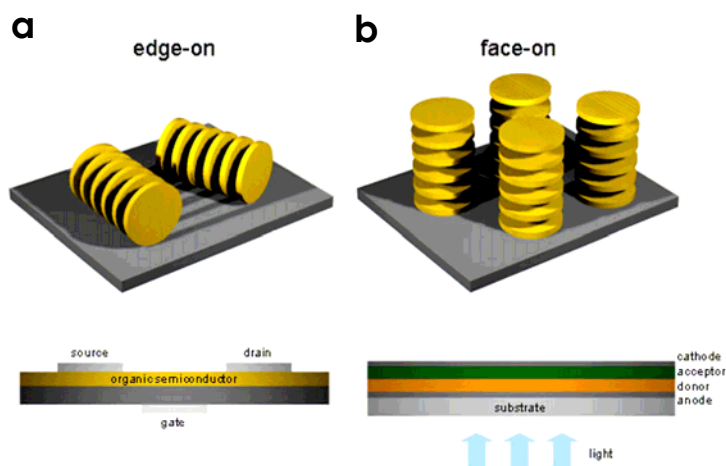


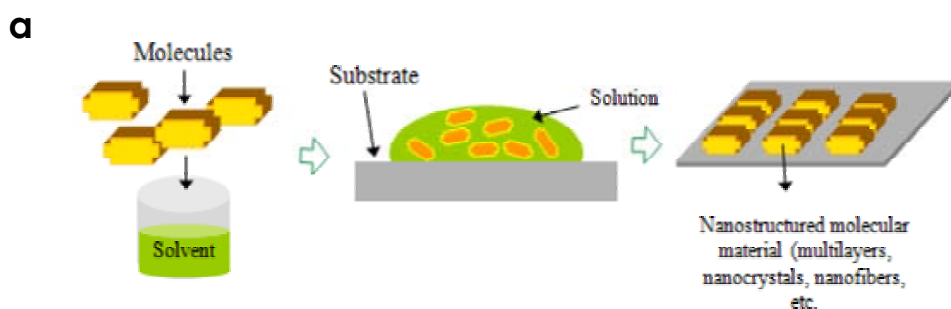
Figure 1.4 Schematic representation of Organic Field-Effect Transistors (OFET) and Organic light-emitting diodes (OLED) with the desired orientation of discotics on substrates.⁴

More in general, the performance of device improves when transport of current and π - π stacking of molecules have the same direction.

As previously said, one main advantage in organic electronics as compared to silicon is the possibility to process materials in solution to produce low cost solar cells and other devices.

The formation of ordered thin films from these systems appears easy: just dissolve your molecules in the right solvent and at the right concentration, then spray or spin coat the solution on a substrate (fig. 1.5).

The molecules will self-assemble, interacting with one another through weak forces such as Van der Waals or electrostatic interactions. π - π and hydrogen bond interactions are also two important secondary interactions created supramolecular structure, because they are selective and directional.



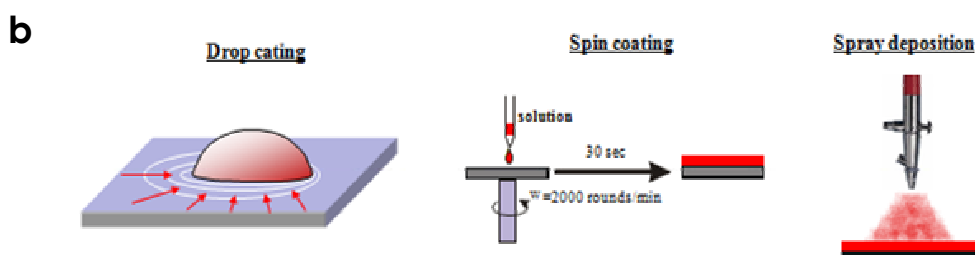


Figure 1.5 a) Schematic illustration of different phase in organic materials process. b) Some different techniques for deposition organic molecules or polymers from solution.

DNA and proteins are two example were hydrogen bond play primary role in supramolecular organization, while in π -conjugated materials, i.e. Polycyclic aromatic hydrocarbons or thiophene derivates, π - π interaction are most important. An example of system were both interaction play role is shown in fig. 1.6, taken from one of our works. In this work we self assembled an oligothiophene derivate with a modified nucleosides in large crystal (fig. 1.6). Here, π - π of the thiophene units and the hydrogen bondings of nucleosides cooperate to give extensive self-assembly and growth of complex mesoscopic crystals.

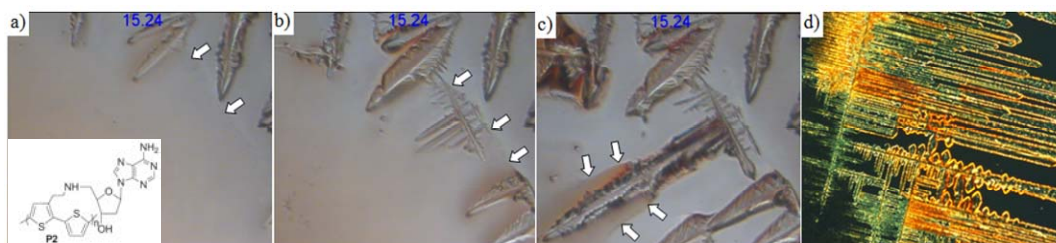


Figure 1.6 a-c) Snapshots of P2 crystal growth. White arrows show roughly the front of receding drop solution. The time span between first and last image is ≈ 40 s. d) Fluorescence microscopy image of crystals.⁵

Although the deposition from solution from the practical (experimental) viewpoint is apparently extremely simple, intrinsically it is a very complex phenomenon to predict and model theoretically, as it involves different materials and phases (the solid substrate, the liquid solvent, the molecules dissolved in the solvent, and the

atmosphere in which the solvent evaporates) as well as their interfaces. This is a fundamental issue in the case of organic solar cells (as example in bulk-heterojunction devices) where two complementary materials, an electron acceptor and an electron donor, are typically present forming two highly percolated structures (fig. 1.7). Upon absorption of solar light, the different nature of the two materials favours exciton splitting and generates free charges which are then collected by the two highly percolated structures, and transported towards the opposite poles of the cell. To maximize charge generation the two phases should have a high surface area and be intercalated on the nanometer scale, while to favour charge transport each of them should be highly percolated, without having dead ends or bottlenecks.

To obtain such a high control on nanoscale morphology, a subtle balance of all the interactions involved must be achieved, as shown in fig. 1.7 in which three major types of interactions are considered. Extreme cases, which are characterized by one

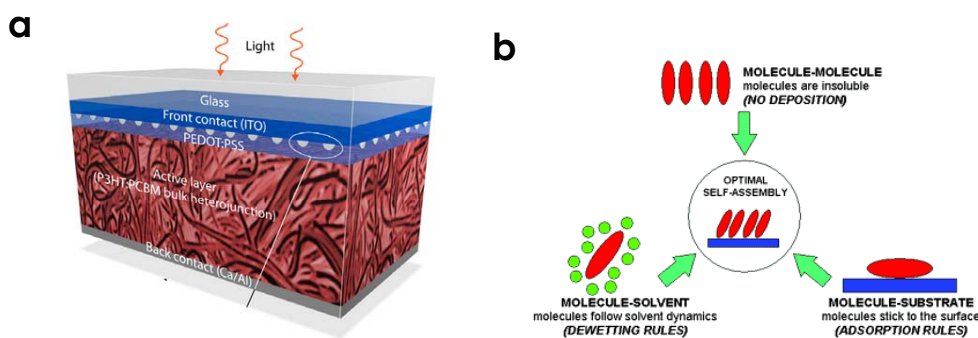


Figure 1.7 a) Cartoon representing a bulk-heterojunction solar cell, from www.spie.org. b) Schematic representation of the major types of interaction that play a role during processing from solution.⁶

of the three interactions dominating over the others, can lead to the following three scenarios:

1. If molecule–molecule interactions are too strong, the molecules will be poorly soluble in the chosen solvent, and thus difficult to process in solution.

2. If molecule–substrate interactions are dominant, the molecules will be kinetically trapped on the surface instead of interacting with each other and thus forming optimal nanostructures (fibers, crystals, network) for charge transport.

3. If molecule–solvent interactions are too strong, the molecule–molecule interactions will be shielded and the molecules will tend to follow the solvent during the dewetting to ultimately give amorphous structures.

Throughout our scientific works, we have used the competition between all these different forces to self-assemble organic molecules and polymers into different kinds of ordered materials, in the next section we can see some of this examples and how is possible to control the self-assembly also after deposition with post-treatment.

1.3 NANO-GRAPHENES

Polycyclic aromatic hydrocarbons (PAHs) also known as polyarenes can be considered as small pieces of graphene; on the other hand, graphene can also be considered as an indefinitely large PAHs “The suffix -ene is used for fused polycyclic aromatic hydrocarbons, even when the root of the name is of trivial origin, e.g. naphthalene, anthracene, coronene, etc. A single carbon layer of the graphitic structure can be considered as the final member of this series...”.¹³

The most important sources of PAHs are crude oil, coal and oil shale⁷ and are one of the most prevalent organic pollutants. Polycyclic aromatic hydrocarbons and their heterocyclic analogs attracted huge interest for the potential application in organic electronics.

To improve the molecules' processability from solution, thereby their solubility in organic solvents, large PAHs i.e. Hexa-peri-hexabenzocoronenes (HBC) are usually functionalized with different alkyl side chains; while aromatic core drives the self-assembly in columnar structure and gives the electronic properties (fig. 1.8), these materials are promising candidates in devices like OFETs, OLEDs and Organic Solar Cells.

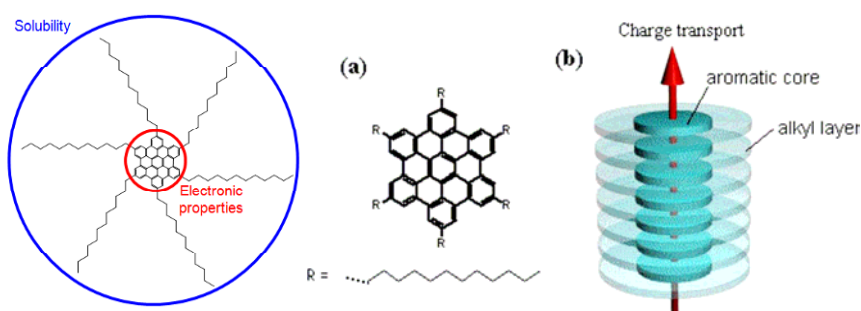


Figure 1.8 Chemical structure of HBC-C₁₂, and charge transport along the columnar HBC-C₁₂ stack.⁸

Hexa-peri-hexabenzocoronenes (HBCs) derivatives are prone to aggregate in organic solvents, forming i) highly crystalline structures, ii) rigid needles, and iii) fibers once they are deposited on a solid substrate.^{9,10}

HBC functionalized with alternating hydrophilic and hydrophobic side chains (see fig. 1.9a HBC-PEO) films exhibit a variety of different morphologies on the micrometer scale when molecules are spin-coated on Si/SiO_x substrate using solutions in a mixture of different solvent (fig. 1.9).

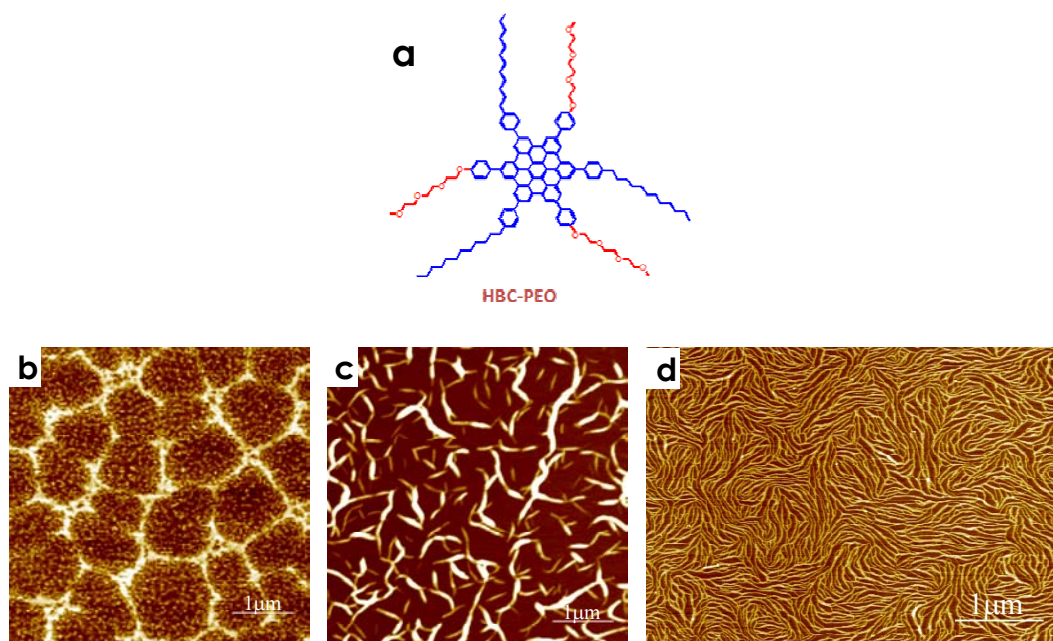


Figure 1.9 a) Molecular structures of the HBC derivatives. AFM image of HBC-PEO deposited on Si/SiO_x by spin-coating from solution in different solvents: b) chloroform, c) chloroform/methanol 2:1, d) dichloromethane/methanol 2:1.¹¹

Making use of chloroform as solvent (fig. 1.9b), a continuous amorphous film coating the substrate surface is covered by a discontinuous network. By mixing chloroform with methanol in a volume ratio of 2:1 (fig. 1.9c), needles, having a length of some 100 nm and a width of some 10 nm, and aggregates thereof, have been observed. By using dichloromethane blended with methanol (2:1 volume ratio fig. 1.9d), bundles of thinner fibers have been found.

Using chloroform, a good solvent for our molecular system, solvent-molecule interactions govern the self-assembly and final morphology is mainly dictated by solvent evaporation dynamics, yielding a broken network of material, due to dewetting, which resembles a Marangoni pattern.¹² By using a mixture of solvent with chloroform and methanol, the molecules are prone to aggregate due to local

phase separation and thus form short fiber-like structures. Using a different solvent mixture such as dichloromethane/ methanol the tendency of aggregation is reduced yet not fully hindered, leading to the formation of a very uniform, continuous network of smaller fibrillar-like structures.

Also post-treatment procedures such as thermal annealing or solvent vapour annealing (SVA) are often required to increase the level of order within the self-organized architectures and improve the performance of the associated devices. Temperature or solvent help materials to reorganize in more stable and ordinate system, they give at the system an activated energy to win a barrier between two different states (fig.1.10).

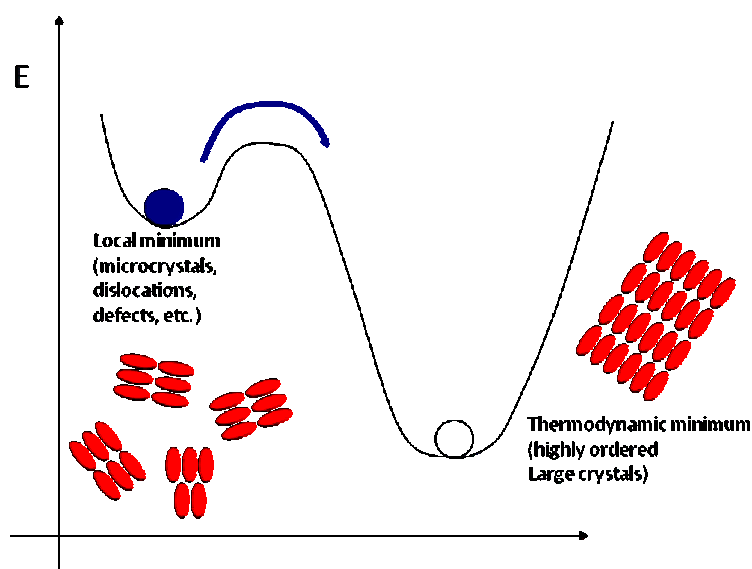


Figure 1.10 Schematic representation of energy state of materials in annealing process.

The modulation of the experimental conditions makes it possible to promote reorganization from the scale of a few nanometers up to several hundreds of micrometers, leading to the formation of crystalline functional architectures.

figure 1.11 shows a film of HBC-PEO deposited on Si/SiO_x and subjected to SVA treatment in chloroform for 80 min (fig. 1.11b) or 18 h (fig. 1.11c) at room temperature.

After 80 min of SVA, the fibrillar network is partially destroyed and more isotropic islands are formed. On top of these islands spatially uncorrelated anisotropic features are observed.

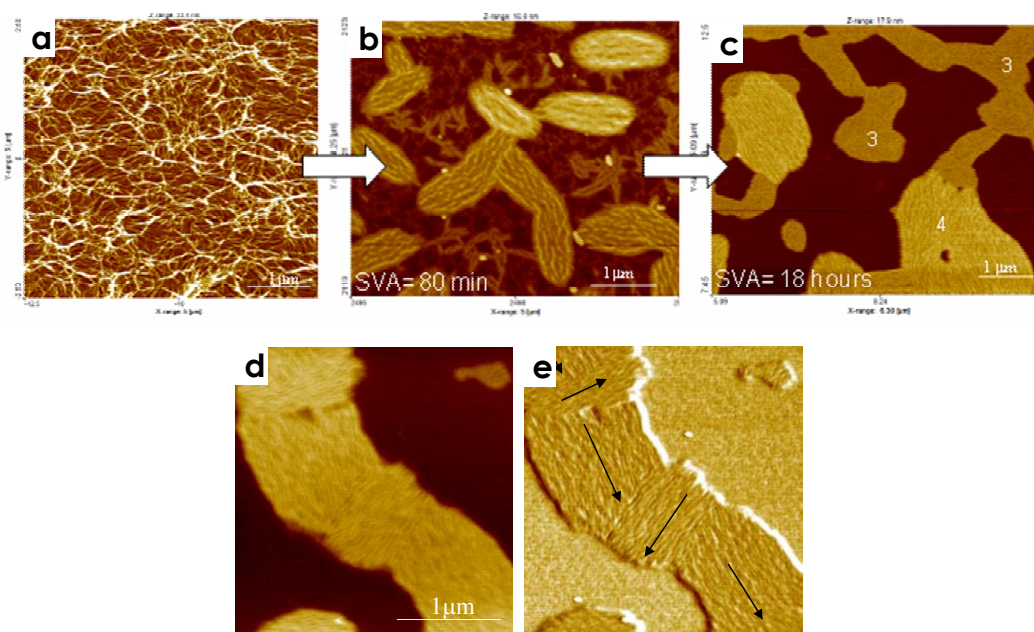


Figure 1.11. AFM images of HBC-PEO deposited on Si/SiOx a) Original morphology after spin-coating. b) After 80 min of SVA. c,d) After 18 h of SVA. e) Phase image of the area shown in d. The numbers 3 and 4 in the image indicate islands formed by three and four layers, respectively.¹¹

Upon prolonged SVA (fig. 1.11c), the isolated fibrils adsorbed on the neat substrate completely disappear and all the material assembles into micrometric islands, having a random orientation. Therefore, upon SVA treatment at room temperature a self-healing within the film is observed: the fibers obtained by spin-coating completely disappear, being substituted by islands showing uniform thickness and exposing tightly packed fibers aligned preferentially along the main axis of the islands (fig. 1.11c). The vast rearrangement observed in figure 1.11 is due to solvent that absorbs on the surface, triggering the molecules' reorganization into islands. Initially small islands are formed, which eventually grow, removing material from the surrounding fibers. The islands show an anisotropic structure,

with a preferential director orientation running parallel to the substrate. When two growing islands touch each other they coalesce but retain their director orientation. Solvent Vapor Annealing represents a viable strategy featuring a controlled, versatile, and cost-effective self-assembly of ordered structures on surfaces. For more details see reference 11.

1.4 GRAPHENE

Geim and Novoselov in the paper published on Nature Materials “The rise of graphene” give this definition of graphene: graphene is the name given to a flat monolayer of carbon atoms tightly packed into a two-dimensional (2D) honeycomb lattice, and is a basic building block for graphitic materials of all other dimensionalities. It can be wrapped up into 0D fullerenes, rolled into 1D nanotubes or stacked into 3D graphite.¹⁴

Graphene is not only a new material with incredible properties but is also a new approach of science to study and play with Materials in two dimensions. Dimensionality is a novel important tool for discover new 2D crystal materials or other form with different property from 3D precursor, graphene is only the first of a list of new, 2D materials (BN, MoS₂, etc.). Nanotechnologies are actually pushing the research in a new world all to discover.

1.4.1 Carbon allotropes

Carbon is the basis of organic chemistry and therefore of life on Earth, the reason of this extraordinary role is probably related to the high number of carbon compounds, which have a great variety of physical and chemical properties.

Atomic carbon exists in three bonding states with different geometry, shape and

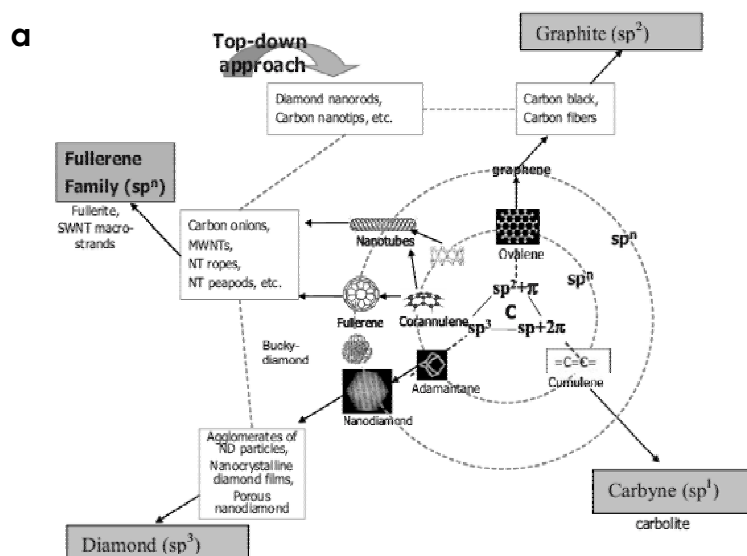




Figure 1.12 a) Allotropes of the element carbon¹⁵ b) optical image of diamond and graphite crystals, two of most famous allotropes of carbon.¹⁶

dimension, corresponding to sp^3 , sp^2 and sp hybridization of the atomic orbitals, these different bonds lead to diverse carbon allotrope structures. In figure 1.12 we can see some overviews of this family.

Diamond, graphite, carbyne, fullerenes, carbon onions, nanotubes, graphene, amorphous carbon are only some of allotrope forms of carbon. We think that carbon science, especially related to nanotechnologies, has great potential and in the next years can offer more interesting discoveries and new solution for industry and everyday life.

1.4.2 Graphene, production and applications

Emerging technologies, no matter how revolutionary they are, initially face significant cost barriers to compete with established technologies. Thus, cheap production of large amounts of graphene with controlled electrical, chemical and structural properties is fundamental for graphene to have a significant impact on society. While high-end electronic devices need highest quality material in terms of electronic and crystalline properties, applications like transparent electrodes demand cost efficient solutions. A major advantage of graphene is that, despite its young age, it can be already produced with many different techniques, which offer

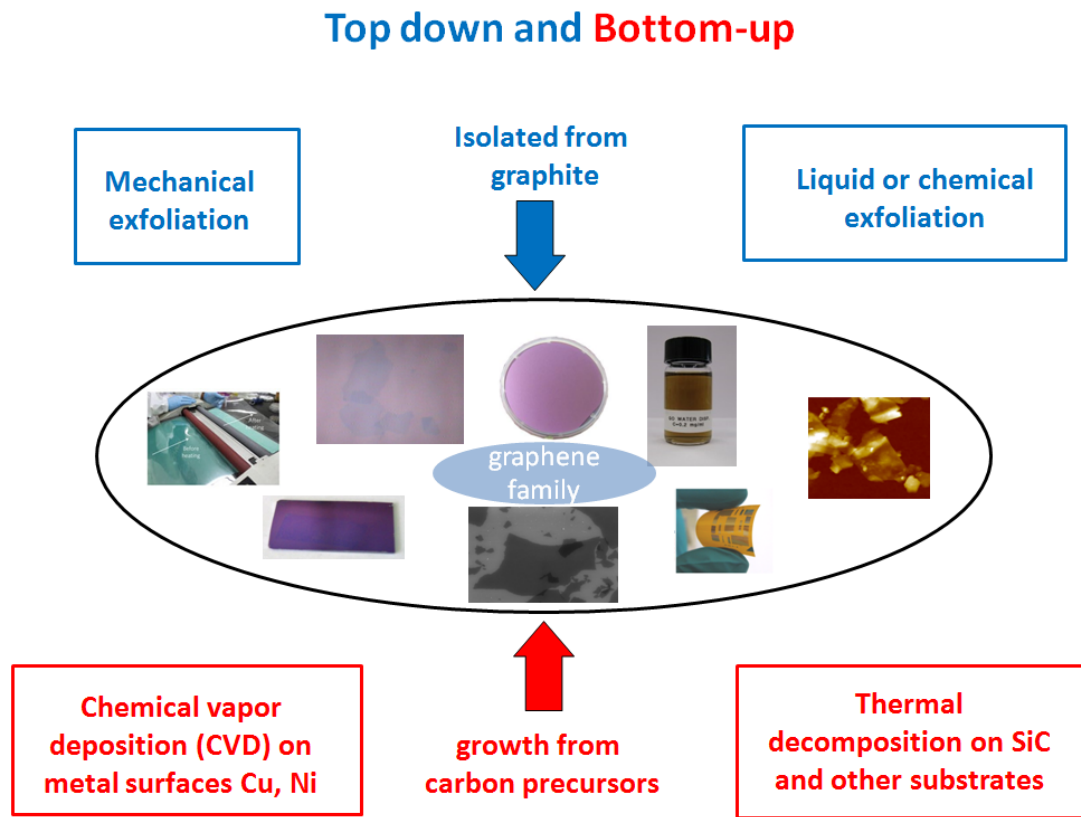


Figure 1.13 Top down and bottom-up approaches in graphene production.

a different mix of high quality and low cost, which will be suitable for different kinds of applications.

Mainly there are two kind of approach in the graphene production, the first is top down approach where the starting material is graphite and by mechanical, liquid or chemical exfoliation it is possible to isolate a graphic monolayer. The second is top down approach where it is possible to grow graphene layers from carbon precursors at high temperature and in inert atmosphere (fig. 1.13).

Scotch tape method: this technique is based on the possibility to use adhesive tape to repeatedly divide graphite into increasingly thinner pieces, transfer few or single layers obtained in this way on silicon oxide, where they can be detected by optical microscope. Advantages: high quality of graphene produced, no special equipment needed. Disadvantages: inappropriate for large-scale production, uneven

films, difficult processability, low yield, single sheets difficult to localize. Applications: suitable for fundamental research.

Chemical method: graphene is produced by reducing graphene oxide (GO) usually via thermal, chemical or electrical methods. Graphene oxide was synthesized from oxidation (i.e. Hummer method) of graphite and dissolved in water due to the presence of polar groups. Water solutions of graphene oxide can be used to prepare film or composite. Advantages: graphene oxide is suitable for large area and up-scaling production, cheaper, easy processable (soluble in water) and can be chemically functionalized. Disadvantages: poor quality of graphene produced, necessary reduction techniques for conducting materials.

Applications: transparent conductors, biological and energy applications, sensors, composites, coating and gas barrier.

Solution-based exfoliation: it is possible to produce graphene from sonication of graphite in special solvents (i.e. dimethylformamide) or with particular molecules (i.e. pyrene derivatives). These molecules, under sonication, have ability to interact strongly with graphite, infiltrating between the planes and making possible the exfoliation of graphite into graphene. Advantages: suitable for large area and up-scaling production, easily processable. Disadvantages: use of poisonous or high boiling solvents, solvent or molecules tend to fix on graphene, not high quality of graphene, low yield. Applications: transparent conductors, sensors, composites, coating and gas barrier.

Thermal decomposition of SiC: another approach to the production of graphene is thermal treatment of silicon carbide under vacuum or in inert ambient, this causes sublimation of the silicon atoms while carbon can reorganize, due to the high temperature, from graphenic domains to continuous film.

Advantages: Insulating substrate, thus no transfer necessary, wafers scale available, good quality of graphene produced. Disadvantages: high temperature process,

difficult control of morphology. Applications: high frequency transistors, sensor, electronic.

Chemical vapour deposition: in this method graphene is grown on metal catalyst from gaseous carbon source (i.e. methane, ethylene) at high temperature and inert ambient. Carbon precursor dissociates of at high temperature on the catalyst surface, carbon dissolves in the catalyst and then precipitates out during the cool down to room temperature. Advantages: Roll-to-roll production on plastic substrates demonstrated, good quality of graphene produced. Disadvantages: high temperature process, difficult control of morphology, requires transfer after synthesis. Applications: flexible display or transparent conductors, sensor, solar cells, OFETs.

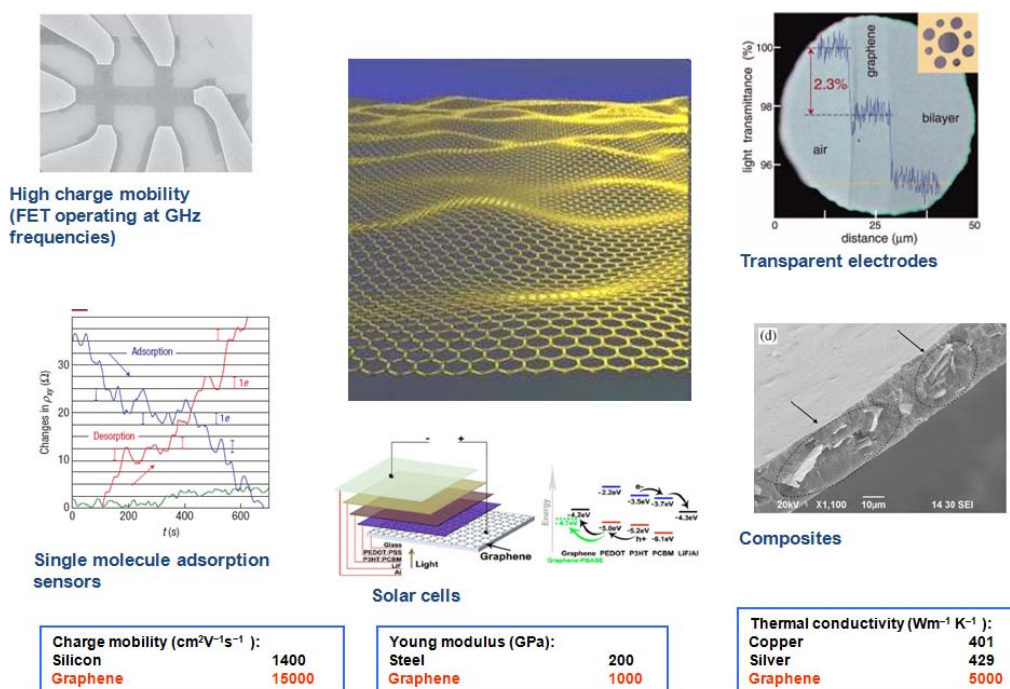


Figure 1.14 Some properties and applications of graphene.¹⁷⁻²¹

1.5 BIBLIOGRAPHY

- 1) Strategic Research Agenda Organic and Large Area Electronics
- 2) Fantastic plastic; R. Gaudiana and C. Brabec. *Nature Photonics* 2008, 2, 287.
- 3) Charge transport in polymeric transistors; A. Salleo. *Materialstoday* 2007, 10, 38.
- 4) Large polycyclic aromatic hydrocarbons: Synthesis and discotic organization; X. Feng, W. Pisula and K. Müllen. *Pure and Applied Chemistry* 2009, 81, 2203.
- 5) Self-Complementary Nucleoside-Thiophene Hybrid Systems: Synthesis and Supramolecular Organization; M. L. Navacchia, L. Favaretto, E. Treossi, V. Palermo, G. Barbarella. *Macromolecular Rapid Communications* 2010, 31, 351.
- 6) Molecular Self-Assembly across Multiple Length Scales; V. Palermo, P. Samorì. *Angewandte Chemie International Edition* 2007, 46, 4428.
- 7) Polycyclic Aromatic Hydrocarbons; R. G. Harvey. 1996.
- 8) Novel organic semiconductors and processing techniques for organic field-effect transistors; H. N. Tsao, H. J. Räder, W. Pisula, A. Rouhanipour, K. Müllen. *Physica Status Solidi (a)* 2008, 205, 421.
- 9) Influence of Alkyl Substituents on the Solution- and Surface-Organization of Hexa-peri-hexabenzocoronenes; M. Kastler, W. Pisula, D. Wasserfallen, T. Pakula, K. Müllen. *Journal of the American Chemical Society* 2005, 127, 4286.
- 10) Synthesis, Helical Organization, and Fibrous Formation of C₃ Symmetric Methoxy-Substituted Discotic Hexa-peri-hexabenzocoronene; X. L. Feng, W. Pisula, M. Takase, X. Dou, V. Enkelmann, M. Wagner, N. Ding, K. Müllen, *Chemistry of Materials* 2008, 20, 2872.
- 11) Temperature-enhanced Solvent Vapour Annealing of a C₃ symmetric hexa-peri-hexabenzocoronene: controlling the self-assembly from nano- to macroscale; E. Treossi, A. Liscio, X. Feng, V. Palermo, K. Müllen, P. Samorì. *Small* 2009, 5, 112.
- 12) Rings and Hexagons Made of Nanocrystals: □ A Marangoni Effect; M. Maillard, L. Motte, A. T. Ngo, and M. P. Pileni. *Journal of Physical Chemistry B* 2000, 104, 11871.
- 13) Nomenclature and terminology of graphite intercalation compounds; H. P. Boehm, R. Setton, E. Stumpp. *Pure and Applied Chemistry* 1994, 66, 1893.

-
- 14) The rise of graphene; A. K. Geim and K. S. Novoselov. *Nature Materials* 2007 6, 183.
- 15) Carbon Family at the Nanoscale; O.A. Shenderova¹, Z. Hu, and D. Brenner *Synthesis, Properties and Applications of Ultrananocrystalline Diamond* 2006, 3.
- 16) Wikipedia.
- 17) Detection of individual gas molecules adsorbed on graphene; F. Schedin, A. K. Geim, S. V. Morozov, E. W. Hill, P. Blake, M. I. Katsnelson, K. S. Novoselov *Nature Materials* 2007 6, 652.
- 18) Fine structure constant defines visual transparency of graphene; R. R. Nair, P. Blake, A. N. Grigorenko, K. S. Novoselov, T. J. Booth, T. Stauber, N. M. R. Peres A. K. Geim, *Science* 2008 320, 1308.
- 19) Graphene Oxide, Highly Reduced Graphene Oxide, and Graphene: Versatile Building Blocks for Carbon-Based Materials O.C. Compton and S.T. Nguyen *Small* 2010, 6, 711.
- 20) Large area, continuous, few-layered graphene as anodes in organic photovoltaic devices Y. Wang , X. H. Chen , Y. L. Zhong , F. R. Zhu , K. P. Loh , *Applied Physics Letters* 2009 , 95 , 063302 .

CHAPTER 2

COVALENT AND SUPRAMOLECULAR INTERACTION BETWEEN GRAPHENE OXIDE AND ORGANIC MOLECULES**2.1 GRAPHENE OXIDE**

Graphene oxide (GO) is a oxidized derivative of graphene, containing a mixture of sp² and sp³ hybridized carbon atoms, it is obtained by treating graphite with strong oxidizers in acid environment. It is an electrically insulator due to the disrupted sp² bonding network, in the structure carbon aromatic clusters are isolated by a continue network of oxidized regions.

There are different methods to produce graphene oxide, in table 2.1 we can see an overview of them.

	Brodie	Staudenmaier	Hummers	Modified Hummers	
Year	1859	1898	1958	1999	2004
Oxidants	KClO ₃ , HNO ₃	KClO ₃ (or NaClO ₃) HNO ₃ , H ₂ SO ₄	NaNO ₃ , KMnO ₄ , H ₂ SO ₄	pre-ox: K ₂ S ₂ O ₈ , P ₂ O ₅ , H ₂ SO ₄ ox: KMnO ₄ , H ₂ SO ₄	NaNO ₃ , KMnO ₄ , H ₂ SO ₄
Reaction times	10 h / 4 days	1 / 10 days	2 / 10 h	6 h pre-ox + 2h ox	≈ 5 days

Table 2.1. Methods for the oxidation of graphite to graphite oxide.¹

In this work graphene oxide is prepared using a modified Hummers method²⁻⁵ starting from graphite flakes.

Synthesis of Graphene oxide:

Graphite (5g) and 3.8 g of NaNO₃ is introduced in a 2L flask equipped with a mechanical stirring apparatus. Then, H₂SO₄ (375 ml) is added at 0°C (ice bath), and the solution is stirred until homogeneous. KMnO₄ (25 g) is slowly added over 1h, keeping the temperature below 10°C with an ice bath. The solution is removed

from the ice bath after 2 hours, and is further stirred for 5 days at room temperature (color change from dark green to brown).

700 ml of H_2SO_4 5% aqueous solution are added to the brown suspension dropwise (temp. $< 40^\circ\text{C}$) and the mixture is stirred for 2 h at room temperature. Then, 20 ml of H_2O_2 (30%) are added drop-wise to destroy the excess of permanganate, and stirred for 2 h. The solution is diluted to 2 L with 5% H_2SO_4 and, after one day of sedimentation, 1 L of supernatant is removed and replaced with water (1 L) and H_2O_2 (10 ml). After vigorous shaking, the suspension is allowed to sediment overnight. The supernatant solution is removed and the solid washed with an aqueous mixture of 5 wt% H_2SO_4 and 0,3% H_2O_2 (12 times), then HCl 4% (3 times), milli Q water (10 times) and centrifuged after each step. Finally, the GO is dried at 60°C under vacuum.

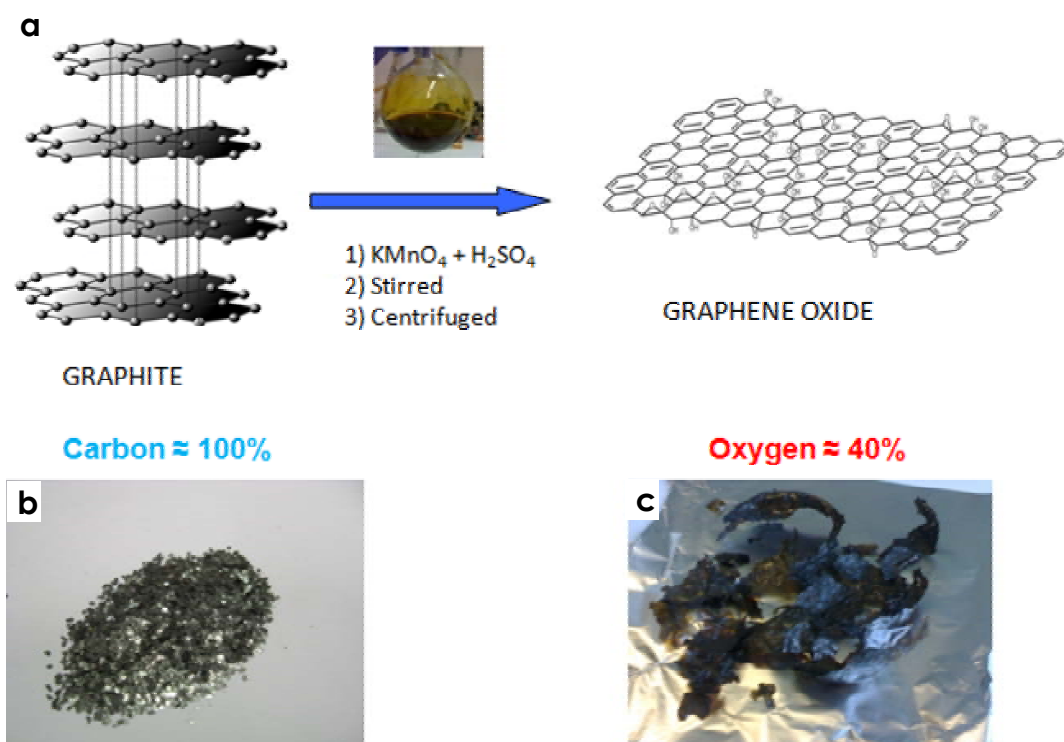


Figure 2.1 a) Schematic representation of graphene oxide synthesis. Optical images of graphite b) and graphite oxide c).

As-synthesized GO is suspended in water to give a brown dispersion, centrifuged to remove aggregates and deposited on the different substrates to obtain continuous film or isolated flakes, fig. 2.2 a-b (The solutions are subjected to dialysis).

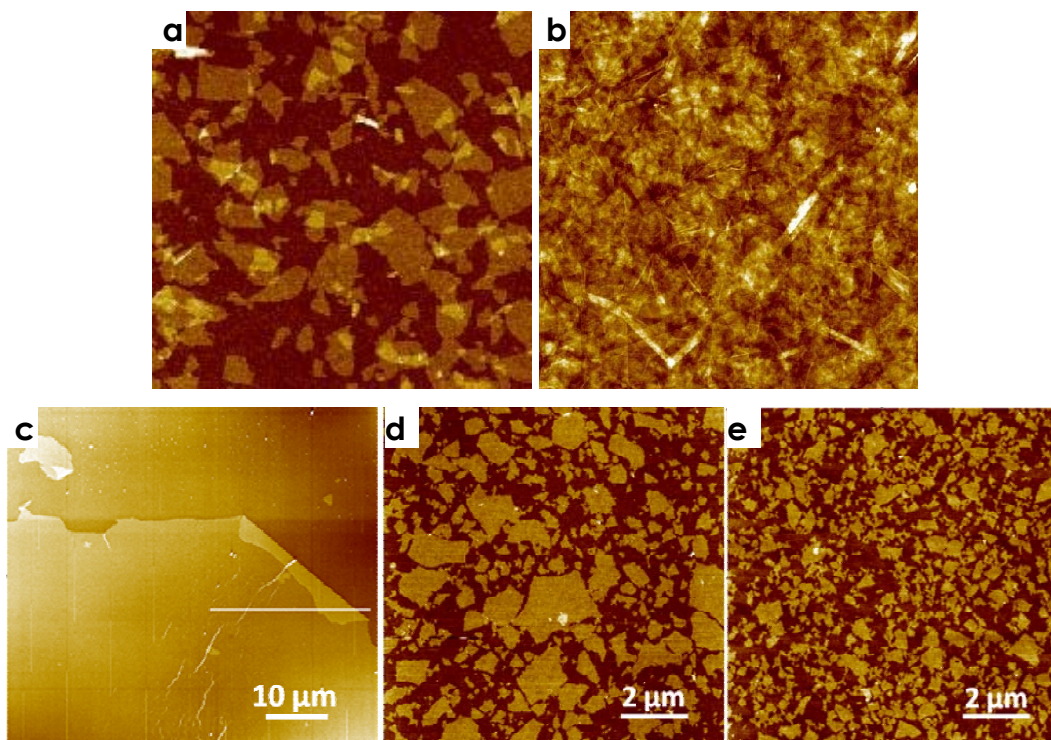


Figure 2.2 a,b) AFM images of graphene oxide a) flakes, b) thin film on silicon substrate. (size of images is 5 micron). c,d,e) AFM images of GO flakes obtained by spincoating of graphene oxide solution sonicated respectively 0h – 2h or 26 hours.

XRD measurements performed on GO membranes gave a value of 0.82 nm (see fig.2.3a), in this material the distance of carbon planes is larger than graphite (0,34 nm) due the presence of oxygen and reorganization of carbon in sp³ arrangement.

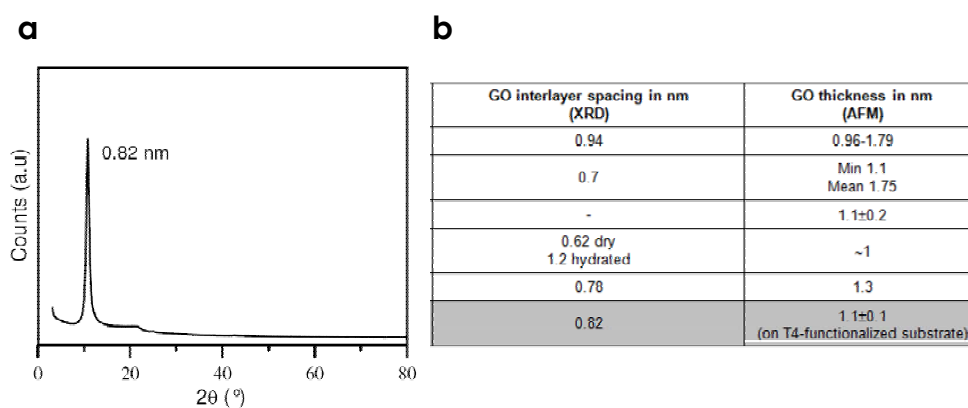


Figure 2.3 a) XRD patterns of GO membrane. b) GO thickness, as measured by XRD, AFM and modeling from S.I. reference 10.

The measured thickness of the GO monolayer is ≈ 1 nm; similar values have previously been detected using AFM (fig.2.3b) and are always somewhat larger than the real GO thickness, depending upon the measurement conditions and the presence of adsorbed water.

In nanotechnology use of graphene oxide can offer many advantages due the easy processability and huge variety of its derivatives and composites, in addition GO:

- can be produced in large scale;
- is soluble in water and in some organic solvents;
- in solution is present as monoatomic single sheets;
- sheet size can be tuned from submicron to 100 μm by sonication time of solution (see fig 2.2);
- can be chemically functionalized (see section 2.3);
- and it is possible to tune the degree of reduction i.e. by thermal treatment a different temperature see fig 3.1 This means that GO can be used as insulating or conductive material.^{6,7}

2.2 VISUALIZING GRAPHENE SHEETS BY FLUORESCENCE QUENCHING

One of the keys to the successful discovery of graphene in 2004 was the possibility of detecting single graphene sheets deposited on a silicon substrate covered by a 300 nm thick oxide layer due to a weak interference-like contrast, which currently is the most practical way of identifying graphene sheets adsorbed on surfaces fig.3.3. Without this simple yet effective way to scan substrates for single or multiple-layer sheets, graphene would have probably remained undiscovered.

This principle has been studied systematically and improved using various illumination setups. Under optimal conditions, the highest observable contrast of graphene on SiOx is 0.12.⁸

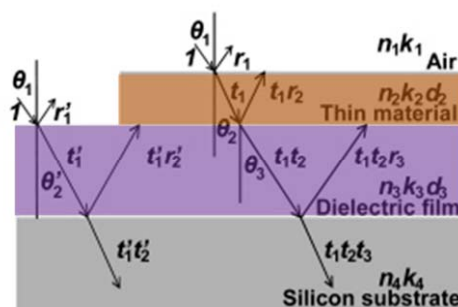


Figure 2.4 Optical reflection and transmission for layered thin film system: dielectric film on silicon substrate (left), thin sheet added on dielectric film (right).⁹

Graphene oxide, although easier to produce and process than graphene, shares the same “visibility” problems. Since GO can be produced in large quantities and deposited as single layers on a wide variety of substrates, it is being intensively studied for applications in microelectronics, photovoltaics, and even biology.

We demonstrate a novel approach for detecting and mapping GO sheets on surfaces derivatized with an organic dye whose fluorescence is quenched in the presence of GO. In this way, visualization of GO sheets with high optical contrast

(up to 0.78) can be easily accomplished on various substrates, including quartz and glass, without the need to use interference methods.

In this approach, a triethoxysilane fluorescent thiophene-based dye, N-(3-(triethoxysilyl)propyl 2,2':5',2'':5'',2'''-quaterthiophene- 5-carboxamide (T4, Figure 2.5), is covalently grafted onto the silicon dioxide, quartz, or glass surface through a microwave-prompted silanization reaction (i.e., reaction of Si-O-Et moieties with the OH groups of the SiO_x substrate).

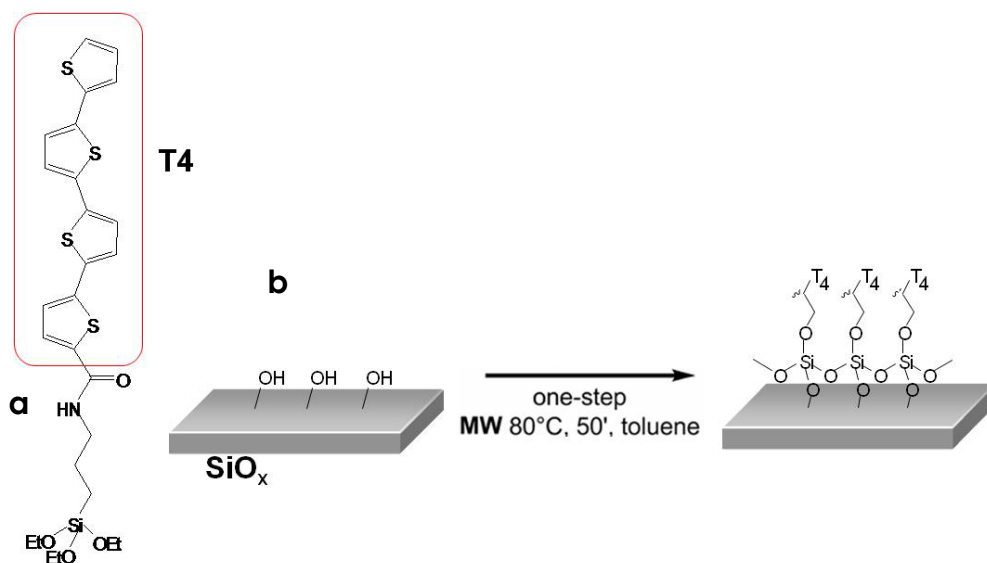


Figure 2.5 a) Structure of the T4 molecule used for functionalization, b) Scheme of preparation of SAM T4-functionalized substrates.

After T4 functionalization, intense green emission from the functionalized substrate is observed under UV excitation (Hg lamp, λ_{exc} 330-380 nm), confirming the formation of a T4 layer.

On the nanometric scale, the T4-SiO_x surface appears flat and uniform, as revealed by atomic force microscopy (AFM); the root-mean square roughness (R_{rms}) is comparable to that of unfunctionalized SiO_x (≈ 0.2 nm as measured on $2 \times 2 \mu\text{m}^2$ areas). GO is then spin-coated onto the surface from a water solution. Through the use of thorough stirring instead of prolonged GO sonication, a large number of

large, single GO sheets were formed on the surface, with lateral dimensions of up to 100 μm fig.2.2.

After deposition on the functionalized substrates, GO multilayers or folded single sheets were visible on the surface by optical microscopy (fig. 2.6a), albeit with low contrast. Conversely, the fluorescence image of the same area ($\lambda_{\text{exc}} = 330\text{-}380\text{ nm}$, $\lambda_{\text{em}} = 487\text{ nm}$) displayed a green emission from the T4 layer. Remarkably, while the correspondence of many quenched areas of Figure 2.6b to the thicker GO deposits already visible in Figure 2.6a is straightforward, fluorescence imaging allows one to monitor smaller GO sheets that went undetected using normal light.

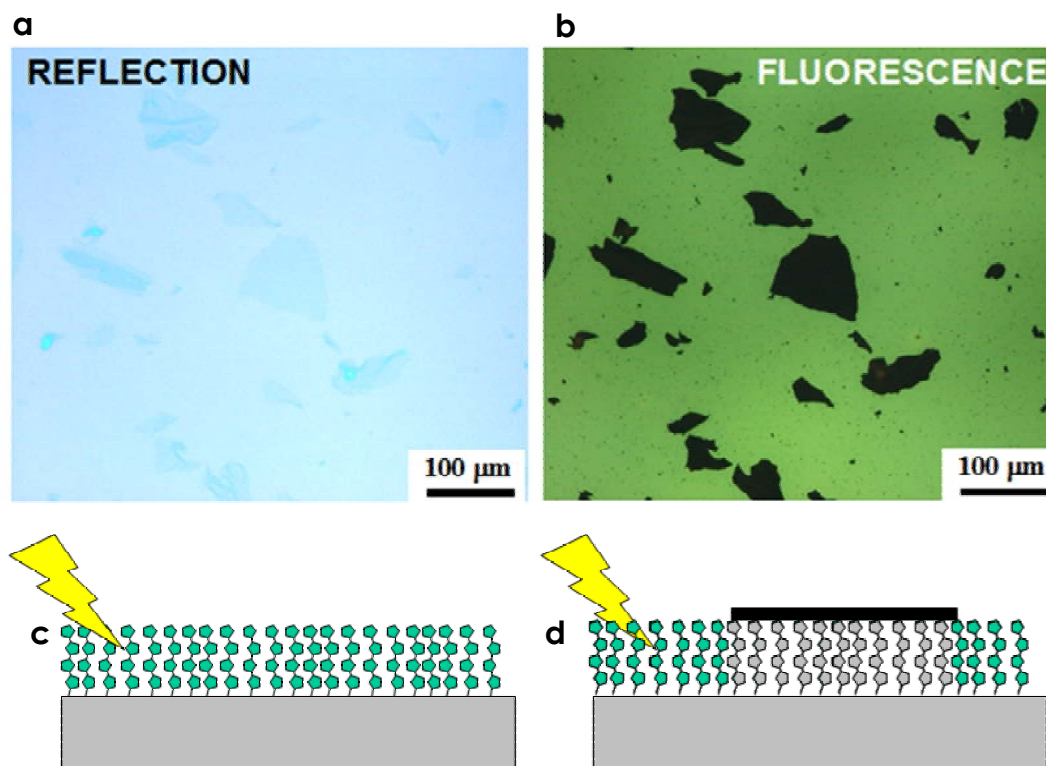


Figure 2.6 a) Optical microscopy (OM) image of GO sheets on T4-functionalized, 300 nm thick SiO_x and b) Fluorescence image of the same area. c,d) Scheme of graphene oxide quenching on surface.

The fluorescence quenching observed can be attributed to charge transfer from the T4 molecules to GO, as demonstrated by Raman spectroscopy and density functional theory calculations;¹¹ comparison of fluorescence and AFM

measurements recorded over the same areas (Figure 2.7) confirmed that even a single GO sheet can completely quench the fluorescence. The measurements shown in Figures 2.6-2.7 were performed using a 300 nm thick SiO_x layer (i.e., one possessing optimal conditions for graphene detection). The expected theoretical contrast^{8,9} for phase interference is either ≈ 0.02 (considering an excitation wavelength of 330-380 nm) or below 0.05 (considering the T4 emission wavelength, which peaks at 487 nm). The contrast C measured in fluorescence images, however, reached values of 0.78, which is about 6 times the theoretical limit expected for light interference on 300 nm SiO_x.

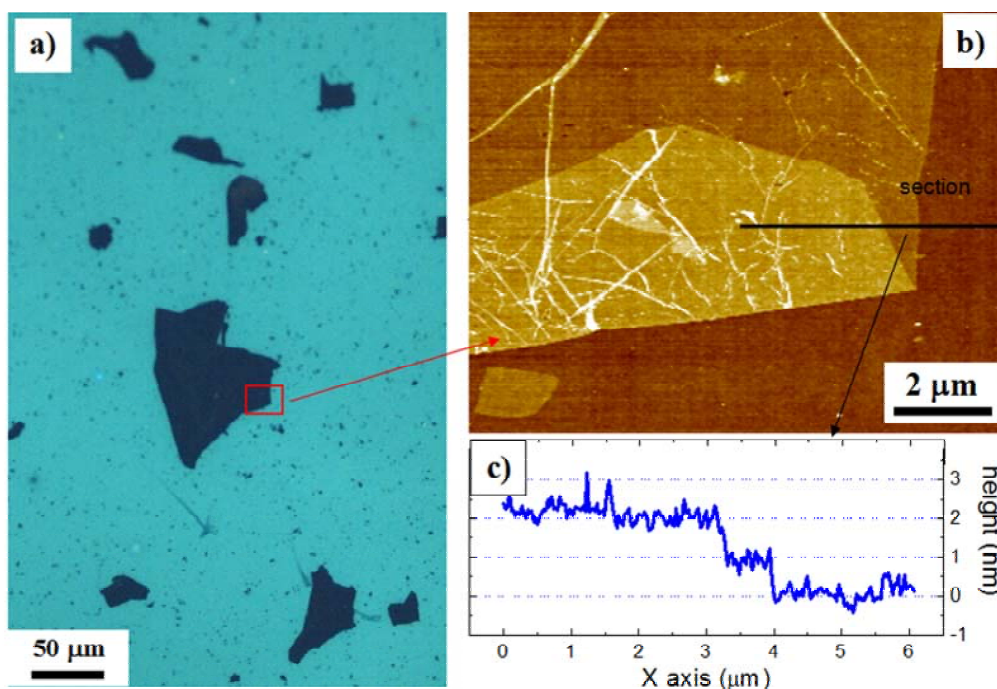


Figure 2.7 a) Fluorescence image of a GO monolayer deposited on T4-functionalized, 300 nm thick SiO_x. b) AFM of the area indicated in a. c) Height profile taken across the black line in b.

The contrast C is obtained in fluorescence images by comparing the intensity of light IGO (I_0) emitted from areas with (without) GO sheets, using the formula:

$$C = (I_0 - I_{GO}) / I_0$$

This gives a contrast >0 for objects darker than the surrounding substrate, and <0 for lighter ones. To calculate the contrast we used the Weber formula, suitable for small objects located on a large background, in analogy with ref. 8

GO is clearly visible even on quartz and glass, where no hidden SiO_x-Si interface is present to give interference.

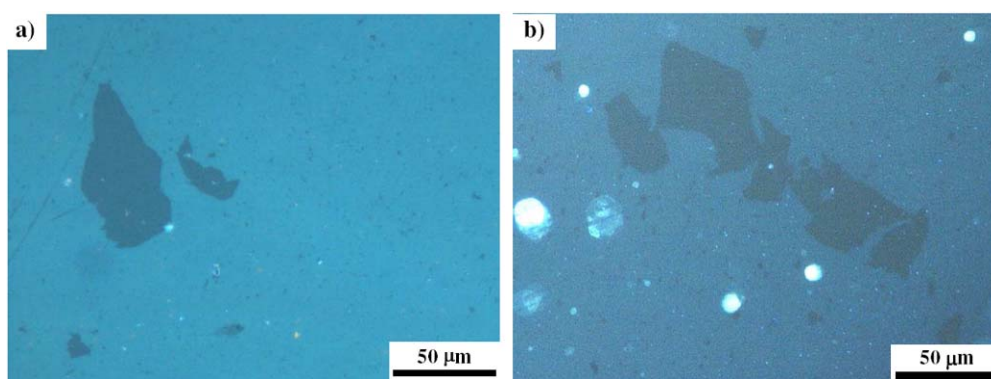


Figure 2.8 Fluorescence images of GO sheets deposited on a) quartz and b) glass substrates which have been T4-functionalized.

The only equipment required to obtain this result was a low-pass optical filter, which was needed to exclude the excitation wavelength emitted by the lamp. The main advantage of this strategy is not only higher contrast but also the possibility of obtaining this result even on substrates other than 300 nm SiO_x without the need to change the illumination setup or optimize the substrate dielectric thickness.

GO sheets deposited on 100 nm SiO_x, quartz, and glass substrates gave contrast values of 0.52, 0.20, and 0.07 which, although lower than in the previous case, are still more than sufficient for a clear visualization.

The contrast can be observed on so many different surfaces because it is due not to the mesoscopic structure of the substrate (which gives light interference) but rather to the “chemical” interaction between the GO and the T4 molecules on the molecular scale. T4-functionalized substrates possess high stability, and although slow quenching takes place under intense illumination, it is possible to visualize the

GO sheets even after storing the samples for several days under ambient illumination in air.

The approach presented here represents a simple strategy to study the interactions between graphene and organic molecules with a good control, thanks to the layer structure, of the molecule's position relative to the graphene sheet.

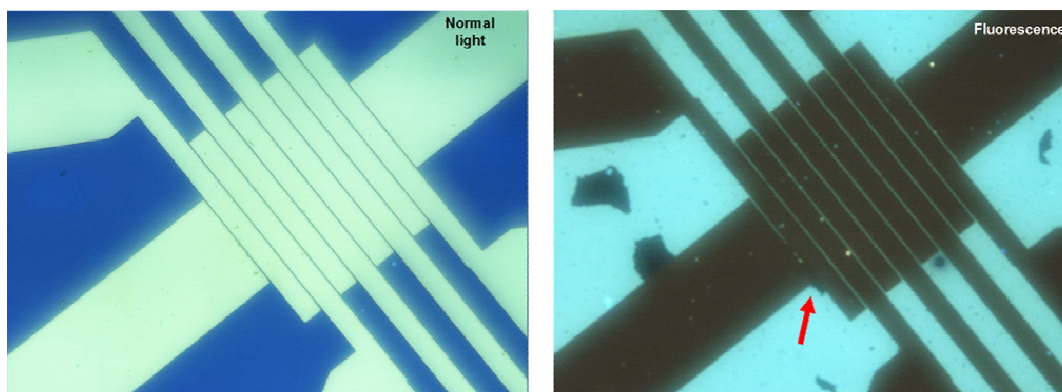


Figure 2.9 Example of use of fluorescence quenching to find flakes of graphene derivatives, the red arrow indicates a flake between electrodes.

Moreover, this kind of approach is not limited to GO and SiO_x substrates and can in principle be applied to a wide variety of different systems from biology to sensing and for many molecules.

The work present here led to the realization of the article “High-Contrast Visualization of Graphene Oxide on Dye-Sensitized Glass, Quartz, and Silicon by Fluorescence Quenching; E. Treossi, M. Melucci, A. Liscio, M. Gazzano, P. Samorì, V. Palermo *Journal of the American Chemical Society* 2009, 131, 15576.

2.3 COVALENT FUNCTIONALIZATION OF GRAPHENE SHEETS WITH OPTICALLY ACTIVE OLIGOTHIOPHENES.

Among carbon based materials, graphene represents the most thrilling discovery of the last decade. While a great effort has been addressed to the detailed investigation and optimization of its physical properties, the chemistry of graphene is still a rather unexplored field of research. Current challenges include the controlled chemical functionalization of graphene with functional units to achieve both a good processability in various media and a fine tuning of various physico-chemical properties of the 2D architecture, paving the way towards its technological application in chemical engineering. In this frame graphene oxide, because of its easier production and processability as well as simple chemical functionalization if compared to graphene, is emerging as a versatile material for applications in nanoscience and nanotechnology.

GO can be obtained in high yield by controlled chemical oxidation of graphite; the resulting oxidized single sheets are characterized by the presence of epoxy and hydroxyl groups covalently linked to the C atoms of the graphene basal planes, as well as carbonyl and carboxyl groups placed at the edges. Such functional groups can be exploited for the selective intercalation or adsorption of ions and molecules as well as for covalent modifications. In particular, GO–organic hybrid materials hold great promise for filling, sensing, imaging and electronics applications.¹³

For both fundamental science and technological applications in all these fields, it is crucial to lay the foundation for a new “chemistry” of graphene and graphene oxide, by devising synthetic methodologies able to add specific functionalities to these interesting materials, ultimately providing them with new and tunable electronic and optical properties.

Common methodologies for the covalent functionalization of GO rely on two-step procedures, i.e. activation of carboxylic acids followed by nucleophilic substitution by amines or epoxides ring opening. Functionalization of hydroxyl groups, largely present on the sheets basal planes, has received only minor attention. Triethoxysilane as well as halosilanes are widely exploited components for the

functionalization of metal oxide surface spanning from two dimensional (2D) substrates to silica nanoparticles having interfacial hydroxyl groups. Concerning GO substrate, amino catalyzed silylation through alkylchlorosilanes or sol-gel methods has been exploited to tailor the solubility and mechanical properties of GO.^{3,14} In this context we report a new, facile and rapid synthetic approach based on microwave-assisted (MW) silanization protocol to tether functional p-conjugated oligomers on GO sheets surface (Fig. 2.10). MW irradiation is currently employed in many sub-fields of organic synthesis to shorten reaction times, to enhance both reaction yields and product purity, and eventually to provide eco-sustainable synthetic methodologies, by replacing or reducing the use of polluting reagents.

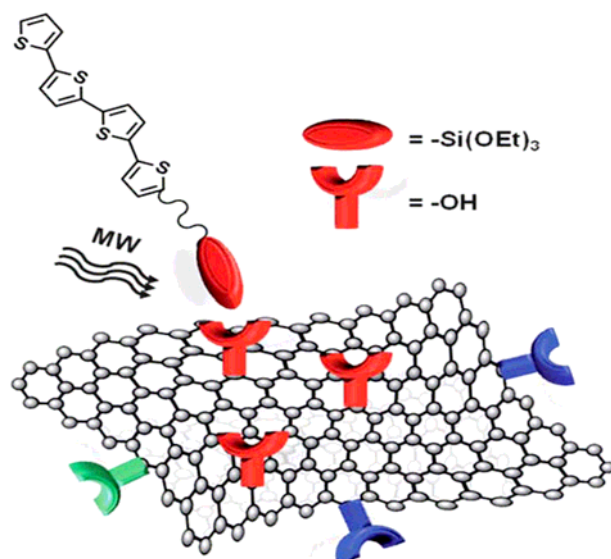


Figure 2.10 Sketch of the one-step functionalization approach presented here. The oligothiophene molecules are tethered by Si–O bonds. Blue: carboxylic groups, green: carbonyl groups.

Concerning graphene chemistry, MW activation has been employed so far for graphite pre-exfoliation, and more recently for the GO chemical reduction. Due to the chemical versatility and excellent photophysical and electrical properties of oligothiophene materials, quaterthiophene was selected as model system to be tethered to GO. GO was prepared by a modified Hummers method and exfoliated in dimethylformamide (DMF) by sonication for 24 h. The resulting black

suspension and T4-Si molecule **2** (Fig. 2.11) were introduced in a microwave oven reactor and irradiated at 80 °C (100 W) for 40 min.

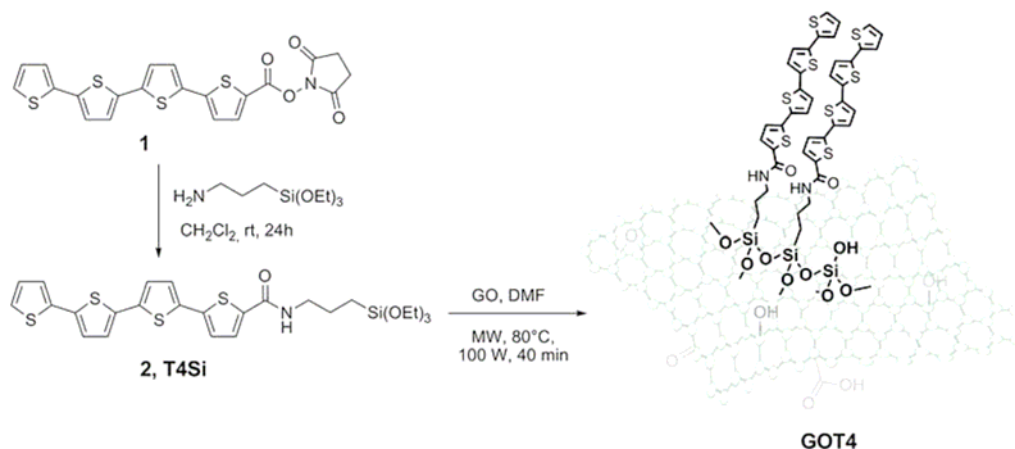


Figure 2.11 Synthetic route to T4-Si and GOT4.

After 40 min of irradiation, the DMF was evaporated under vacuum and the resulting solid was washed several times with fresh DMF, CH_2Cl_2 and acetone until the supernatant solution was not fluorescent under UV irradiation at 364 nm. After drying, GOT4 self-consistent membranes of a dark-green color were obtained. The sheets showed deep-yellow fluorescence under UV illumination (Fig. 2.12b).

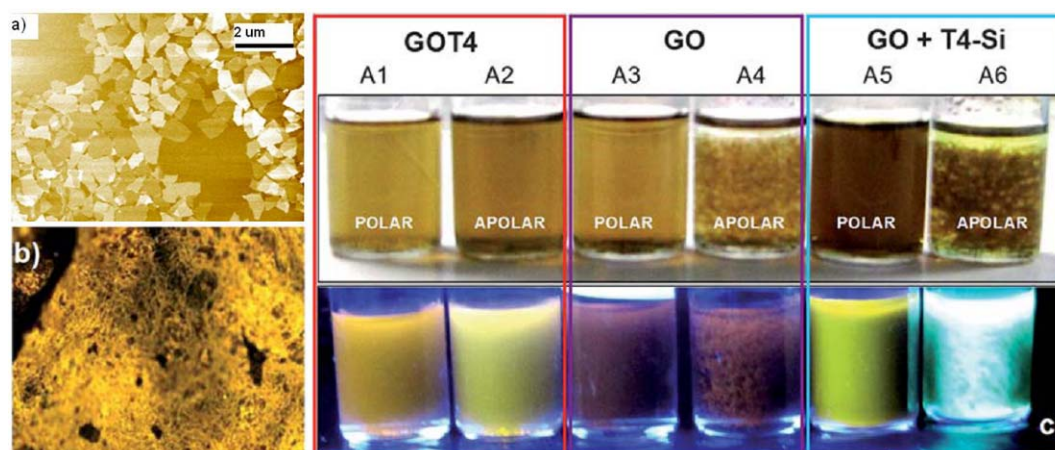
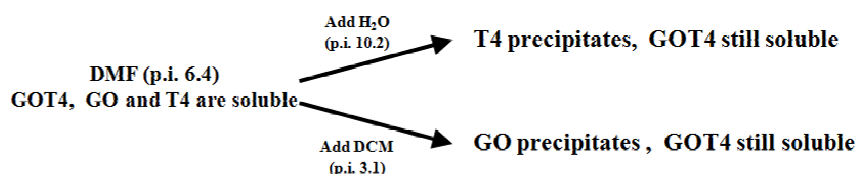


Figure 2.12 a) AFM image of exfoliated GOT4 sheets spin-coated on silicon. b) Fluorescence microscopy image of a GOT4 membrane illuminated by a mercury lamp. c) Suspensions of GOT4, pure GO and a mixture of free T4-Si with GO in polar ($\text{DMF-H}_2\text{O}$, 1 : 5 in volume) and apolar ($\text{DMF-CH}_2\text{Cl}_2$, 1 : 5 in volume) either in normal light (top) and under UV lamp (bottom).

Simple, combined tests of solubility and fluorescence unambiguously proved the successful chemical functionalization, by comparing the new properties for GOT4 with the ones of both its precursors (Fig. 2.12c, samples A1–A6). In these experiments, starting solvent was always DMF (polarity index p.i. = 6.4), where GO, T4-Si and GOT4 are all soluble. Then, selective GO or T4-Si precipitation was obtained by adding an excess of either water (p.i. = 10.2), in which T4-Si is not soluble, or dichloromethane (DCM, p.i. = 3.1), in which instead GO is not soluble.

New solubility properties of GOT4



Surprisingly, GOT4 did not precipitate in both polar and apolar media, i.e. upon addition of either H₂O and DCM (Fig. 2.12c, samples A1, A2 respectively). Instead, GO precipitation was always observed in apolar media, either for GO alone (sample A4) or mixed with free T4-Si (A6). Moreover the new compound, under UV illumination, did not show the typical bluish fluorescence of free T4-Si in solution (sample A6), but always showed a yellow emission similar to the one of aggregated T4-Si in water (A5).

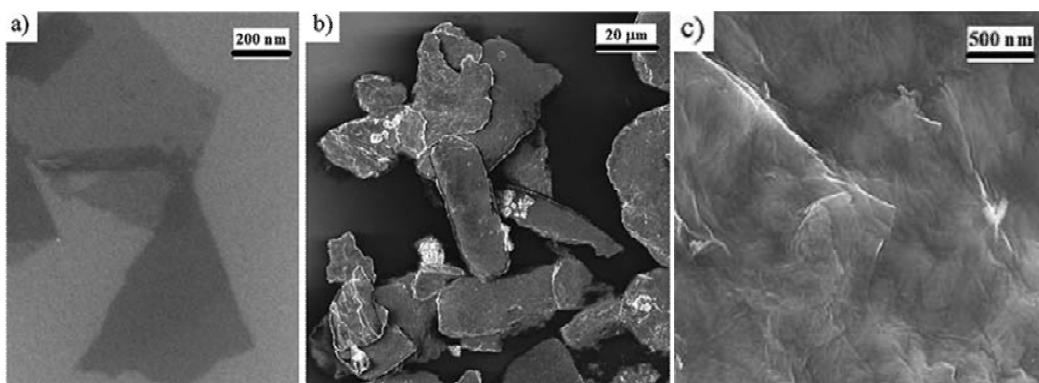


Figure 2.13 SEM images of: a) thin, sheets and b) thick, micron-sized stacks of GOT4 drop-cast on silicon from a DMF solution. c) Zoom-in on the surface of one of the stacks, showing the layered structure.

GOT4 sheets were deposited on silicon substrates for Scanning Electron Microscopy (SEM) observations, Fig. 2.13 show SEM images of GOT4 drop cast on silicon. Both thin layers a) and large platelets, with sizes of tens of microns b), were observed. On the surface of the platelets, the layered structure of the GOT4 sheets was clearly observed c). SEM analysis does not allow the determination of whether the thin sheets shown are single sheets or not. By spin coating a diluted solution on silicon it was also possible to obtain thinner layers of GOT4, down to deposition of even single sheets on the substrate, as unambiguously proved by Atomic Force Microscopy (AFM). Fig. 2.14 shows AFM images of highly exfoliated GOT4 sheets deposited on silicon, where single, bi- and multi-layers are clearly resolved, having variable lateral size of ca. 1 μm .

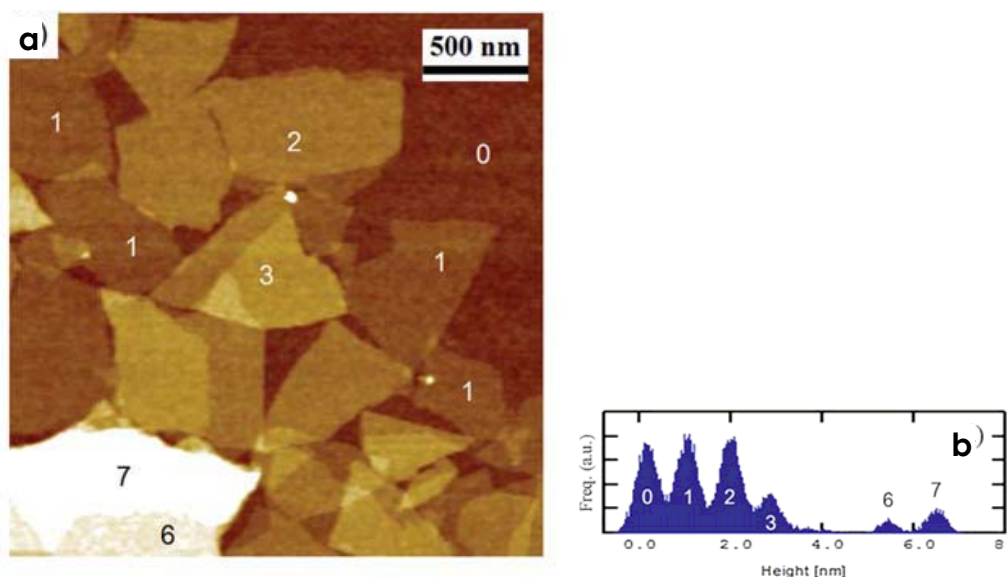


Figure 2.14 a) AFM image of exfoliated GOT4 sheets spin-coated on silicon, labels show the number of layers in different areas. b) Height histogram performed on a. The peak numbers correspond to the number of layers present in the area.

By using spin coating, basically all the GOT4 was deposited as single, bi- or tri-layer sheets, differently from what was obtained with drop casting, where only a small amount of thin sheets were found together with a majority of larger platelets. By performing statistical histogram analysis, an average height of 0.9 ± 0.2 nm was obtained. This value should be considered indicative, because even the thickness of

“simple” GO sheets, as measured by AFM, has been shown to vary greatly, ranging from 0.9 to 1.3 nm (see fig 2.3), due to the presence of adsorbed water on the surface, and the different hydrophilicity of the sheets with respect to the Si substrate. Nonetheless, the measured height can be compared to the one of “unfunctionalized” GO, thus suggesting a low density of T4 moieties on the surface, which, even if affecting significantly solubility and optical properties, does not change the apparent sheet thickness.

The optical properties of GOT4 in DMF were compared to those of T4-Si in a diluted (10^{-5} M) solution, featuring a poor interaction between T4-Si fluorophores dispersed in the chosen solvent, and to a cast film of T4-Si, featuring instead strong interactions between the packed molecules. To gain a complete understanding on the optical properties, absorption (Fig. 2.15a) and emission spectra (Fig. 2.15b) have been recorded.

In DMF solutions, T4-Si molecules show an unstructured absorption band located at 405 nm, and emission at 487 nm. The unstructured emission of T4-Si in solution suggests that the molecule adopts a distorted conformation. The absorption band of T4-Si in the solid state is strongly blue shifted instead, with a maximum placed at 350 nm (Fig. 2.15a). Blue shift of the major absorption band in the solid state was already observed for α quarter-, α quinque- and α sexi-thiophene and ascribed to the formation of H-aggregates with cofacially aligned molecules in the solid state.¹⁵⁻¹⁷ The red shift of the T4-Si emission in the solid state (peaks at 544 nm and 585 nm) also supports the occurrence of H-aggregation.

Both absorption and emission spectra of GOT4 (Fig. 2.15a and 2.15b) are comparable to those of T4-Si in diluted solutions, suggesting poor T4-T4 interactions. In particular, GOT4 exhibits a broad and structurless absorption band located at $\lambda_{\max} \approx 397$ nm and a broad emission band located at $\lambda_{\max} \approx 482$ nm. The emission is more similar to that of T4-Si in solution ($\lambda_{\max} = 487$ nm) rather than that of T4-Si solid film. This can be ascribed to the fact that in GOT4 the grafted T4-Si molecules are more distant from each other than T4-Si molecules in a conventional solid film. As a consequence, in GOT4 hybrid, strong T4-T4

interactions, yielding the red shifted PL spectrum of T4-Si solid films, are prevented.

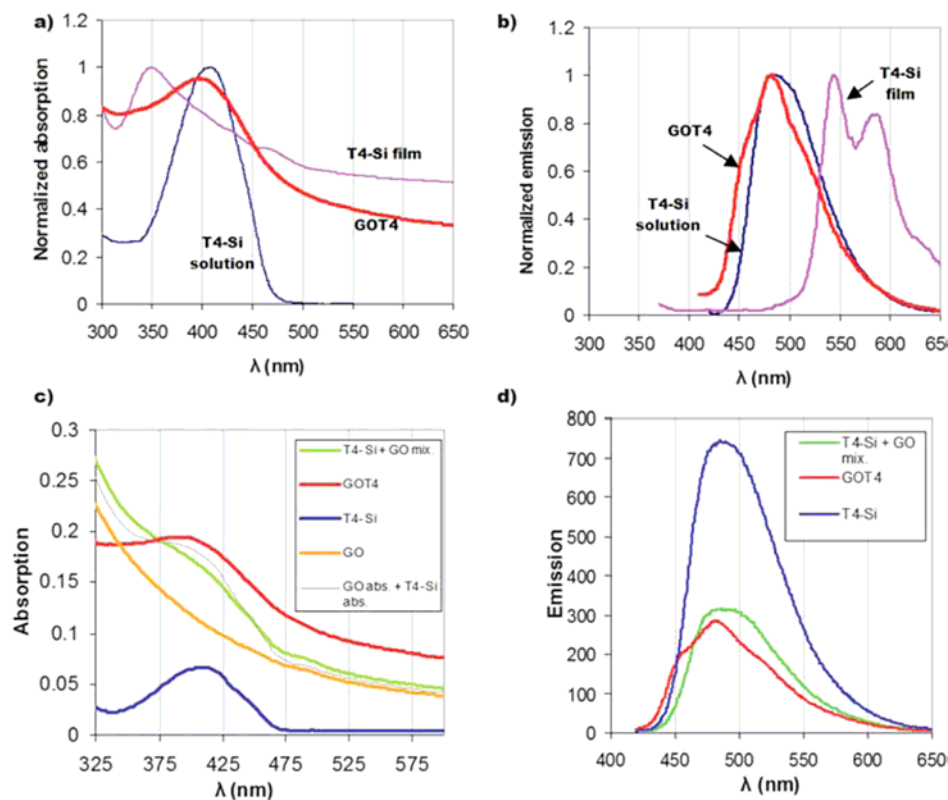


Figure 2.15 Normalized (a) absorption and (b) emission spectra of T4-Si monomers in DMF solution, T4-Si monomers in cast film, and of GOT4 in DMF (conc. 1 mg/ml). (c) and (d) Comparison of (c) absorption and (d) emission spectra of neat T4-Si, neat GO, a mixture of GO and T4-Si having the same T4-Si content of GOT4, and GOT4.

Fig. 2.15c and 2.15d show the comparison of the optical properties of T4-Si, GO, GOT4 and of a mixture of GO and T4-Si. The amount of T4-Si present in the mixture was based on the one estimated to be in GOT4, as obtained by TGA results (see below), i.e. $\approx 2.6\%$ in weight. The absolute molar concentration of T4-Si moiety in T4-Si sample and in the GO + T4-Si mixture was the same. The absorption spectrum of the mixture can be considered simply the sum of the absorption spectra of the two components (grey thin line in Fig. 2.15c); conversely, the GOT4 spectrum is qualitatively different both in the slope of the featureless GO absorption part and in the shape of the emission spectrum, indicating a strong perturbation of the T4 electronic structure. Fig. 2.15d shows the emission spectrum

for GOT4, having a different shape as compared to either T4-Si or a GO + T4-Si mixture.

Even if GOT4 material was carefully washed with different solvents before use, to eliminate physisorbed frameworks, this cannot exclude the presence of traces of free dye molecules on the sheets; though, the different shape of the absorption and emission spectra observed for GOT4 compared to T4 and the GO + T4 mixture, and the solubility tests (Fig. 2.12) indicate that GOT4 is not a mere mixture of the two components. A simple physisorption of T4-Si on GO would eventually take place as well in the GO + T4-Si mixture, given that both GOT4 preparation is performed in the same solvent used for the mixture (DMF), and thus would give similar solubility and spectroscopic properties between GOT4 and the mixture. Fluorescent quenching of organic fluorophores by GO has been already observed. It can be ascribed both to either short-range charge transfer or long-range energy transfer.

Thermal characterization of T4-Si, GO and GOT4 Thermal behavior of the GOT4 and of its basic components was investigated by TGA/MS under nitrogen atmosphere (FIG. 2.16). The T4-Si monomers show two distinct weight losses which have been unequivocally attributed to the thermal decomposition of the aliphatic triethoxysilane tail.

From 150 to 375 °C a weight loss of 16.2% is ascribed to the partial thermal decomposition of the triethoxy groups (m/z 45; m/z 46), while the residual aliphatic moiety entirely decomposes with a marked weight loss between 421 °C (T_{onset}) and 476 °C (T_{offset}) (m/z 113; m/z 112; m/z 97; m/z 84) (wt loss % between 150–500 °C; 45.7%). Over 500 °C a gradual weight loss due to the partial oxidative decomposition of the T4 fragment (m/z 44, CO₂ evolution) is observed.

The initial weight loss of GO below 150 °C (10.6%) is ascribed to the elimination of adsorbed water while a 2.5 wt% loss for functionalized GOT4 sample, within the same temperature range, is reasonably due to the elimination of adsorbed solvents.

A larger weight loss around 200 °C is observed for GO thermal profile and it is attributed to the oxydryl groups elimination from the graphene oxide layers.^{18,19}

Accordingly, a lower weight loss is measured at this temperature for the GOT4 sample compared to the pure GO, as a direct consequence of the T4 functionalization (GO vs. GOT4 in the 150–230 °C range, 32.2% vs. 27.8%). In the temperature range from 400 to 500 °C, a weight loss of 0.6% in the GOT4 sample (calculated as weight difference between the TG profiles of GOT4 and GO in the selected range of temperatures) is attributed to the thermal decomposition of the aliphatic linker between the GO and the T4 moiety. The MS analysis of volatiles in the latter range of temperatures (m/z 113 M^+ ; m/z 112 $M^+ -1$; m/z 97; m/z 84), accounts for the aforementioned decomposition. On this basis, one may roughly conclude that a 2.6 wt% of T4-Si is ultimately grafted to the graphene GO. Both the T4 unit and the GO do not undergo significant decomposition at $T < 500$ °C, and no decomposition of T4 fragments was observed below 500 °C from the TGA/MS of the GOT4, neither from the TGA/MS of pure T4-Si.

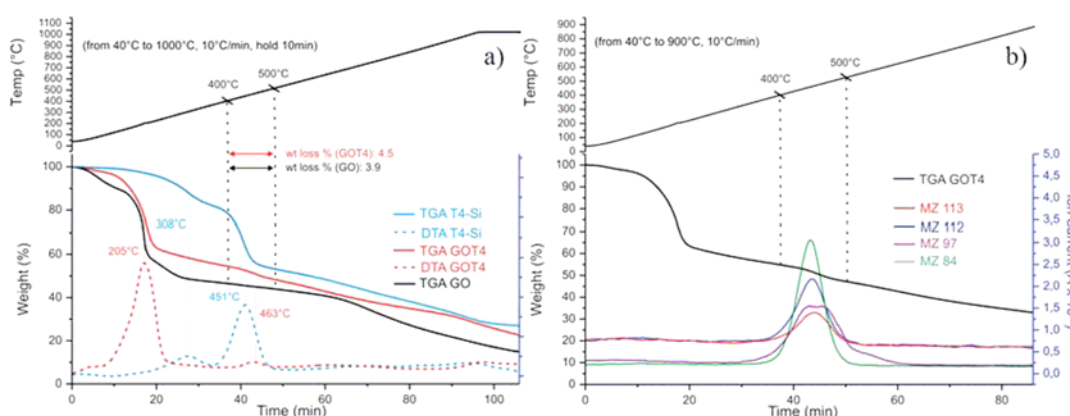


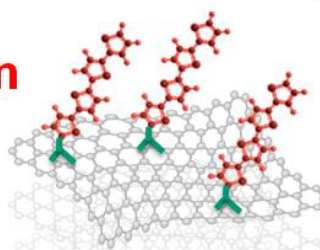
Figure 2.16 a) TGA-DTA of T4-Si, GO and GOT4 from 40 to 1000 °C. DTA of GO does not provide additional information and it has been omitted for clarity. Weight losses for GO and GOT4 have been calculated as average value over three runs. (b) TGA-MS of GOT4 from 60 to 900 °C. Evolution of volatiles ($m/z = 113$, $m/z = 112$, $m/z = 97$ and $m/z = 84$) have been monitored throughout the temperature range.

Elemental analysis conducted on the GOT4 sample has provided the following C, N and S contents: C, 49.47%, N, 0.3%, S, 2.69%. Accordingly, one may conclude that a 2.6 wt% T4-Si grafting roughly corresponds to 1 T4-Si group every 750 carbon atoms. However, it should be pointed out that the presence of intercalated

molecules of solvent (DMF) does not ultimately allow for an accurate estimation of the grafted fluorophore.

By assuming one T4 unit every 750 C atoms and the carbon atom surface density for a “perfect” graphene sheet ($38.2 \text{ C atoms nm}^{-2}$), an average T4-T4 distance of $\approx 6.2 \text{ nm}$ can be roughly estimated (much larger than the T4-Si long axis, which is $\approx 2.5 \text{ nm}$ including the flexible aliphatic tail), thus suggesting that the T4 molecules on average do not touch each other. The real T4-T4 distance is likely much larger, giving that GO has a much lower density of C atom, due to the presence of defective sites. According to this estimate, around $\approx 10^4$ T4-Si molecules can be tethered on both sides of a single GO sheet having lateral size of $1 \mu\text{m}$.

**Mixed properties between
a solid film of T4 and a
solution of free T4**



The hybrid system consisting of T4-Si covalently linked to the GO sheets exhibits new chemical and optical properties with respect to the pristine components. Optical spectroscopy shows that GOT4 can be seen as a multifluorophoric array,²⁰ where a high number of fluorophores is fixed to a common mesoscopic, flexible scaffold. It can be solution-processed from both water and organic solvents, to give platforms of main interest for optoelectronics. Application of multifluorophoric arrays in optoelectronic devices such as transistors and solar cells has been already demonstrated by some of us by using perylenes and oligothiophenes as fluorophores and organic polymers as scaffolds (polyisocyanides or polyvinyls). The use of GO as scaffold instead of synthetic polymers gives major advantages: GO can be produced on large scale and at low cost by graphite oxidative exfoliation, and can form 2-dimensional sheets with sizes up to $100 \mu\text{m}$, as compared to polymeric scaffolds which instead are 1-dimensional and have typical lengths $< 1 \mu\text{m}$.

Alongside the peculiar characteristic of the GOT4 material itself, a major synthetic outcome is that the use of microwaves assisted silanization represents a ‘user friendly’ methodology to engineer GO properties. Indeed, readily available building blocks and mild conditions are required to perform this reaction.

Conventional silanization of silicon and glass substrates, as well as GO functionalization by other methods, generally require reaction times of 1–7 days. Our procedure allows reduction of the functionalization time down to 40 min. It is well known that coupling microwaves (energy source) with graphite (support) is responsible for a high temperature gradient leading to increased reaction rates as compared to conventional procedures.

It is well known that graphene oxide does not have the same outstanding electrical properties of pristine graphene. Although GO can be considered an insulator, it is a peculiar one, where irregular aromatic patches of sp²-hybridized C atoms can exist, surrounded by insulating areas of sp³-hybridized C atoms. In light of this, GO can be considered as an irregular (macro)- molecule bearing different kinds of polyaromatic moieties, whose electronic properties depend significantly on the size of the aromatic domains. The results obtained here show that, despite GO is not fully conjugated as graphene, it can exchange efficiently charges with adjacent T4 fluorophores, which will interact preferentially with GO rather than with each other.

We have reported an efficient synthetic approach to build GO-based multifluorophoric array, in which GO acts as a flexible planar template and p-conjugated oligomers (in this case T4) as antennas.

The above described functionalization methodology is not limited to T4-Si attachment, but can be useful for both fundamental science and technological applications to covalently tether different functional moieties to GO.

The work present here led to the realization of the article “Facile covalent functionalization of graphene oxide using microwaves: bottom-up development of functional graphitic materials” M. Melucci, E. Treossi, L. Ortolani, G. Giambastiani, V. Morandi, P. Klar, C. Casiraghi, P. Samori, V. Palermo. *Journal of Materials Chemistry* 20, 9052, 2010.

2.4 BIBLIOGRAPHY

1. Graphene Oxide, Highly Reduced Graphene Oxide, and Graphene: Versatile Building Blocks for Carbon-Based Materials; O. C. Compton, S. T. Nguyen *Small* 2010, 6, 711.
2. Large-area ultrathin films of reduced graphene oxide as a transparent and flexible electronic material; G. Eda, G. Fanchini, M. Chhowalla *Nature Nanotechnology* 2008, 3, 270.
3. Evaluation of Solution-Processed Reduced Graphene Oxide Films as Transparent Conductors; H. A. Becerril, J. Mao, Z. Liu, R.M. Stoltenberg, Z. Bao, Y. Chen, *Acs Nano* 2008, 2, 463.
4. High Yield Preparation of Macroscopic Graphene Oxide Membranes; Z. T. Luo, Y. Lu, L. A. Somers, A. T. C Johnson, *Journal of the American Chemical Society* 2009, 131, 898.
5. Thin-film particles of graphite oxide 1: High-yield synthesis and flexibility of the particles; M. Hirata, T. Gotou, S. Horiuchi, M. Fujiwara, M. Ohba, *Carbon* 2004, 42, 2929.
6. Evolution of Electrical, Chemical, and Structural Properties of Transparent and Conducting Chemically Derived Graphene Thin Films; C. Mattevi, G. Eda, S. Agnoli, S. Miller, K. A. Mkhoyan, O. Celik, D. Mastrogiovanni, G. Granozzi, E. Garfunkel, M. Chhowalla *Advanced Materials* 2009 19, 2577.
7. Determination of the Local Chemical Structure of Graphene Oxide and Reduced Graphene Oxide; K. Erickson, R. Erni, Z. Lee, N. Alem, W. Gannett, A. Zett *Advanced Materials* 2010, 22, 4467.
8. Making graphene visible; P. Blake, E.W. Hill, A.H.C. Neto, K.S. Novoselov, D. Jiang, R. Yang, T.J. Booth, A.K. Geim, *Applied Physics Letters* 2007, 91, 063124.
9. Simple Approach for High-Contrast Optical Imaging and Characterization of Graphene-Based Sheets; I. Jung, M. Pelton, R. Piner, D.A. Dikin, S. Stankovich, S. Watcharotone, M. Hausner, R.S. Ruoff, *Nano Letters* 2007, 7, 3569.
10. High-Contrast Visualization of Graphene Oxide on Dye-Sensitized Glass,

Quartz, and Silicon by Fluorescence Quenching; E. Treossi, M. Melucci, A. Liscio, M. Gazzano, P. Samori, V. Palermo *Journal of the American Chemical Society* 2009, 131, 15576.

11. Graphene: The New Two-Dimensional Nanomaterial; C.N.R. Rao, A.K. Sood, K.S. Subrahmanyam, A. Govindaraj, *Angewandte Chemie International Edition* 2009, 48, 7752, and references therein.

12. Facile covalent functionalization of graphene oxide using microwaves: bottom-up development of functional graphitic materials; M. Melucci, E. Treossi, L. Ortolani, G. Giambastiani, V. Morandi, P. Klar, C. Casiraghi, P. Samori, V. Palermo. *Journal of Materials Chemistry* 20, 9052, 2010.

13. Graphene oxide as a chemically tunable platform for optical applications; K.P. Loh, Q. Bao, G. Eda, M. Chhowalla *Nature Chemistry* 2010, 2, 1015.

14. Preparation and characterization of silylated graphite oxide; Y. Matsuo, T. Tabata, T. Fukunaga, T. Fukutsuka, Y. Sugie *Carbon*, 2005, 43, 2875.

15. Conjugated polymers and oligomers as active material for electronic devices; F. Garnier, G. Horowitz and D. Fichou *Synthetic Metals* 1989, 28, C705.

16. Exciton Coupling Effects in the Absorption and Photoluminescence of Sexithiophene Derivatives; A. Yassar, G. Horowitz, P. Valat, V. Wintgens, M. Hmyene, F. Deloffre, P. Srivastava, P. Lang and F. Garnier *Journal of Physical Chemistry* 1995, 99, 9155.

17. Effect of substituents on electronic properties, thin film structure and device performance of dithienothiophene-phenylene cooligomers S. M. Zhang, Y. L. Guo, H. X. Xi, C. A. Di, J. Yu, K. Zheng, R. G. Liu, X. W. Zhan and Y. Q. Liu, *Thin Solid Films*, 2009, 517, 2968.

18. Structure of Graphite Oxide Revisited; A. Lerf, H. Y. He, M. Forster and J. Klinowski *Journal of Physical Chemistry B* 1998, 102, 4477.

19. Synthesis of graphene-based nanosheets via chemical reduction of exfoliated graphite oxide; S. Stankovich, D. A. Dikin, R. D. Piner, K. A. Kohlhaas, A. Kleinhammes, Y. Jia, Y. Wu, S. T. Nguyen and R. S. Ruoff *Carbon* 2007, 45, 1558.

20. The Relationship between Nanoscale Architecture and Function in Photovoltaic Multichromophoric Arrays as Visualized by Kelvin Probe Force Microscopy; V. Palermo, M. B. J. Otten, A. Liscio, E. Schwartz, P. A. J. de Witte, M. A. Castriciano, M. M. Wienk, F. Nolde, G. De Luca, J. J. L. M. Cornelissen, R. A. J. Janssen, K. Mullen, A. E. Rowan, R. J. M. Nolte, P. Samori, *Journal of the American Chemical Society* 2008, 130, 14605.

CHAPTER 3

ELECTROCHEMICAL REDUCTION AND PATTERNING OF GRAPHENE OXIDE

3.1 REDUCED GRAPHENE OXIDE

To exfoliate graphene via chemical method we introduces in graphitic plane polar groups to improve the solubility in water and lead the interaction between different planes.

Mattevi in the paper “Evolution of Electrical, Chemical, and Structural Properties of Transparent and Conducting Chemically Derived Graphene Thin Films” shows how after oxidation of graphite about 40% of compound was oxygen

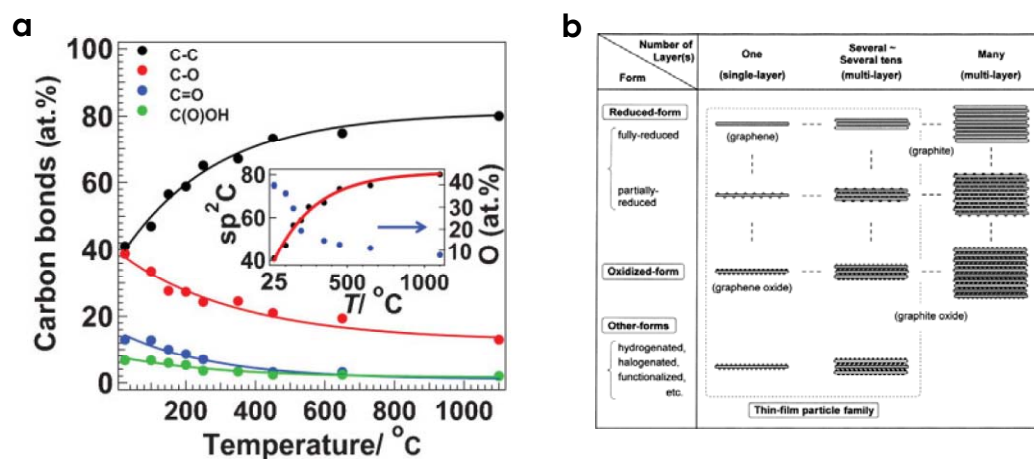


Figure 3.1 Percentages of different carbon as a function of annealing temperature. The aromatic carbon and oxygen concentration are reported as a function of the annealing in the inset.² b) Category of thin-film particles.¹

and the carbon atoms in function of chemicals bonds can be divided into 4 different types:

C=C/C-C bonds = aromatic carbon are $\approx 40\%$ of carbon atoms

C-O bonds = epoxy and hydroxyl groups are $\approx 40\%$ of carbon atoms

C=O bonds = carbonyl groups are $\approx 13\%$ of carbon atoms

CO-OH bonds = carboxyl groups are $\approx 7\%$ of carbon atoms

Usually aromatic carbons are organized in domains surrounded by epoxy, hydroxyl and carbonyl groups while carboxyl groups are present in the edges of flakes.

By thermal, chemical or electrochemical treatment is possible to restore the conducting network, increasing and connecting the previously isolated aromatic domains, the resulting compound is known as reduced graphene oxide (RGO).

In figure 3.1 it is possible to see how 80% of sp^2 carbon can be restored by thermal annealing at $1000\text{ }^\circ\text{C}$.

The structure of graphene, graphene oxide and reduced graphene oxide obtained by transmission electron microscopy are shown below from Erickson's paper "Determination of the Local Chemical Structure of Graphene Oxide and Reduced Graphene Oxide"

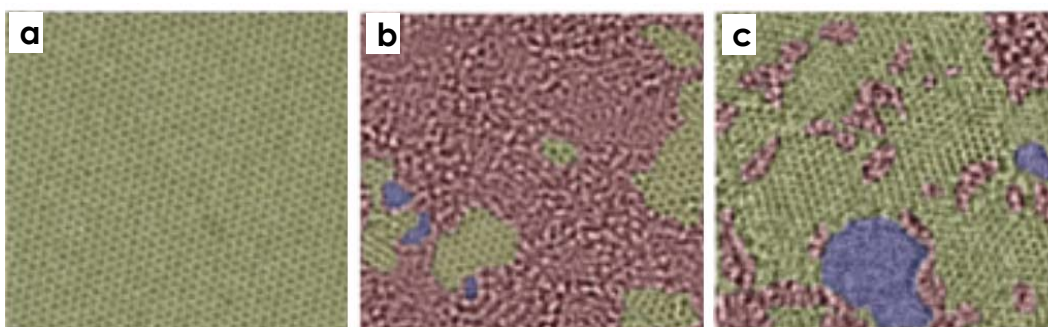


Figure 3.2 Aberration corrected TEM images of a) suspended sheet of graphene. b) suspended sheet of GO and c) suspended sheet of RGO. Graphitic area indicated in yellow, disordered regions (indicating oxygen functionalities) in red and holes are indicated in blue.³

In our work the GO was reduced to RGO by thermal annealing at $\approx 700\text{ }^\circ\text{C}$ in vacuum. We used a low rate heating ramp, in order to ensure efficient removal of oxygen containing groups with minimum carbon losses.

In the following figures we can see graphene oxide flakes or film before and after thermal treatment. The optical contrast increases after reduction we can see by

optical images of flakes on silicon oxide 300 nm thick or in the transmittance spectra of GO and RGO films on quartz.

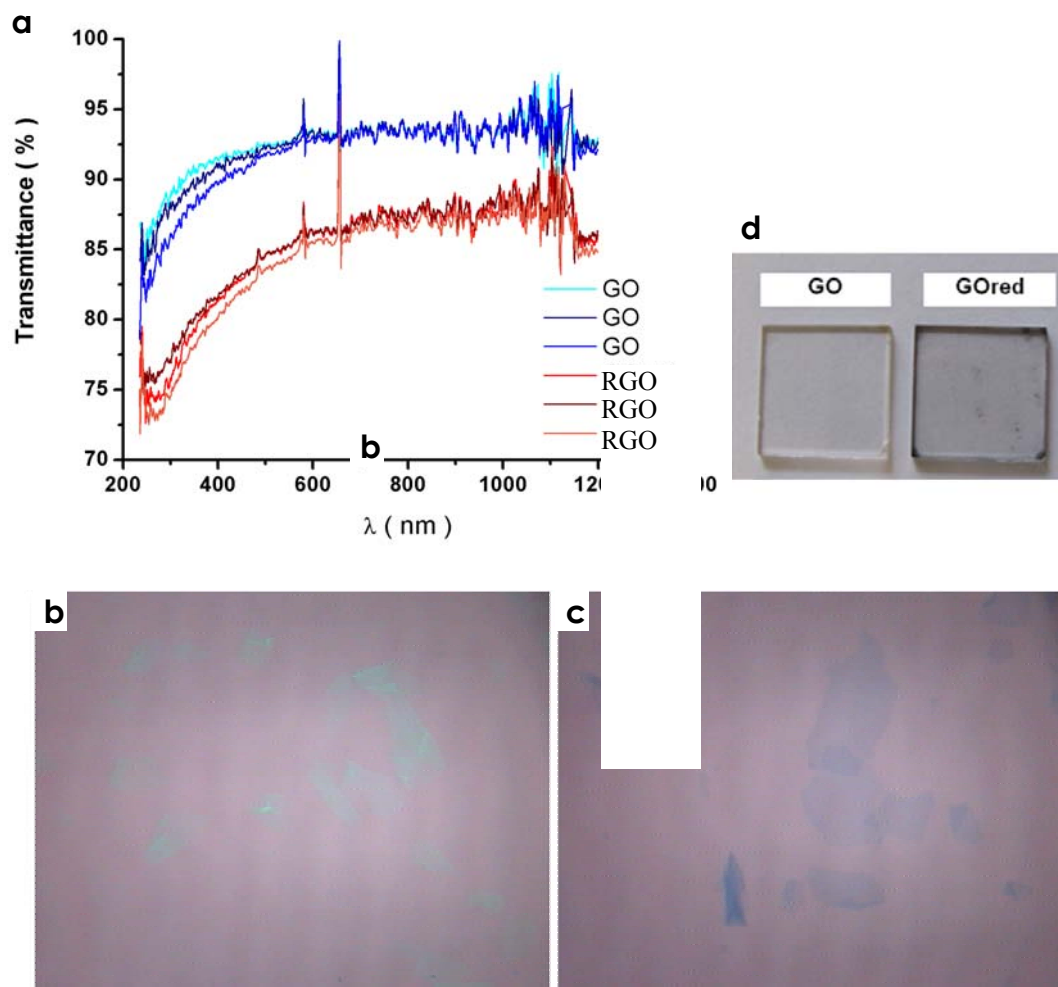


Figure 3.3 a) Transmittance spectra of GO and RGO films on quartz b,c) optical images of GO and RGO flakes on silicon oxide 300 nm. e) optical images of GO and RGO films on quartz.

While rapid progress in measuring electrical transport in multilayer films and single graphene sheets has been achieved, little is known about the local spatial dependence of the electrical properties. Here we show that conductive atomic force microscopy (C-AFM) is a powerful tool for obtaining direct measurements of the local variations in current-carrying capacity in graphene sheets and films over length scales ranging from tens of nanometers to tens of micrometers. These

measurements make it possible to correlate the detailed morphology of graphene (e.g., wrinkles, multilayer regions) to its electrical characteristics.

In this approach, a metal-coated AFM tip is used as a movable electrode that can be positioned with nanometer-scale precision and a controlled nanonewton-range force. In contrast to scanning tunneling microscopy (STM), the use of force feedback decouples the regulation of the tip-sample separation from the current measurement, providing a better-defined tip-sample interaction and the capability of measuring samples with insulating regions. Previous applications of C-AFM include studies of self-assembled monolayers, organic semiconductors, and low-dimensional nanostructures such as carbon nanotubes. We demonstrate here that C-AFM is well-suited for mapping the local electronic properties of RGO.

GO was produced by a modified Hummers method as previously described see chapter 2 and then spin-coated onto Si substrates with a 300 nm thick SiO₂ layer. We first tested the applicability of C-AFM for current mapping on few-layer-thick thermally reduced RGO films.

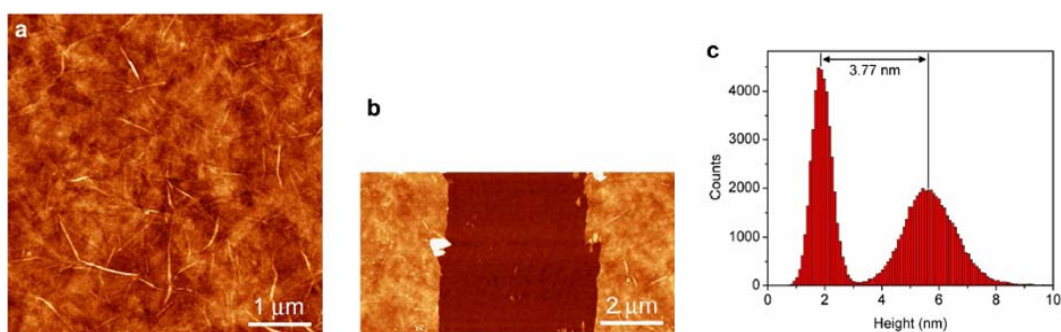


Figure 3.4 Topographic tapping mode AFM images showing a) the RGO film structure, and b) a scratched region, for measuring the film thickness c) The height of the film is measured from a histogram of the height distribution.

The morphology of the reduced graphene-oxide films was measured by tapping mode atomic force microscopy (AFM), revealing a flat, smooth structure and some visible sheet edges. The thickness of the films was measured at several positions by gently scratching the surface with a sharp needle, and measuring the height difference between the film and substrate surfaces (fig. 3.4).

C-AFM imaging was performed by applying a voltage between a Pt/Ir-coated AFM tip and a vacuum-deposited Au top electrode and scanning the tip over the sample with a constant force in the contact mode. A schematic of the setup is shown in figure 3.5.

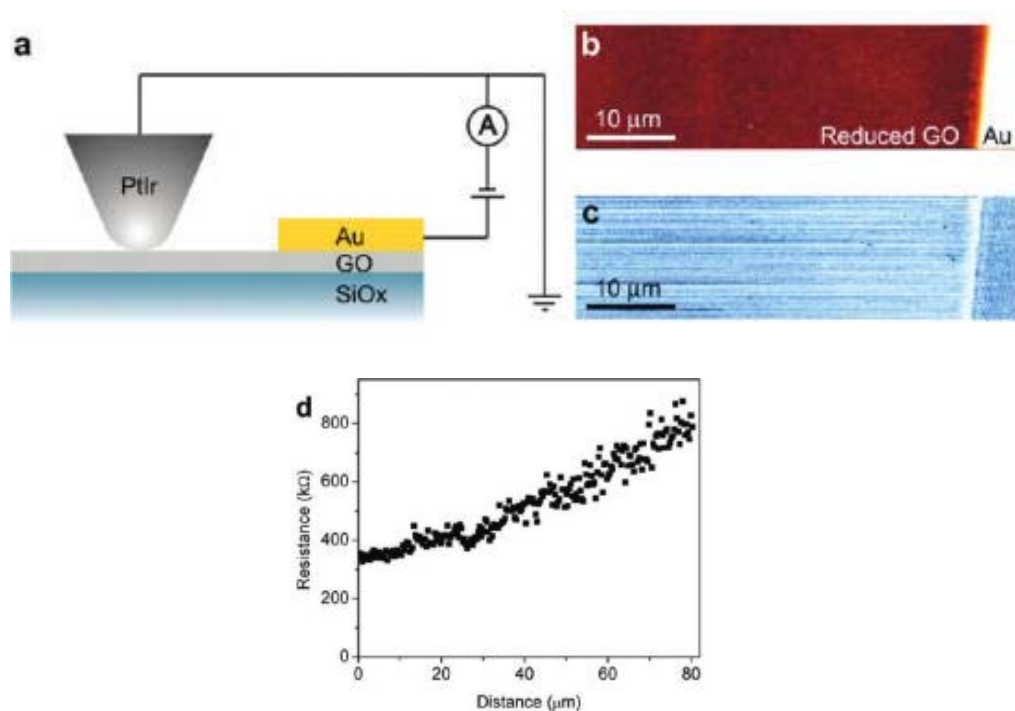


Figure 3.5 a) Schematic of the setup employed for C-AFM current mapping and current-voltage acquisition. b) Contact-mode topographic AFM image of a few-layer reduced GO film and c) the simultaneously recorded current map obtained using a 100 mV sample voltage. d) Dependence of the electrical resistance on the separation between the tip and the counter electrode.

The recorded current as a function of position provides a map of the local capacity of the sample to transport charge between the tip position and the Au counter electrode. As shown in figure 3.5b,c, the current measured on RGO film is highly uniform over a scale of tens of micrometers, highlighting the potential of RGO as a transparent electrode material.⁴

Small line-to-line variations are visible, probably caused by microscopic structural changes in the tip-sample interface during scanning, particularly at the Au step edge.

The bright appearance of the Au edge in the current image is related to the large topographic height difference at the edge (100 nm in this instance), which causes the side of the tip rather than the sharp apex to electrically contact the sample; this results in a larger contact area and an increased current. In addition, over the Au, the current map has a speckled appearance due to the formation and loss of contact with individual nanometer-scale Au grains by the tip as it scans over the surface. A relatively constant electrical contact between tip and sample was formed over the RGO as a result of its smooth morphology. Interestingly, there were no abrupt changes in conductivity associated with the RGO sheet edges, indicating efficient transport between adjacent sheets. This is in contrast to the case of organic semiconductors, where grain boundaries represent a major transport bottleneck.⁵

The resistance of the RGO film as a function of tip-electrode separation yielded a nearly linear relation (figure 3.5d). Some nonlinearity is to be expected given the measurement geometry: the current spreads as it flows through the sample from the sharp tip to the extended Au electrode. Nonlinearities may also originate from the conduction mechanism.

Fitting the curve to a second-order polynomial yielded a contact resistance of 340 k Ω , representing the sum of the resistances at the RGO-electrode and RGO-tip interfaces. The latter is expected to be the dominant contribution, given the relatively small contact area of about 7 nm².

Topography and current images of a region with incomplete RGO coverage on SiO₂ (figure 3.6 a,b) show that defects in the RGO film are far more easily visualized in the current channel than in the topography. As displayed in figure 3.6b, the electrical connectivity of the film and the local capacity to transport charge is immediately clear from the current image, while the topography (Figure 3.6 a) provides little information with respect to these. The resolution of the current images was determined to be less than 20 nm on the basis of the minimum distance between distinct features. Current-voltage (I-V) measurements (90 in total) at 16 positions on the surface revealed currents over single-layer regions that were 3.9 \pm 0.5 times smaller than the currents over multilayer regions at similar electrode distances.

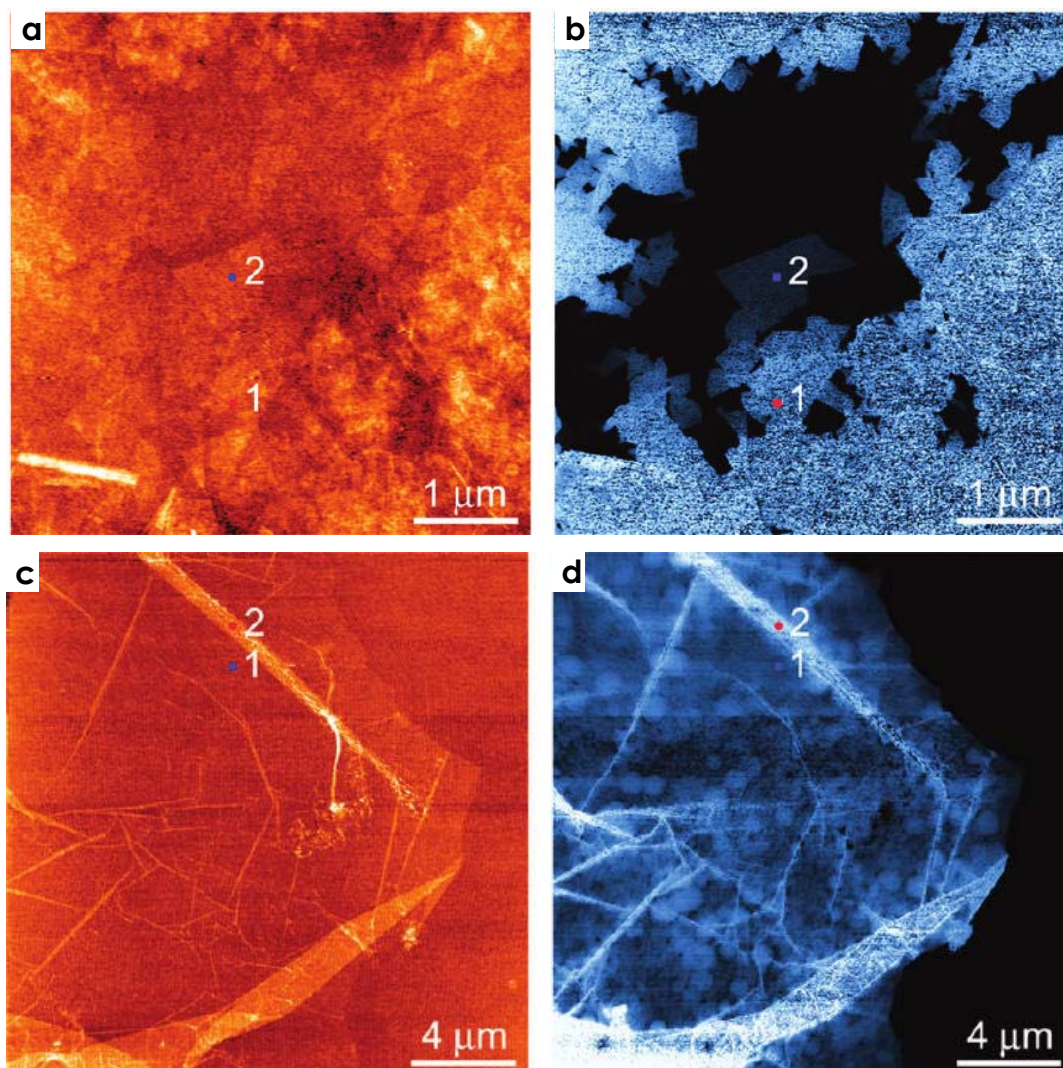


Figure 3.6 Contact-mode image of a defect region of an RGO a) film and b) the corresponding current image, the differences in the current over regions of different thickness. c) Contact-mode topographic image of a single-layer RGO sheet exhibiting some folds and multilayer regions d) Simultaneously recorded current map showing increased currents over the folded and multilayer regions as well as local variations over the single-layer areas.

The film thickness of 3.7 ± 0.7 nm, which was measured over several areas of the sample, indicates that the film consisted of about three RGO layers, given the measured single-layer thickness of 1.2 ± 0.1 nm, the latter closely matching that of earlier studies. By considering as an approximation the stacked RGO layers as parallel conductors, we see that the current per layer in the multilayer is 1.3 times

larger than the current in the single layer. A similar effect was measured by Kern and co-workers,⁶ who suggested that decreased conduction in the first layer results from interactions with the substrate. An additional factor may be that in multilayer graphene, there is an increased number of percolation pathways around defects. Moreover, in few-layer RGO films, the band structure is expected to depend on the number of layers. In the case of pristine graphene, as the number of layers increases, the band structure becomes increasingly semimetallic (i.e., there is increased band overlap).⁷

Further support for increased conductivity in multilayers was provided by C-AFM measurements on single RGO sheets. A topographic AFM image is shown in Figure 3.6 cd along with the corresponding current image. These measurements revealed a morphology of smooth single-layer with narrow folds and two-layer segments; moreover, the current image shows that folded and two-layer regions are more conductive than the single-layer RGO, provided that the regions are in direct contact with the surface electrode.

In instances where folded and multilayer regions are surrounded by single-layer RGO, the current is limited by the intervening single layer. I-V measurements (44 curves at 22 points) showed that the current over the directly contacted two-layer regions was 3.0 ± 0.4 times larger than the current over the single layer.

Assuming equal conduction in each layer, the current per layer in the bilayer was thus 1.5 times the current in the single layer.

Upon close inspection of the current image (Figure 3.6d), some round features and small local variations in current are visible over the single-layer regions, which may be due to the thermal reduction process (e.g., outgassing of the oxygen-containing defects).

The resistance as a function of distance from the Au electrode was measured on a single-layer flake, and a nearly linear relation was obtained, similar to the multilayer case. The extracted contact resistance of $1.1 \text{ M}\Omega$ is slightly more than 3 times higher than that in the multilayer.

3.2 TIP-INDUCED REDUCTION OF GRAPHENE OXIDE.

There is great interest in patterning graphene for largescale integration into electronic devices and for prototyping lab-scale test systems. Large-scale patterned graphene films have been grown by chemical vapor deposition and transferred to flexible substrates. Stencil masks have been used in conjunction with electrochemical or camera-flash reduction to produce macroscopically patterned RGO. Moreover, quantum confinement and opening of an energy band gap have been observed in graphene nanoribbons patterned by standard lithography methods.⁸ However, it has been shown that lithography can leave residual photoresist on patterned graphene, potentially obscuring the intrinsic device characteristics. We demonstrate a resistless single-step C-AFM-based approach for patterning GO with conductive micrometer-scale regions under ambient conditions. As a proof of principle, we have employed this technique to fabricate micropatterned graphene field-effect transistors featuring high charge-carrier mobilities.

Not surprisingly, GO multilayers (7 ± 1 nm thick) without reduction exhibited limited electrical transport. At $2 \mu\text{m}$ from the Au electrode, picoampere-range currents were measured at voltages above 2 V (figure 3.7a).

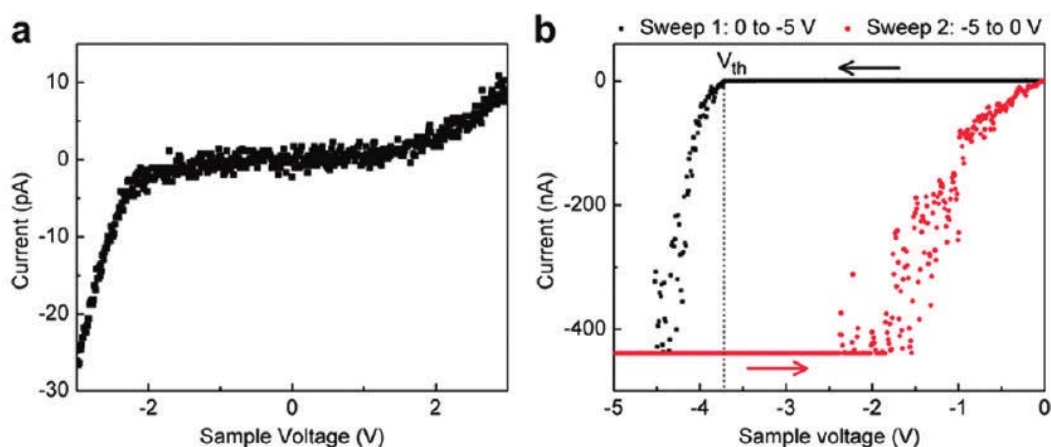


Figure 3.7 AFM-tip-induced modification of GO leading to conductive regions. (a) Current-voltage measurement on a few-layer GO film. (b) As the current was swept to large negative voltages, beyond a threshold voltage $V_{th} = -3.6 \pm 0.3$ V, the current suddenly increased to saturation levels of the current detection.

Interestingly, a change took place when the tip was in close proximity to the Au electrode (e.g., within 1 μm) at negative sample voltages beyond -3.6 ± 0.3 V: the current rapidly increased with voltage from current levels below the minimum detection limit (<1 pA) to beyond the maximum detection limit (>500 nA), spanning more than 5 orders of magnitude.

This change was marked by hysteresis in the I-V traces (figure 3.7b). Subsequent C-AFM imaging revealed that the GO surface was rendered conducting over a small patch of the surface. Sweeping the sample voltage to a large negative voltage (below -3.6 ± 0.3 V) at evenly spaced intervals (e.g., 500 nm) starting from the electrode allowed conducting lines to be patterned on the GO. The width of the features depended linearly on the magnitude of the applied voltage within the measured range, with lines as narrow as 1 μm at voltages of -3.6 V and features as wide as 6 μm at -6 V. No significant increase in conductivity was observed at positive sample biases. Similar results were obtained on multilayer and single-layer GO.

To ensure that the observed conductivity was not related to damage to the underlying oxide, the tip-induced modification was reproduced on quartz substrates. There was no significant change in the GO surface topography following surface modification, as confirmed by AFM height measurements, demonstrating that the process is nondestructive.

The surface modification experiments were performed at relative humidity (RH) levels between 40 and 60%. In order to test the possible role of an adsorbed water layer during the tip-induced modification of GO, the RH level in the AFM chamber was gradually reduced using flowing argon. As the RH decreased, the surface modification became less pronounced see fig. 3.8, and the widths of the features were reduced to submicrometer dimensions. Below about 25% RH, surface modification was no longer observed. This suggests that water has a significant role in the surface modification process.

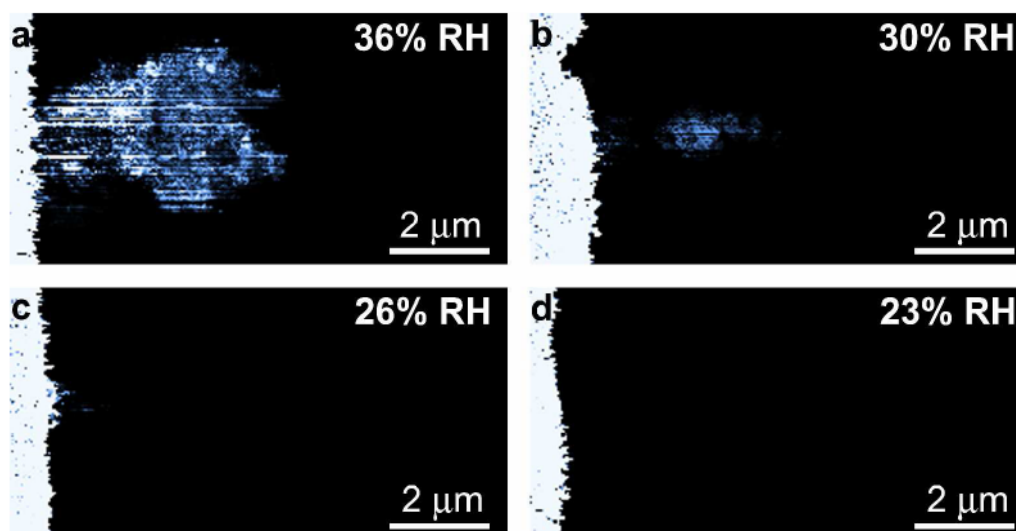
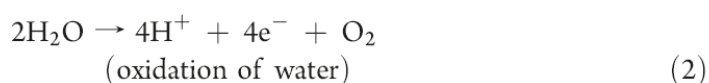
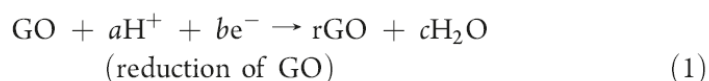


Figure 3.8 Current images of a tip-modified GO film at RH levels of a) 36%, b) 30%, c) 26%, and d) 23%. The reduction was performed with a minimum sample bias of -5V. The Au surface electrode is at the left edge of the image.

It is well-known that in air, a several-monolayer-thick water layer readily adsorbs on hydrophilic surfaces. Moreover, when the AFM tip is in contact with the sample, a water meniscus forms around the tip and acts as a localized electrochemical environment. Previous studies have shown that through the application of a positive voltage between the tip and sample, it is possible to locally oxidize various substrates, including silicon⁹ and graphene.¹⁰ In the case of our experiments, it is expected that the GO was electrochemically reduced by the negative tip-sample voltage. Previous work on macroscopic electrochemical GO reduction revealed that reduction is facilitated at low pH levels, indicating an essential role of hydrogen ions.¹¹

The suggested reaction scheme leading to GO reduction is hypothesized to comply with the following:



Repeated tip-induced modification of the same GO region resulted in increased conductivity. After 10 modification cycles, the measured currents in the I-V traces were 10 times higher than after the first modification and within an order of magnitude of the results for thermally reduced GO. In the case of GO, it is expected that the decrease in reduction rate with time is related to the depleted supply of oxygen-containing defects available to under GO reduction over time. A contact resistance of 1.3 M Ω was extracted for a GO region that was modified 11 times. With the assumption that the current was transported along the entire modified area, which had a width of 3.7 μm , a sheet resistance of 1 M Ω /square was determined; this is lower than the sheet resistance of 4 M Ω /square for hydrazine-reduced few-layer GO¹¹ but more than an order of magnitude higher than that for thermally reduced fewlayer GO.⁷

Further evidence that the tip-induced GO modification corresponds to a reduction process was provided by confocal Raman spectroscopy, which is a particularly effective tool for identifying the structure and degree of disorder in carbon-based materials. Large conductive GO features were patterned and subsequently measured by C-AFM, optical microscopy, and Raman spectroscopy (figure 3.9). In accordance with previous studies fig.3.3, the reduced region had a lower optical transmittance, resulting in a darker appearance under the optical microscope (Figure 3.9b). Raman spectra for the GO and modified GO exhibited two prominent peaks, at about 1350 and 1600 cm^{-1} , corresponding to the D and G bands. The G band is due to the E_{2g} phonon mode in the sp^2 carbon network, while the D band is correlated to disorder in the lattice. In agreement with other studies,^{12,13} the intensity of the D band increased relative to the G band upon reduction. This has been interpreted as resulting from the creation of new graphitic domains that are smaller in size but greater in number than those present prior to reduction.¹²

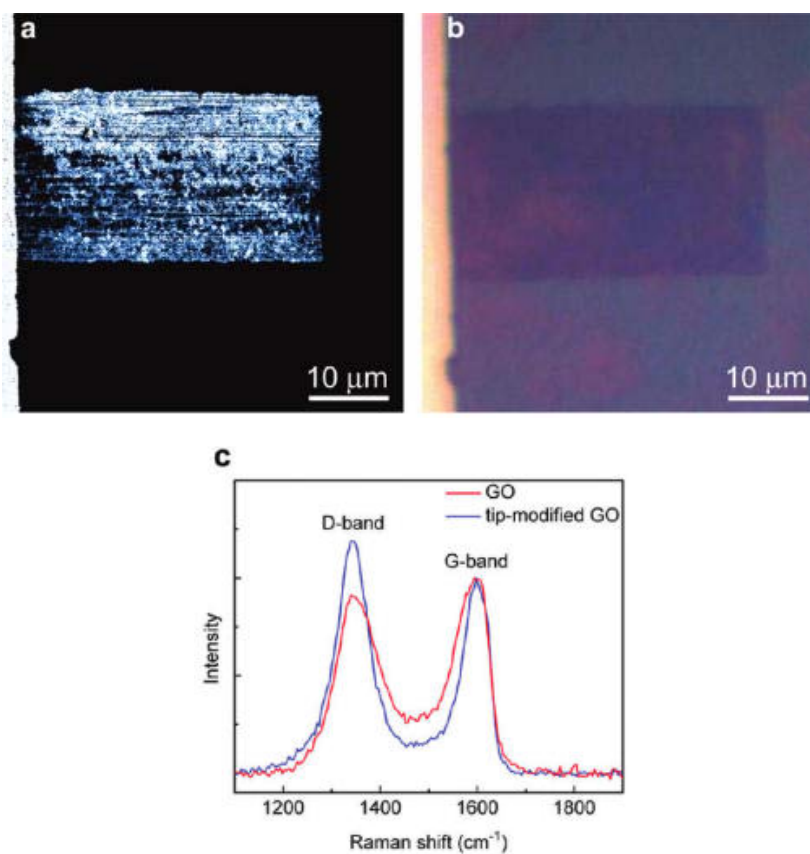


Figure 3.9 a) C-AFM current map of a tip-modified rectangular region of a few-layer GO film and a top-contact gold electrode. b) Optical image of the same region showing contrast between the modified and unmodified GO. c) Raman spectra obtained on modified and unmodified GO

3.3 THIN-FILM TRANSISTORS BASED ELECTROCHEMICAL REDUCED GRAPHENE OXIDE.

The tip-induced reduction of GO was used to successfully bridge prepatterned fig. top- (fig.3.10 c,d) or bottom-(fig. 3.10 a,b) contact electrode pairs. Current images of a source-drain electrode pair (left and right side) bridged by an electrically conducting tip-reduced GO region. As expected the currents were not registered over the electrodes in bottom configuration because the Au was covered by a film of unreduced GO unlike of top contact configuration.

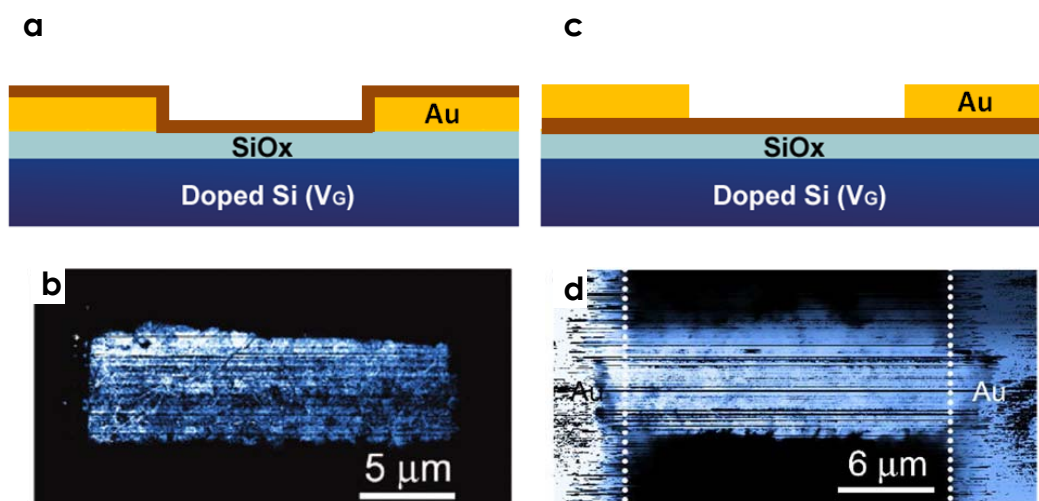


Figure 3.10 Thin-film transistors based on tip-reduced GO. a,c) Schematic representation of the devices top or bottom contact before the reduction b,d) current image of a source-drain electrode pair after tip-reduction graphene oxide.

Figure 3.10 a,b, show a bottom-gate bottom-contact RGO transistor with channel width of 6 μm was defined with the AFM tip and then characterized by C-AFM, which revealed an estimated sheet resistance of 1.6 $\text{M}\Omega/\text{square}$.

Transistor measurements on several GO and tip-reduced GO devices in a nitrogen environment showed a significant current increase, approaching a factor of 10^8 , obtained by means of tip reduction (Figure 3.11a). The transport can be consistently considered ambipolar, as previously observed for reduced GO,¹⁴ a hole

mobility of $0.3 \text{ cm}^2 \text{ V}^{-1} \text{ s}^{-1}$ and an electron mobility of up to $0.1 \text{ cm}^2 \text{ V}^{-1} \text{ s}^{-1}$ were determined. These values are comparable to the ones measured by Chhowalla and co-workers,¹⁴ who found p- and n-type mobilities of 1 and $0.2 \text{ cm}^2 \text{ V}^{-1} \text{ s}^{-1}$, respectively, providing further evidence that the performance of the micropatterned AFM-tip-reduced GO is similar to that of GO reduced by combined hydrazine and thermal treatments.

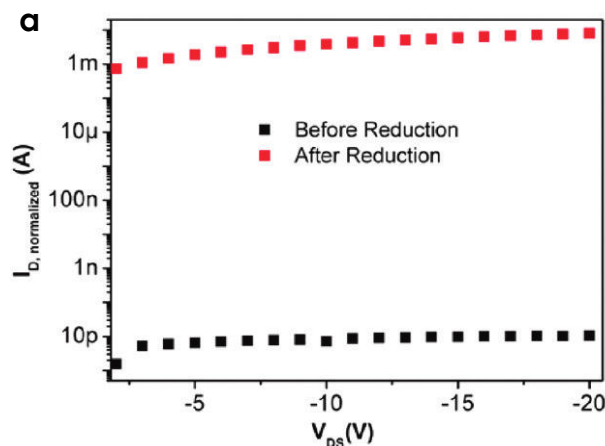


Figure 3.11 Drain current (I_D) normalized to the effective channel width vs drain-source voltage (V_{DS}) measured on graphite oxide films before (black) and after (red) tip reduction.

We demonstrate that the voltage-induced reduction of GO under ambient conditions is not restricted to the C-AFM configuration. We show that the electrochemical conversion of GO under ambient conditions is broadly applicable and can be achieved by applying a voltage across nano- and micro-electrode pairs in close proximity on a surface.

A topographic AFM image of the system is shown in figure 3.12a. C-AFM current mapping (figure 3.12b) provided further confirmation that the GO was rendered electrically conductive. The GO over the gold electrodes remains insulating, with only some nanoscopic pinholes in the film passing current. However, between the electrodes, the film is highly conducting.

These measurements demonstrate a simple approach to for tuning the conductivity of graphene between electrodes. The voltage-induced reduction process works under ambient conditions and does not require specialized equipment, making it attractive for the large-scale, low-cost processing of graphene for electronics.

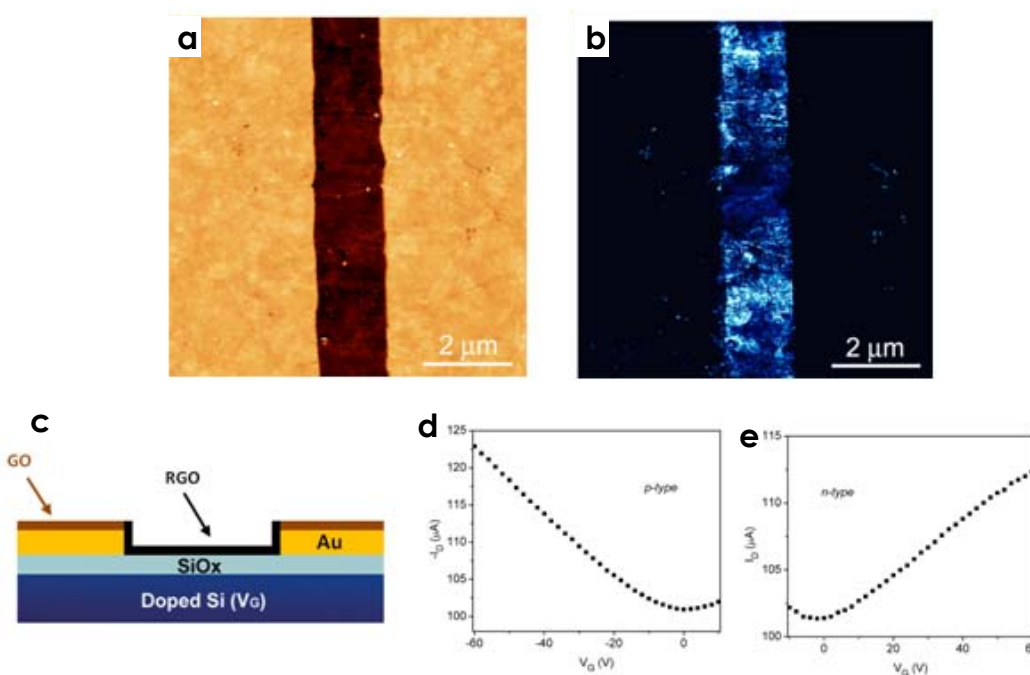


Figure 3.12 a) AFM image and corresponding b) current image of voltage-reduced GO in an FET channel c) schematic representation of device. Transfer curves measured on voltage-reduced GO transistors, in the d) p-type ($V_{SD} = -2$ V) e) n-type ($V_{SD} = +2$ V), transport regimes. Channel length = 1.6 μm.

This kind of approach is interesting for sensing because the active area is only the material between the electrodes so we have less noise for the signal and less problem of current leakage to the gate.

The work present here led to the realization of the articles:

“Local Current Mapping and Patterning of Reduced Graphene Oxide” Jeffrey M. Mativetsky, Emanuele Treossi, Emanuele Orgiu, Manuela Melucci, Giulio Paolo Veronese, Paolo Samori and Vincenzo Palermo *Journal of the American Chemical Society* 132, 14130, 2010; and

“Graphene transistors via in-situ voltage-induced reduction of graphene-oxide under ambient conditions” Jeffrey M. Mativetsky, Andrea Liscio, Emanuele Treossi, Emanuele Orgiu, Alberto Zanelli, Paolo Samori, Vincenzo Palermo *Journal of the American Chemical Society* 133, 14320, 2011.

3.4 BIBLIOGRAPHY

1. Thin-film particles of graphite oxide 1: High-yield synthesis and flexibility of the particles; M. Hirata, T. Gotou, S. Horiuchi, M. Fujiwara, M. Ohba, *Carbon* 2004, 42, 2929.
2. Evolution of Electrical, Chemical, and Structural Properties of Transparent and Conducting Chemically Derived Graphene Thin Films; C. Mattevi, G. Eda, S. Agnoli, S. Miller, K. A. Mkhoyan, O. Celik, D. Mastrogiovanni, G. Granozzi, E. Garfunkel, M. Chhowalla *Advanced Materials* 2009 19, 2577.
3. Determination of the Local Chemical Structure of Graphene Oxide and Reduced Graphene Oxide; K. Erickson, R. Erni, Z. Lee, N. Alem, W. Gannett, A. Zett *Advanced Materials* 2010, 22, 4467.
4. Graphene as Transparent Electrode Material for Organic Electronics; S.P. Pang, Y. Hernandez, X. L. Feng, K. Müllen, *Advanced Materials* 2011, 23, 2779.
5. Gate Voltage Dependent Resistance of a Single Organic Semiconductor Grain Boundary; T.W. Kelley, and C. D. Frisbie, *Journal of Physical Chemistry B* 2001, 105, 4538.
6. Electronic Transport Properties of Individual Chemically Reduced Graphene Oxide Sheets; C. Gomez-Navarro, R. T. Weitz, A. M. Bittner, M. Scolari, A. Mews, M. Burghard, K. Kern, *Nano Letter* 2007, 7, 3499.
7. Evaluation of Solution-Processed Reduced Graphene Oxide Films as Transparent Conductors; H. A. Becerril, J. Mao, Z. Liu, R. M. Stoltenberg, Z. Bao, Y. Chen *ACS Nano* 2008, 2, 463.
8. Electronic Confinement and Coherence in Patterned Epitaxial Graphene; C. Berger, Z. M. Song, X. B. Li, X. S. Wu, N. Brown, C. Naud, D. Mayou, T. B. Li, J. Hass, A. N. Marchenkov, E. H. Conrad, First P. N., W. A. de Heer, *Science* 2006, 312, 1191.
9. Atomic force microscope tip-induced local oxidation of silicon: kinetics, mechanism, and nanofabrication; P. Avouris, T. Hertel, R. Martel *Applied Physics Letters* 1997, 71, 285.

10. Atomic force microscope local oxidation nanolithography of graphene L. S. Weng, L. Y. Zhang, Y. P. Chen, , L. P. Rokhinson Applied Physics Letters 2008, 93 093107.
11. A Chemical Route to Graphene for Device Applications; S. Gilje, S. Han, M. Wang, K. L. Wang, R. B. Kaner Nano Letter 2007, 7, 3394.
12. Synthesis of graphene-based nanosheets via chemical reduction of exfoliated graphite oxide; S. Stankovich, D. A. Dikin, R. D. Piner, K. A. Kohlhaas, A. Kleinhammes, Y. Jia, Y. Wu, S. T. Nguyen, R. S. Ruoff, Carbon 2007, 45, 1558.
13. High-throughput solution processing of large-scale graphene; V. C. Tung, M. J. Allen, Y. Yang, R. B. Kaner, Nature Nanotechnology 2009, 4, 25.
14. Large-area ultrathin films of reduced graphene oxide as a transparent and flexible electronic material G. Eda, G. Fanchini, M. Chhowalla, Nature Nanotechnology 2008, 3, 270.

CHAPTER 4

TUNING THE TRANSPORT PROPERTIES OF GRAPHENE BY NONCOVALENT FUNCTIONALIZATION

In chapter three we have seen how is possible partially restore the sp² carbon network in graphene oxide by thermal annealing, in this chapter we show the electronic behavior of this material when it is combine with organic semiconductors i.e. P3ht or Nanographene derivatives.

4.1 TAKING THE BEST OF TWO MATERIALS

Graphene has high conductivity and exhibiting large ambipolar electric field-effect, enabling both electrons or holes doping via electrostatic gating. Single graphene sheets, usually obtained by the “scotch tape” technique, were successfully used to realize high performance transistors and sensors. Graphene can also confer outstanding properties to various material types: when it was incorporated into polymeric or ceramic matrices, a remarkable improvement of the properties of the host materials was found.

Given such an interest in using graphene for the fabrication of functional hybrid architectures, the development of new processing methods, potentially up-scalable, represents a challenging goal as they can pave the way towards large-scale applications of graphene-based composite in electronics.

Organic semiconductors (OSs) are a wide class of small molecules and polymers used as active components for fabrication of (opto)electronic devices such as LEDs, solar cells and field-effect transistors. OSs can be processed from solution at low cost and on different substrates, making it possible to produce light-weight, low-cost, large-area flexible electronic devices.¹ A major limitation of OSs is their poor charge mobility compared to silicon, thereby lowering the performance of OS based electronic devices.

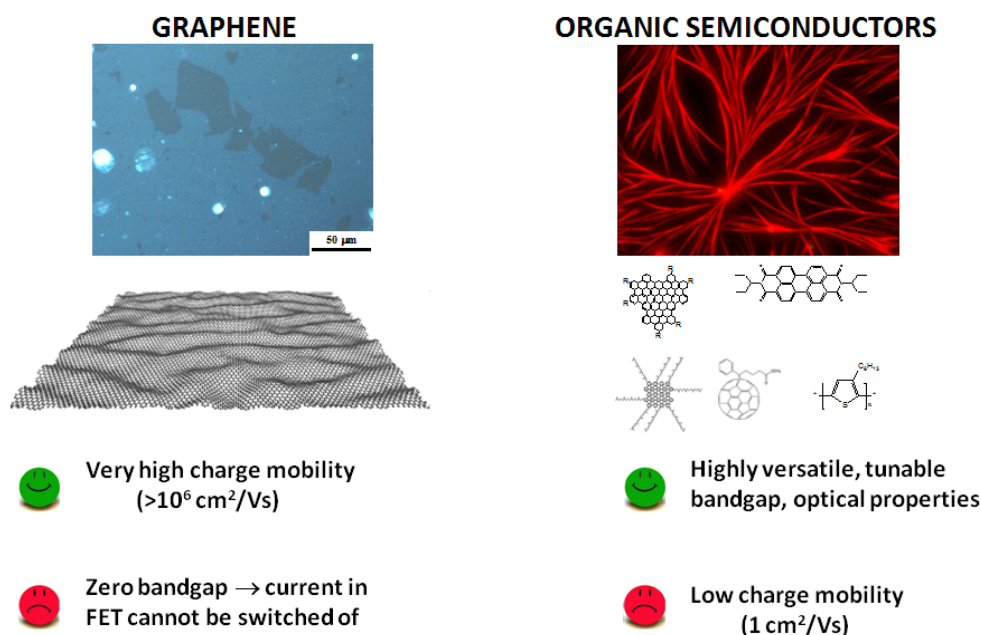


Figure 4.1 Schematic representation of some vantages and limits of graphene and semiconductors for organic electronic.

In order to exploit simultaneously the excellent electronic properties of graphene and the good processability as well as modulable optoelectronic characteristics of organic semiconductors, effort has been recently addressed to the use of blends of soluble graphene with OS in FETs and solar cells, similarly to what has been already reported for carbon nanotubes–OS blends. It is expected that the electrical properties of these blends, and in particular their charge transport characteristics, depend significantly on the graphene/OS ratio used, and on the relative arrangement of the graphene sheets into the OS matrix. Due to the co-deposition process, the blends can have a complex 3D structure. Graphene sheets can be well-dispersed to create percolation pathways for the transport of charges through the less conductive OS matrix. Conversely, in the case of poor solubility and modest affinity with the OS, graphene sheets can stack and phase-segregate during deposition, forming aggregates.

4.2 INTERACTION BETWEEN GORED AND P3HT

To gain a better understanding on the charge transport in graphene–OS blends, we have studied the electrical and morphological properties of a structurally well-defined bicomponent system obtained by physisorption of a p-type organic semiconductor (poly(3-hexylthiophene), P3HT) over a discontinuous layer of atomically thin graphene sheets previously deposited on the electrically insulating silicon oxide substrate.

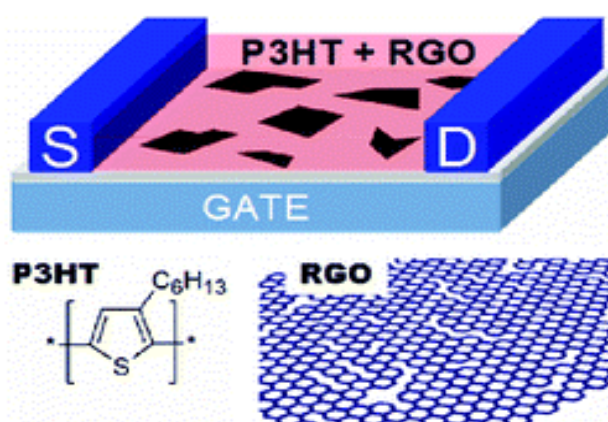


Figure 4.2 Schematic representation of the RGO–P3HT based device

We demonstrate that by changing the density of the sheets it is possible to tune the charge transport from a regime featuring charges that are transported principally through the P3HT layer, having only a few graphene sheets acting as preferential paths for the charge transport, to another in which continuous percolation paths exist through the graphene layer, and P3HT influences only in an indirect way the current passing along the graphene sheets. In both cases, charge transport in the blend results improved with respect to what was observed in either graphene or P3HT alone.

We chose to use reduced graphene oxide (RGO) since it combines good material properties and excellent processability. RGO is obtained from the reduction of chemically exfoliated graphene oxide (GO), which can be produced with high purity and in large quantities and, being water soluble, is well suited for industrial,

large scale applications. Despite the electrical performance of RGO cannot be compared to that of pristine graphene, RGO can be obtained in continuous layers on large areas by thermal and/or chemical reduction of GO. Continuous layers formed by microscopic RGO sheets showed room temperature mobilities amounting between 2 and 200 cm^2/Vs for holes and 0.5 and 30 cm^2/Vs for electrons (i.e. approximately 2 orders of magnitude lower than those observed in mechanically exfoliated graphene single sheets, but much higher than the ones of state-of-the-art organic semiconductors).

The electrical macroscopic properties of the composite material and its potential utility for organic electronics have been studied by fabricating and testing FETs based on different ratios of P3HT and RGO. On microscopic scale, a thorough characterization of both RGO sheets and RGO–P3HT blends has been obtained by Atomic Force Microscopy (AFM), Scanning Electron Microscopy (SEM), optical reflection and fluorescence microscopy, and Kelvin Probe Force Microscopy (KPFM).

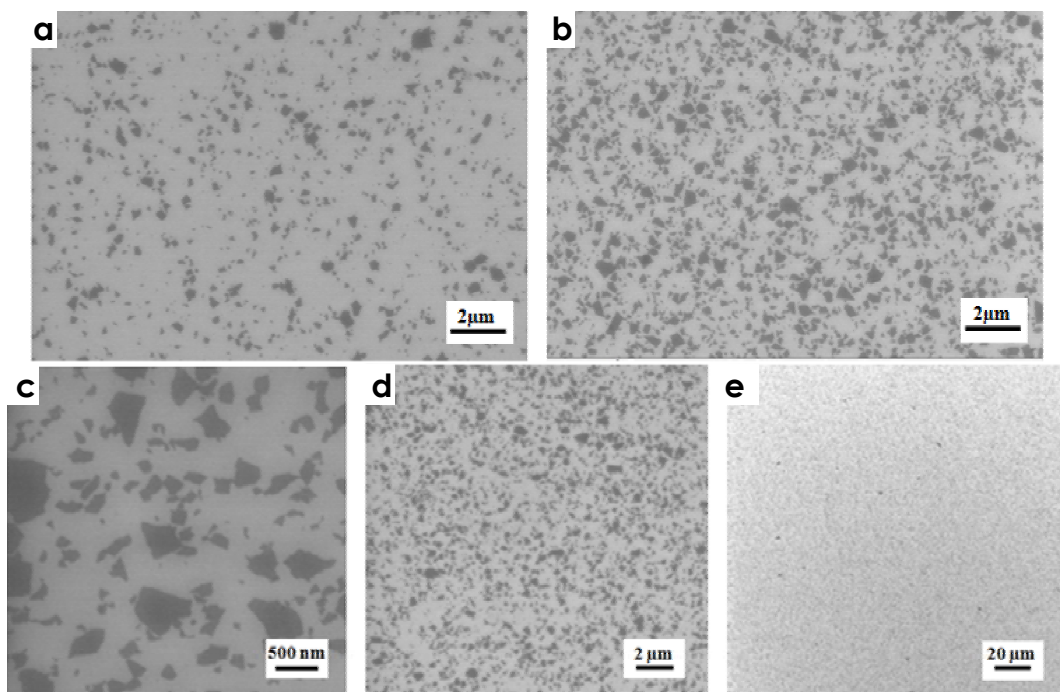


Figure 4.3 a,b) SEM images of GO sheets obtained by spincoating of solutions at two different concentrations, c,d,e) SEM images of GO sheets obtained at different magnifications.

In OFET is very important to have a good control of interface between dielectric and active layer so the uniformity and coverage of RGO sheets on surface is a very important aspect.

Thanks to the high processability of the GO, not only the average sheet size could be controlled using different sonication times fig. 2.2; but changing the concentrations of graphene oxide solutions it is possible by spincoating to tune the density of flakes on substrate (fig. 4.3a and 4.3b) and it is also possible to yield uniform deposition on large areas, ad example in fig. 4.3c-4.3d-4.3e we can see some images of graphene sheets obtained at different magnifications in the same sample.

Figure 4.4 shows AFM and KPFM images of single sheets of GO before (a and b) and after (c and d) thermal reduction at 700 °C.

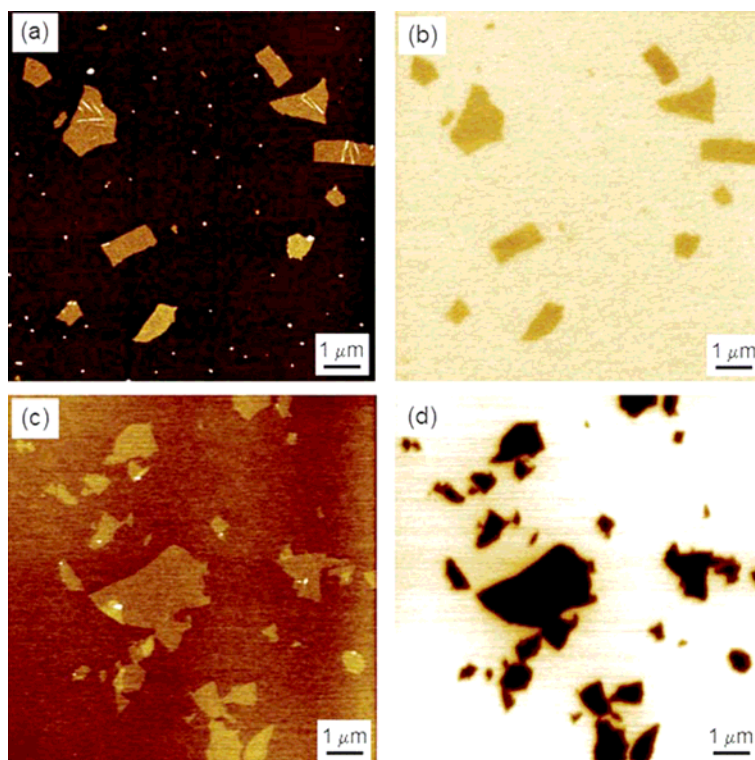


Figure 4.4 a, b) AFM and corresponding KPFM images of GO sheets deposited on SiO_x substrate. c,d) AFM and corresponding KPFM images of the RGO sheets.

The sheet thickness was estimated by AFM before and after the reduction. Fig. 4.5 shows the evolution of the thickness measured by AFM on GO and RGO samples with increasing number of layers.

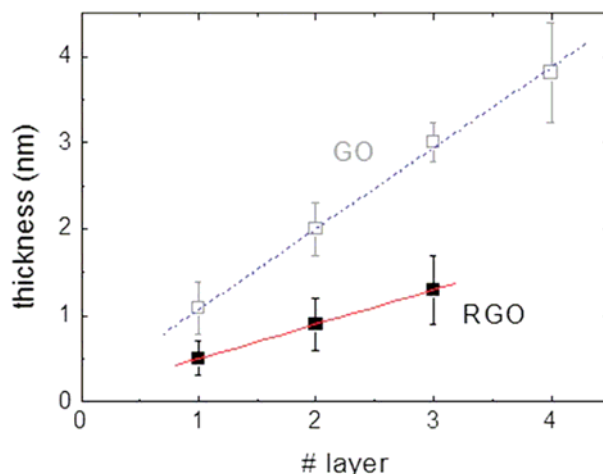


Figure 4.5 Thickness of the GO (□) and RGO (■) sheets of mono- and multi-layers measured by AFM.

The GO monolayers show a thickness of 1.0 ± 0.1 nm, in good agreement with previous results (see fig.2.3). The thickness of RGO monolayer amounted to 0.5 ± 0.2 nm, in line with the expected theoretical value (0.35 nm).²

Electrical characterization of GO and RGO single sheets was also performed with KPFM, a technique which allows to “map” electric potential of nanometric structures with a lateral resolution of few nm, and a potential resolution of few mV. KPFM can be used routinely to measure the work function (WF) of bulk materials, and to characterize working devices such as FETs, light-emitting transistors and solar cells.³⁻⁵ While, when measuring bulk materials and macroscopic objects, the surface potential (SP) measured by KPFM corresponds to the WF of the material, care should be taken when interpreting the potential of nano-sized objects,⁶ especially for very thin layers like graphene, where influence of the underlying substrate is significant. In this case, the measured SP is not simply the WF of the monoatomic layer (in a freestanding graphene layer the Fermi energy coincides with the conical points), since the contact with metallic (or insulating) substrates can alter its electronic properties (i.e. the measured WF) significantly.⁷ Hence, the

measured value should be considered as the result of a complex interplay between the electrical properties of graphene and of the underlying substrate, in addition to a variety of interfacial properties that can arise due to interface dipoles, band-bending effects, etc.

For this reason, the measured WF of graphene sheets mentioned in the following text should be considered as the work function of the sheet–substrate system, i.e. the difference between the potential measured for a sheet deposited on the substrate and the one of bulk graphite.

Figure 4.6 compares the trends observed in the effective WF for different layer thicknesses of GO and RGO deposited on SiO_x. The SP of GO mono- and bi-layers has been measured on a batch of 4 different samples, and shows a large variation of the measured values (blue bars in fig. 4.6) in the range between -50 and 80 meV, with respect to the reference value (i.e. the WF of a bulk substrate of highly oriented pyrolytic graphite). These large variations can be ascribed to (i) the electronic properties of GO which, being an insulator, does not possess a well-defined work function; (ii) the varying percentage of oxygen present in GO influencing its electronic properties; and (iii) the high hydrophilic nature of GO promoting relevant adsorption of water on its surface.

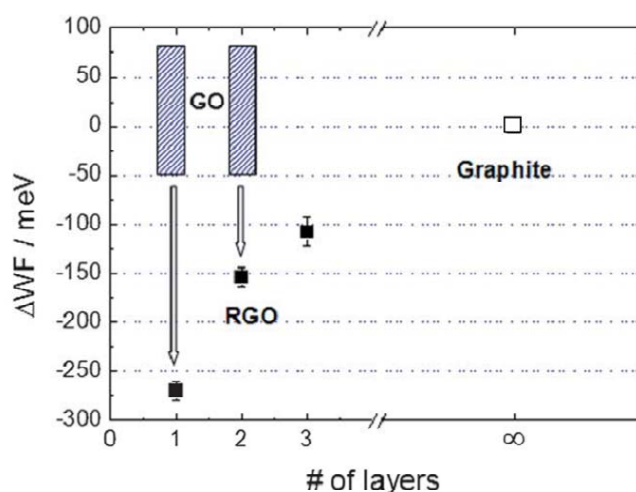


Figure 4.6 WF of RGO mono- and multi-layers as measured by KPFM (■) and the reference value measured on bulk, highly oriented pyrolytic graphite (□). The range of values obtained for mono- and bi-layers of GO before reduction are also shown in shaded blue.

Conversely, the SP of RGO has been estimated with a high degree of precision, i.e. it does not exhibit a big discrepancy on different samples, and it features a distinct increase with the number of layers converging to the graphite value. The measured WF of RGO averaged out on 4 batches scatters within the range of 10 meV, a spread which is much smaller than the one observed for GO.

By using relatively high concentrations of GO solutions, it was possible to obtain and characterize mono-, bi- and tri-layers. In particular the measured WF difference between the bi- and the mono-layers of RGO amounts to 120 ± 10 meV. This value is in good agreement with the WFs reported for epitaxial graphene sheets.⁸ Unfortunately, it was not possible to follow the evolution of WF for a higher numbers of layers because of the difficulty in quantifying the number of layers present in a certain area when the substrate is completely coated, and thus not visible. Overall, the measured WF of graphene can vary up to 250 meV going from one to infinite layers (bulk graphite).

Raman spectroscopy of the GO and RGO has been also performed, and the results have been compared with the spectrum of conventional, “scotch tape” graphene.

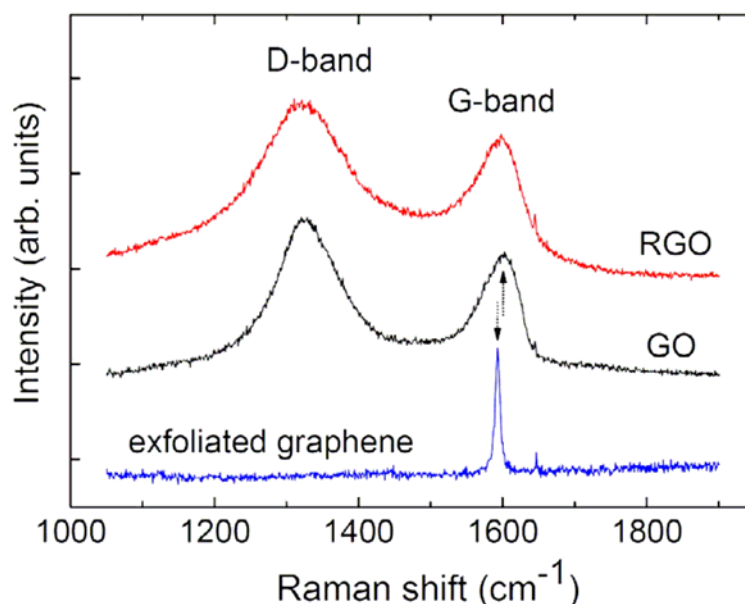


Figure. 4.7. The Raman spectra of GO, RGO and exfoliated graphene in the region of D- and G-band. The spectra were normalized to the G-band intensity.

To better understand the fine structure of the graphene layer, we performed Raman spectra of the GO and RGO, together with the spectrum of “conventional” exfoliated graphene (fig. 4.7). The latter exhibits a sharp G-peak, while GO and RGO show wide D- and G-bands. We find that the Gband of both GO and RGO is shifted to higher frequencies with respect to the G-peak of exfoliated graphene, and this G-peak shift is usually related to doping by chemisorption or physisorption of molecules, ions, functional groups or metal particles, that can take place in the fabrication process of the GO.

Moreover, we find that the overall Raman peak intensities are decreased after the thermal treatment, suggesting a partial loss of carbon during reduction (in fig. 4.7 the spectrum of RGO has been multiplied by a factor ~ 2 in order to equal the G-peak intensity of the spectrum of GO). After reduction we observe a small increase of the intensity ratio $I(D)/I(G)$ (from 1.30 to 1.35), finding a similar trend the area ratio $A(D)/A(G)$. In fact during reduction GO undergoes structural changes due to the loss and rearrangement of oxygen and carbon atoms, which affect the Raman response. Given that the reported measurements were performed on large sheets of GO and RGO, with lateral dimensions larger than the laser spot.

As expected, the GO presents wide D- and G-bands, indicative of large disorder. The same features are observed in RGO indicating that the reduction process creates a material truly different from both graphene and GO. This RGO material has the same irregular structure of GO, as indicated by Raman; though, differently from GO, it features a large number of highly conjugated, conductive paths, as confirmed by charge transport measurements.

The RGO can act as a fluorescence quencher for organic materials,⁹ and this effect has been recently exploited, by us and other groups, to enhance the visualization of graphene sheets using thin layers, even monolayers, of organic molecules interacting with single or multiple graphene or graphene oxide sheets.⁹ fig. 4.7 show the fluorescence images of a RGO–P3HT sample prepared using very large sheets on 300 nm thick SiO₂ to allow direct optical visualization.

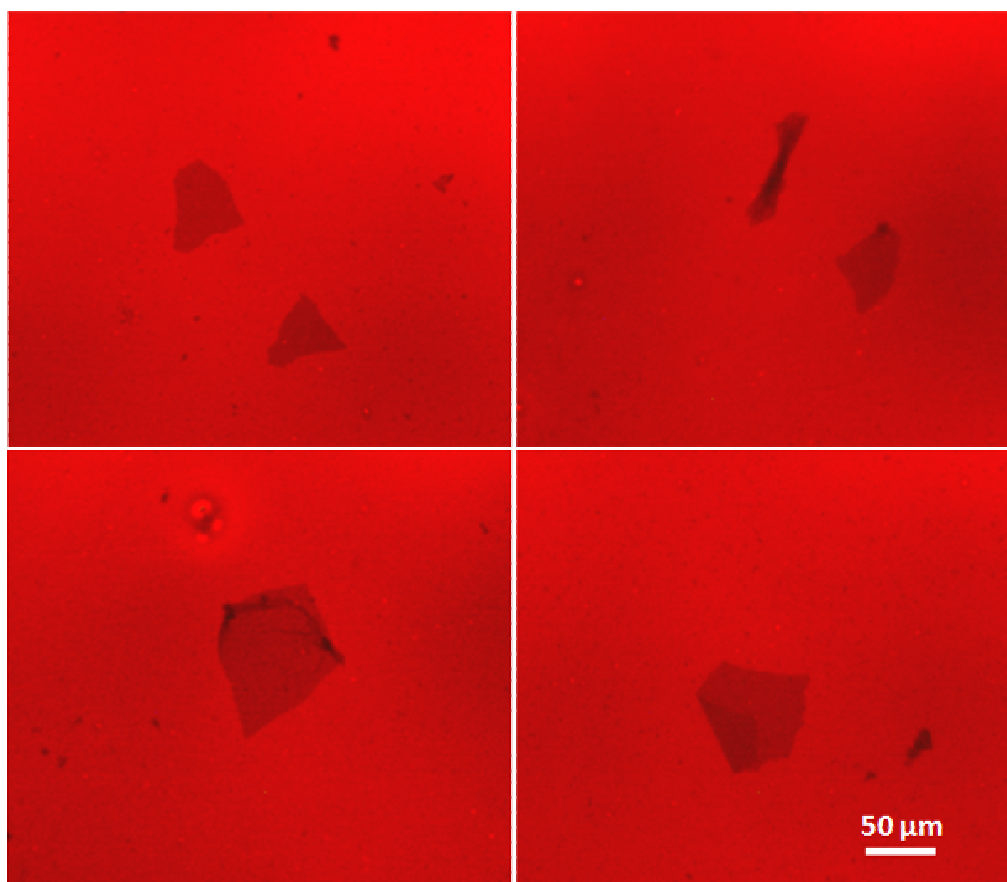


Figure. 4.8. Fluorescence images showing a RGO sheet on 300 nm thick SiO₂, covered by a layer of P3HT.

The fluorescence quenching of graphene and graphene oxide with conjugated polymers (included P3HT) is a well known process which has been studied in different works.^{10,11} The fluorescence quenching confirms visually the good interaction between the two materials. Please note that large, mesoscopic sheets are shown in fig. 4.8 only to give a visual evidence of RGO– P3HT interaction. Instead, much smaller RGO sheets, having a typical size of few hundreds of nm, have been used in the samples for both FET and KPFM measurements, in order to have a very uniform coverage with respect to the adopted FET channel lengths of 10 and 60 nm.

RGO–P3HT blends with different RGO sheet densities have been prepared by (i) spin-coating GO solutions having 4 different concentrations (0.25, 0.5, 1 and 2 g/L) on the SiO₂ surfaces, (ii) reducing the GO to RGO, and (iii) coating with P3HT

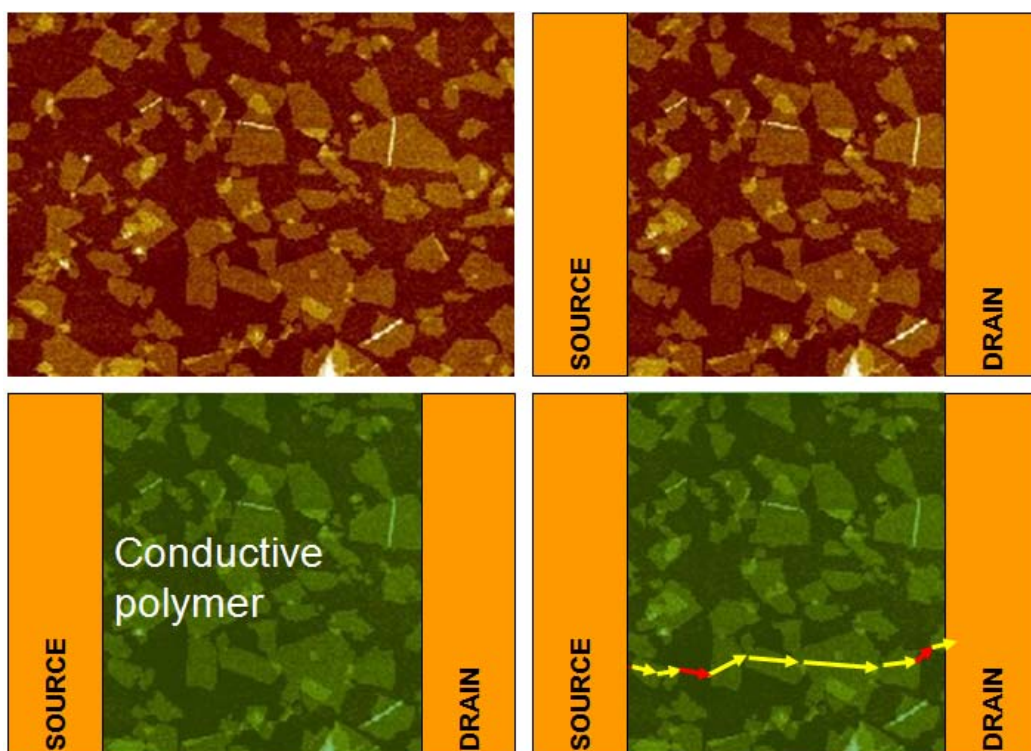


Figure. 4.9. Schematic representation of the various phases present in a realization of RGO-P3HT based device.

After coating, the RGO sheets could still be identified through the P3HT layer by both AFM and KPFM (fig. 4.10a and 4.10b), although with a lower resolution with respect to the bare RGO.

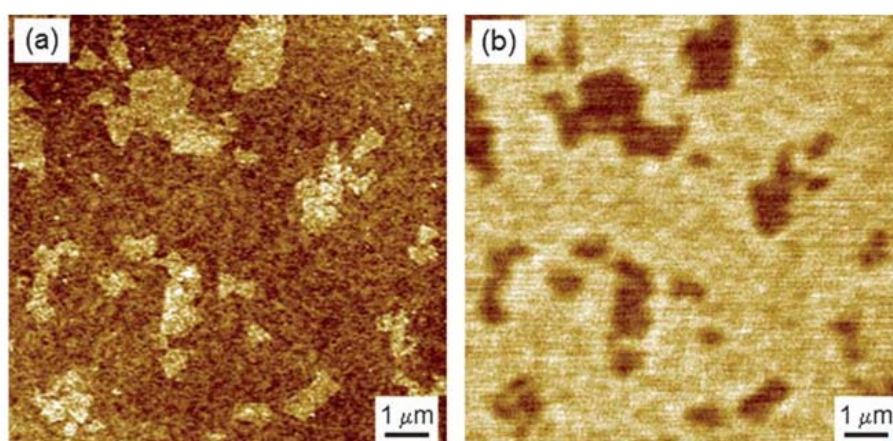


Figure. 4.10 a) AFM and corresponding b) potential images of RGO sheets deposited on native SiO_x substrate, and covered by a thin film of P3HT.

Figure 4.11 shows the statistical trend of the evolution of GO surface coverage as a function of the concentration of GO in solution, as measured by SEM and AFM, only the latter being able to detect the presence of single and multi-layers. In all the topographic images, bare substrate and GO sheets have been unambiguously distinguished using image processing, by applying a threshold filter to the data recorded on AFM and SEM images. This analysis revealed that, due to the high affinity of GO for the substrate, the area coverage increases linearly with GO concentration, allowing a good control of the RGO surface density. At concentrations up to 0.5 g/L, almost all the sheets result to be monolayer thick, with basically no presence of double layers. This is due to the chemical nature of GO sheets, which in solution do not interact significantly with each other, but interact easily both with water molecules and the highly hydrophilic silicon oxide substrate.

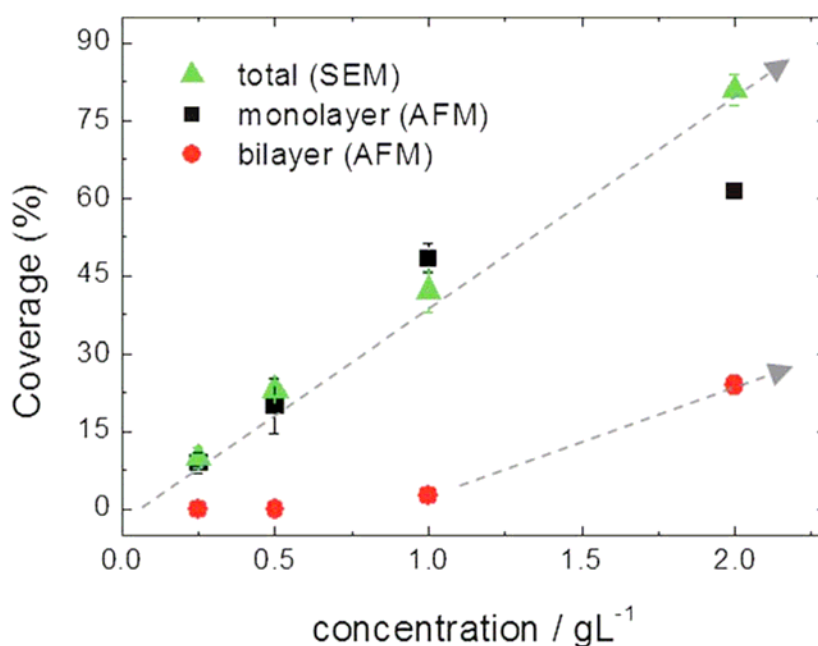


Figure 4.11. Area coverage vs. solution concentration, as measured by SEM (total coverage, ▲) and AFM (mono-■ and bi-layers ●).

Even at the highest concentrations tested (2 g/L), only a 20% of surface is covered by bilayers, and basically no tri- or multi-layers are observed.

The charge transport of the RGO–P3HT having different RGO contents has been tested in FET architectures with 225 nm SiO₂ gate oxide, patterned with source–drain Ni electrodes.

Transistor Architectures:

Silicon substrates (n-type, resistivity 0.01–0.02 Ohm·cm) have been used for the fabrication of the transistors. A 225 nm thick silicon dioxide (SiO₂) has been thermally grown after standard RCA cleaning processes of the native wafers. Interdigitated transistor devices have been fabricated defining source–drain electrodes by means of standard lift-off processes. Channel lengths of 10 and 60 μm have been used, with a constant width-to-length ratio (W/L) of 200.

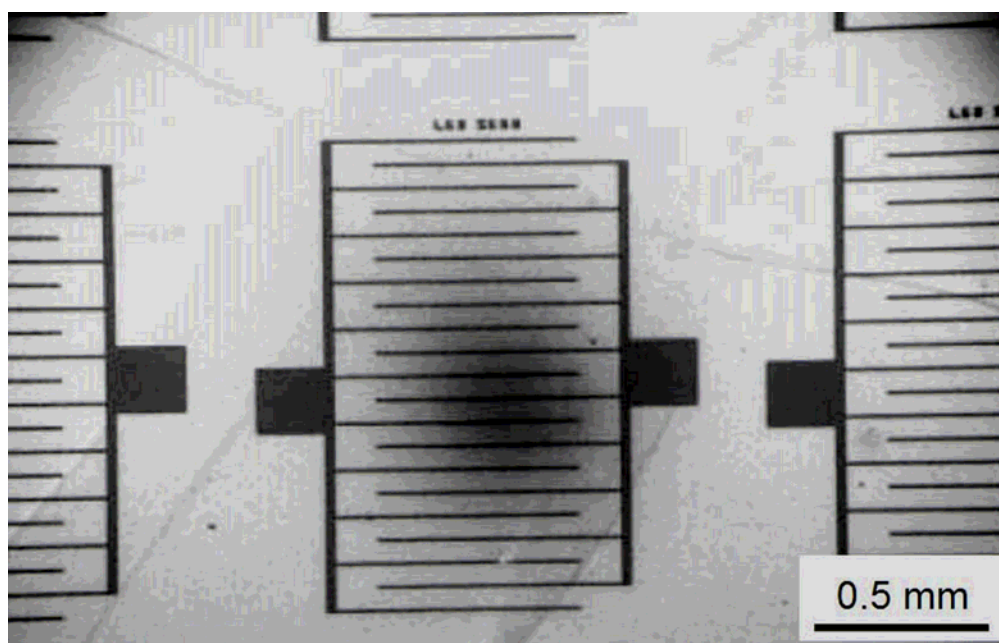


Figure 4.12. SEM image of the transistor architecture used for FET measurements (W/L = 200, channel length of 60 μm)

Both bare silicon oxide substrates and RGO sheets covered substrate have been utilized for the FETs fabrication. Electrodes have been realized by e-beam evaporation of 25 nm thick Ni layer. Silicon substrates have been used as bottom gate electrode. The P3HT thin film, ~30 nm thick, has been then spin coated on the substrates.

The FET performance has then been compared with the one of devices incorporating only pure P3HT.

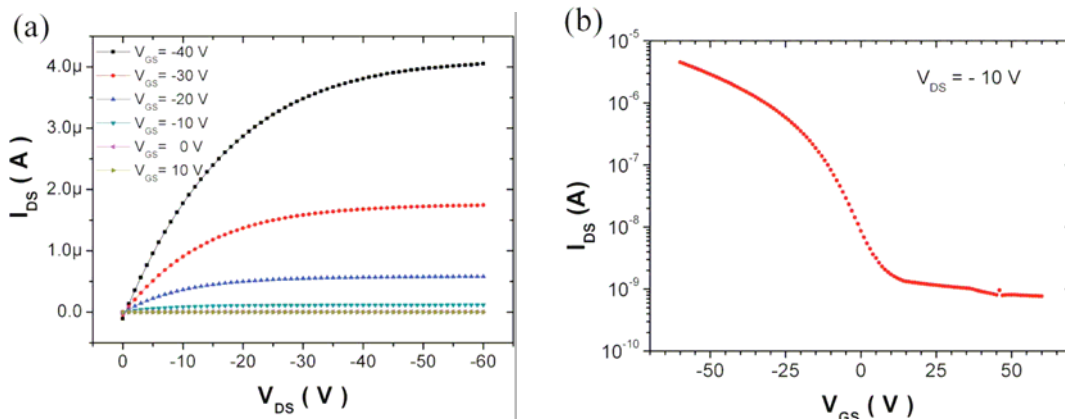


Figure 4.13. Typical (a) output and (b) transfer characteristics for a RGO + P3HT FET device with a 23% coverage area. All measurements have been performed in vacuum.

As a reference, in Fig. 4.13 a and b the output and transfer characteristics for a RGO–P3HT FET with an area coverage $A = 23\%$ are reported.

Fig. 7 shows the change in mobility observed by increasing the RGO content. For an area coverage $A = 10\%$, the presence of sparse, isolated RGO sheets yields only a slight increase in mobility (as compared to pure P3HT FETs), but there is an improvement of ION/IOFF ratio from $3 \cdot 10^3$ to $\approx 1 \cdot 10^5$ due to the improvement of ION current (not shown). For $A = 23\%$, the improvement in hole mobility is larger, and the sheets are still spaced apart, with no percolation. Noticeably, in this case the ION/IOFF ratio is slightly better than the one of pure P3HT.

The most relevant changes take place at $A = 42\%$, where the RGO network is close to its percolation limit. For this coverage, some of the devices show relevant charge transport even before P3HT deposition (red circles in fig. 4.14). By approximating the RGO sheets as randomly deposited disks, theory predicts the onset of percolation for a coverage $A \approx 67\%$.¹² The presence of percolation at $A = 42\%$ can be ascribed to (i) the above mentioned tendency of sheets to avoid overlapping and bilayer formation, while the theoretical model used is based on a completely

random deposition of the disks, and (ii) the irregular shape of the graphene sheets, whose form is usually more similar to a polygon than to a disk.

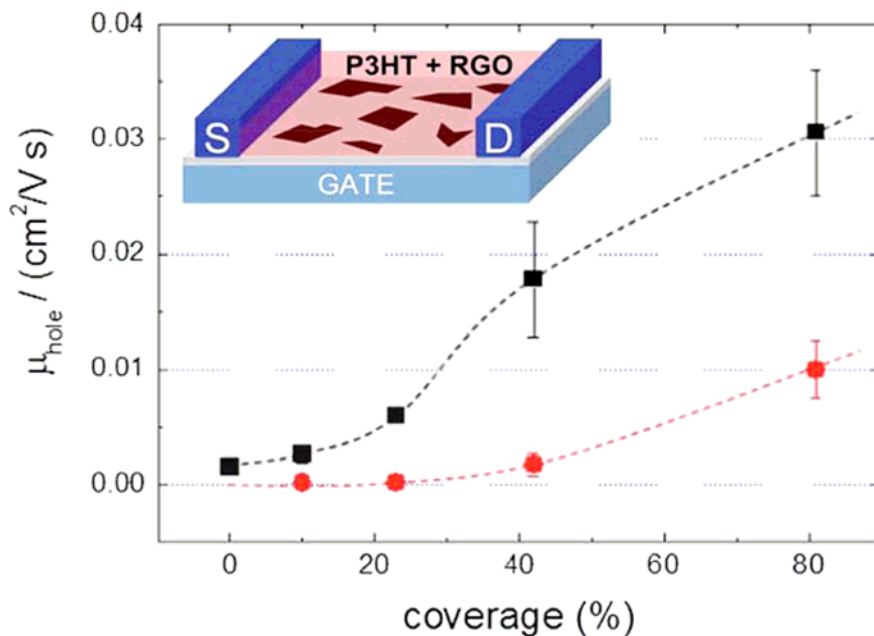


Figure 4.14. Hole mobility vs. area coverage for RGO (●) and RGO + P3HT FETs (■). Continuous lines are shown as a visual guide.

Even without including in the statistics the directly percolated RGO samples, the hole mobility of RGO–P3HT blends at $A = 42\%$ is anyhow significantly higher compared to the pure P3HT ($A = 0\%$), while the I_{ON}/I_{OFF} ratio ($\approx 2 \cdot 10^3$) is comparable to the one of pure P3HT.

For $A = 81\%$, the RGO layer is completely percolated, and all devices show the charge transport even without P3HT. Nonetheless, the addition of P3HT improves greatly the charge transport, although the I_{ON}/I_{OFF} ratio is very low (≈ 2 , i.e. the transistor is always on).

Overall, the addition of RGO layers to P3HT based FETs allows to tune the charge transport by increasing the “effective” mobility of the active layer; however, over a certain threshold, the conduction through the RGO is predominant, and the current cannot be significantly modulated by the gate, in line with previous observations in carbon nanotube–P3HT based FETs.¹³

Interestingly, at intermediate coverage of RGO it is possible to improve mobility without diminishing the ION/IOFF, thus making it possible to have a composite material performing better than the pure P3HT. In these cases, RGO sheets act as preferential paths through which charges can travel much better than in pure P3HT, reducing the effective channel length L of the transistor.

The absence of continuous percolation paths connecting RGO sheets is essential in order to have charges passing through pure P3HT domains, thus maintaining a gate effect to the current through the junction.

The cost of this reduction of effective channel length is that, in a bi-component system, charges will have to face several injection barriers, hopping continuously from P3HT to RGO and vice versa. Though, the WF values measured by KPFM on Ni source–drain electrodes, RGO monolayers on SiO₂ and P3HT resulted to be 5.07, 4.75 and 4.80 eV respectively. These values are measured on both grounded electrodes or by applying 2 V of potential difference between drain and source electrodes. These electrical polarization values are low enough to neglect the WF tuning of RGO due to the electric field-effect.

It should be noted that the WF of organic semiconductors like P3HT depends significantly on molecular packing, which in turn depends on other parameters such as deposition conditions and molecular weight. The value obtained by KPFM measurements for the P3HT is in fair agreement with the HOMO of P3HT estimated by cyclic voltammetry measurements, i.e. 4.9 eV.

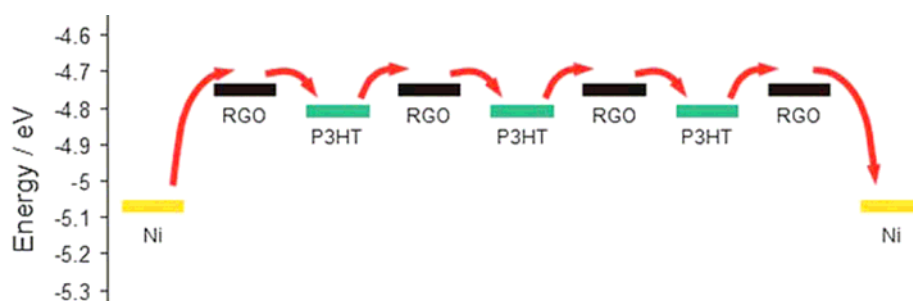


Figure 4.15. Schematic representation of the energy diagram and charge transport in the device.

The WF of P3HT is close to the RGO value allowing us to neglect the contact resistance at their interface, strongly suggesting that the charge injection barrier at the RGO–P3HT interface is much smaller than the one present at the source–drain contacts, as shown in fig. 4.15, which is a schematic representation of the charge transport across the RGO–P3HT blend reporting the experimental WF values as measured by KPFM. The presence of possible charge injection barriers or resistance series has been tested by performing KPFM measurements along the channel of working FETs.

Figure 4.16 shows the potential profiles recorded by KPFM along the channel of working FETs ($V_D = 2$ V, $V_G = 0$ V) based on RGO–P3HT, with increasing coverage of RGO. FETs having a channel length of only $10\ \mu\text{m}$ have been tested to allow simultaneous measurements of the potential on the active layer and on source–drain electrodes with a single scan.

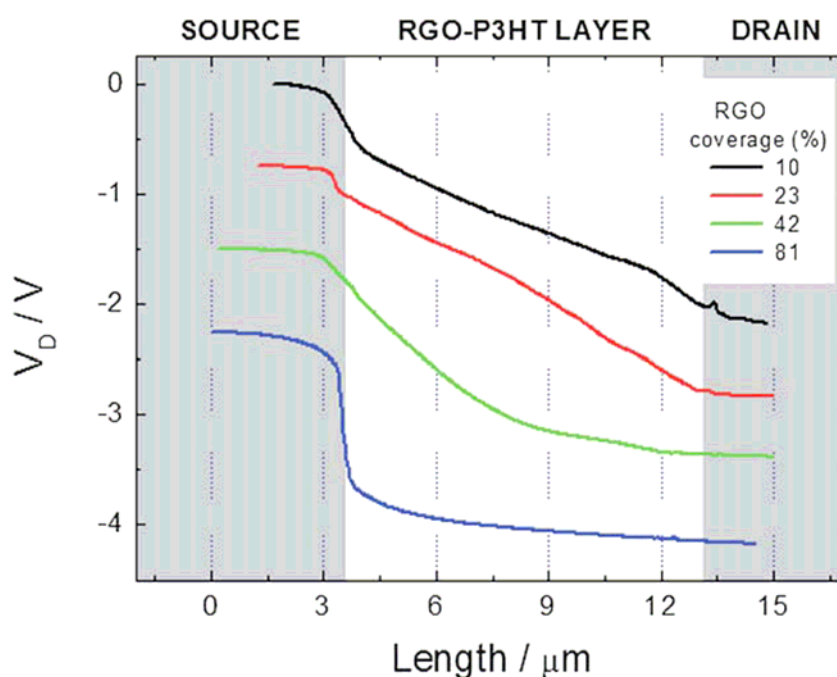


Figure 4.16 Averaged KPFM profiles taken along the channel of FETs based on RGO–P3HT, obtained by GO solutions of increasing concentration. The curves have been shifted for clarity.

For $A = 10\%$, the voltage decays faster at the source–drain interfaces, indicating a relevant contact resistance between Ni and the blend. It is possible to observe that with the increasing content of RGO the active blend material becomes more and more conductive, and the voltage drop becomes more localized at the source interface, with lack of significant voltage drops within the active layer.¹⁴

Thus far we have focused our attention on the effect of discontinuous RGO layers on the charge transport in P3HT.

We can also compare the effect of P3HT on highly interconnected RGO layers, where percolation paths already exist, and thus the current passing through the organic semiconductor layer will be minimal with respect to the one transported through the RGO layer. Figure 4.14 provides evidence that even for RGO coverage as high as 82%, the effect of a P3HT is beneficial, improving the hole charge mobility by a factor of 3. The obtained mobility is much higher than the value obtained by the percolation theory calculated as the harmonic average of the mobilities of pure P3HT and RGO weighted by the coverage,¹⁵ indicating a synergic effect of the two layers which favours the hole transport.

Such an evidence is shown in the transfer curves graphed in fig. 4.17, measured for a continuous RGO layer ($A = 82\%$) with (red line) and without (black line) a P3HT overlayer. RGO exhibits an excellent conductivity both for electrons and holes, and percolated RGO layers show significant drain current at both positive and negative gate voltages.

With the addition of a P3HT overlayer we observe that the electron transport properties do not change significantly, while there is a substantial improvement of hole transport ($V_G < 0$), which can be due to a beneficial effect of the organic polymer on the transport around defects and bottlenecks in RGO layer, e.g. sheet vacancies and defects. In the FET devices, holes or electrons are transported depending on the gate voltage used. P3HT is a hole transporter, and thus can improve the charge transport only for holes transport, at negative gate bias, as observed experimentally.

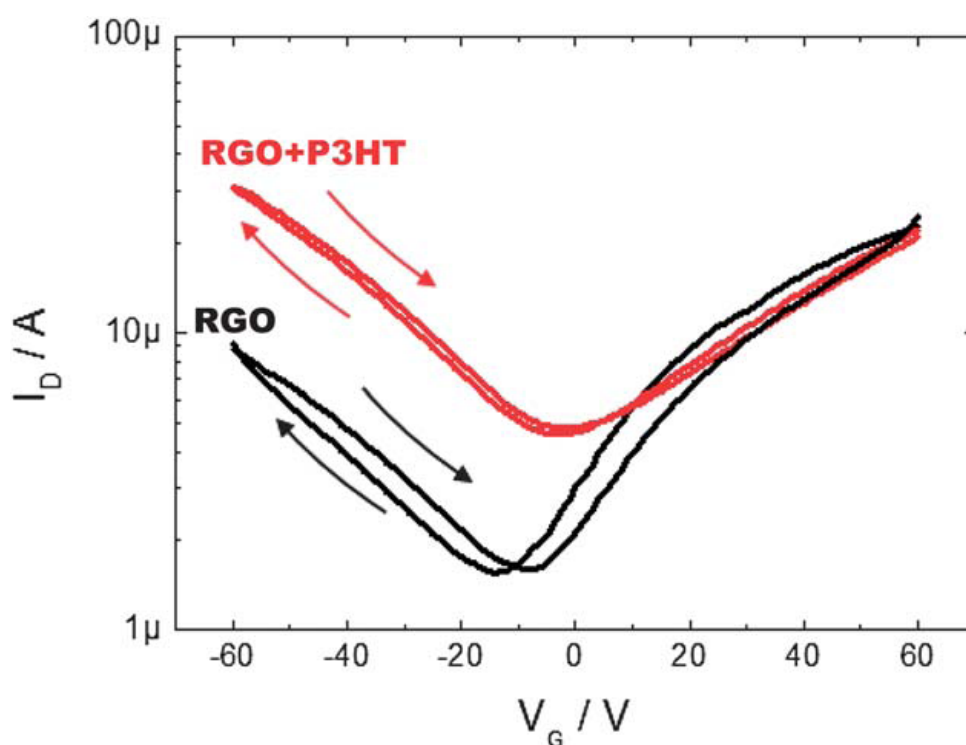


Figure 4.17 Transfer curve for a continuous RGO layer ($A = 82\%$) reporting the drain current in the linear regime ($V_{DS} = -10$ V) with (red line) and without (black line) a P3HT overlayer.

In conclusion, chemical exfoliation, solution processing and successive reduction of graphene oxide allow for the easy preparation of conductive hybrid RGO–P3HT layers featuring a good control of the density of the graphene sheets and thus the presence or absence of percolating paths for charge transport. The preparation technique used yields good, tunable and uniform coverage of graphene sheets on large areas, with basically all sheets present as monolayers, and poor sheet–sheet interactions even for relatively high coverage.

The effective WF of these RGO multi-layers depends significantly on the number of layers, and can be varied by values of up to 250 meV going from single sheets to thick layers, as measured by KPFM.

These layers can be used as a substrate for the deposition of organic semiconductors, modulating different electrical properties of the semiconductor, and improving the overall charge carrier mobility within the layer.

FETs based on P3HT with different amounts of RGO show significant improvements in hole mobility, while electron transport remains unaffected. By comparing the charge transport for different RGO coverage, with or without P3HT, it is possible to observe that graphene sheets can improve the charge transport in continuous P3HT layers by acting as preferential paths for charges, reducing the effective channel length and increasing the overall hole mobility.

Conversely, continuous, fully percolated RGO layers show a certain improvement upon deposition of P3HT overlayer, whose exact cause still needs to be elucidated. KPFM provided evidence for the absence of significant charge injection barrier between the graphene sheets and the P3HT, thus confirming the favourable interaction of the two to have good charge transport.

The interaction of organic molecules with graphene is the subject of intense research both for fundamental science and technological applications.

The approach described in this paper allows to study in a controlled manner the charge transport at multiple graphene–organic interfaces, where the interface graphene/organic contact area corresponds to the effective graphene surface, and the effective path that charges have to travel in graphene and in organic phase can be easily tuned.

This approach can be directly applied to systems different from the P3HT–RGO blend described here, to perform a systematic study of charge transport across graphene–organic interfaces.

From a technological standpoint, the results obtained show that the use of graphene–organic composites allows to have working FETs with variable geometries and channel lengths up to 60 μm , whose performance and characteristics (effective charge mobility, $I_{\text{ON}}/I_{\text{OFF}}$ ratio) can be tuned in a simple way by changing the concentration of the GO solution employed during the spin coating stage.

Overall, these results indicate that the use of nano-sized graphene sheets as additives for organic electronic devices can allow a robust and versatile control of device properties.

The work present here led to the realization of the article “Charge transport in graphene–polythiophene blends as studied by Kelvin Probe Force Microscopy and transistor characterization” A. Liscio, G.P. Veronese, E. Treossi, F. Suriano, F. Rossella, V. Bellani, R. Rizzoli, P. Samorì, V. Palermo, *Journal of Materials Chemistry* 21, 2924, 2011.

4.3 INTERACTION BETWEEN GORED AND NANO-GRAPHENE DERIVATIVES

Small synthetic polyaromatic molecules (nano-graphenes, or NGs), are known to physisorb reversibly on graphitic substrates through π - π interactions forming ordered adlayers, featuring controlled molecular orientation and order on the 1-100 nm scale.

The use of supramolecular interactions, instead of direct covalent functionalization of graphene, has the advantage of keeping intact graphene's sp^2 aromatic network, without compromising its exceptional charge transport properties.

Furthermore, the supramolecular and reversible interactions of NG with graphene will allow reaching at equilibrium a thermodynamically stable, periodic arrangement of NGs on the graphene sheets, with lateral order on a tens of nm scale.

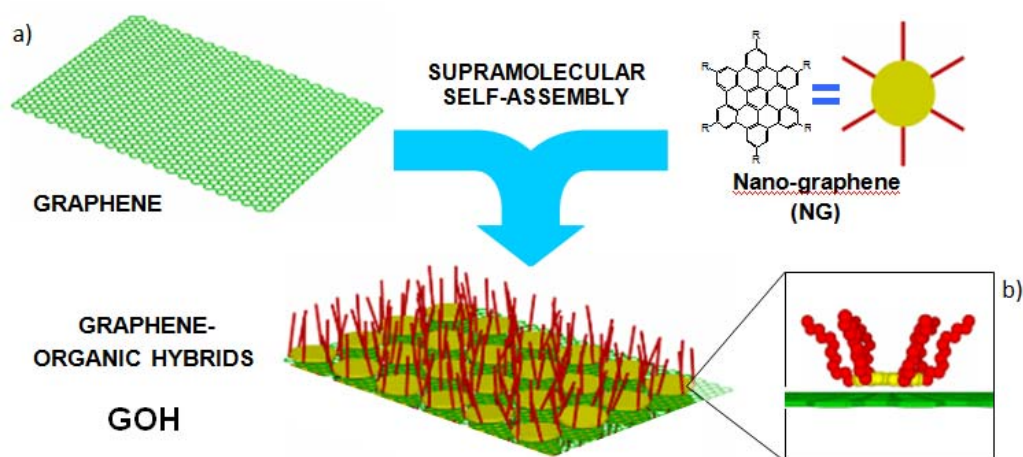


Figure 4.18 a) Cartoon of GOH complex formation. b) schematic representation of a graphene layer with an hexa-benzo-coronene molecule adsorbed on surface.

We are exploring a “supramolecular” approach to develop a radically new class of graphene-based materials, which will combine the excellent electronic and

mechanical properties of graphene with the processability and tunability of organic semiconductors.

Discotic materials see section 1.2 and 1.3 (and also some polymer like P3HT) when interacting with graphene could i) form well-defined graphene–organic hybrids (GOH), where optically/electrically active molecules are arranged in ordered and continuous layers on face of graphene sheets (fig. 4.18) and ii) tune the optical and electronic properties of graphene thanks to the interaction with these organic molecules.

Preliminary results: we worked with different hybrid materials between RGO and Nanographene derivatives, an example is sodium pyrene-sulfonate PSANa

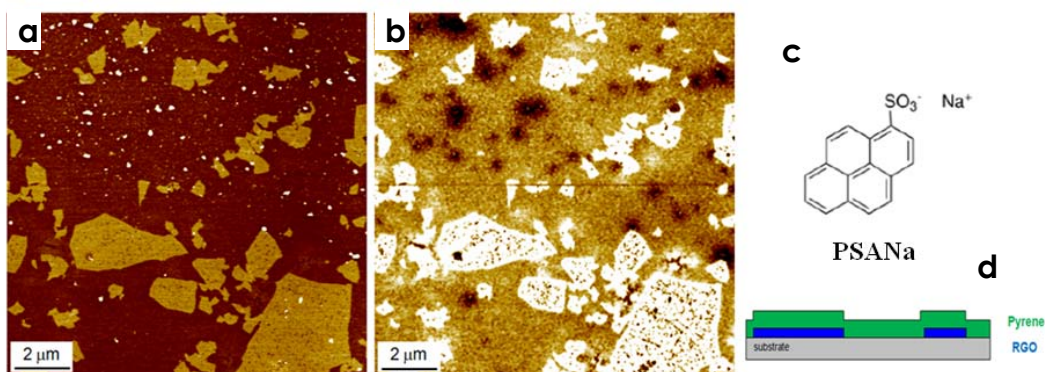


Figure 4.19 a) AFM and corresponding b) potential images of RGO - PSANa hybrid system, c) Molecular structures of the Pyrene derivatives PSANa. d) Schematic representation of sample in a.

Figure 4.19 show AFM and corresponding potential images of RGO sheets deposited on native SiO_x substrate, and covered by a thin film of PSANa. Pyrene derivative was deposited on RGO flakes from methanol solution by spincoating. Different morphology was obtain after deposition of PSANa by drop casting of methanol solution on thin film of RGO, fig. 4.20 a show that pyrene derivatives form aggregates tens of nm thick, due to dewetting of solutions during deposition. The charge transport of the thin film of RGO after deposition of PSANa has been tested in FET architectures with 225 nm SiO₂ gate oxide, patterned with source–drain Gold electrodes.

Figure 4.20 c,d show transfer curve for a continuous film of RGO after deposition of pyrene derivative and the effect of light illumination on the drain-source current of a PSANa -doped RGO field-effect transistor.

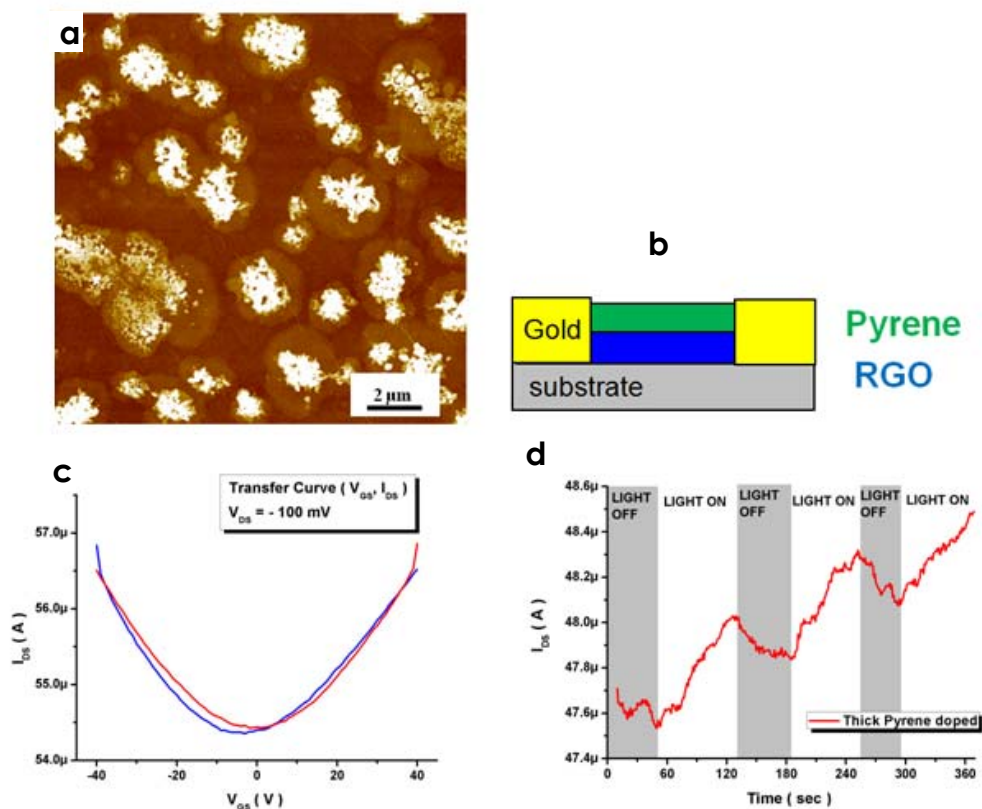


Figure 4.20 a) AFM image of PSANa aggregates formed on RGO thin film b) Schematic representation of the device. c) Transfer curve (I_{DS} , V_{GS}) of the same Pyrene-doped RGO field-effect transistor ($V_{DS} = -100$ mV), d) Effect of Light illumination on the Drain-Source current of a Pyrene-doped RGO field-effect transistor.

This system is still under study, we are monitoring the effect of different nanographenes (pyrene perylene exbenzocoronene etc.) derivatives on the charge transport of graphene.

4.4 BIBLIOGRAPHY

1. Materials and Applications for Large Area Electronics: Solution-Based Approaches; A. C. Arias, J. D. MacKenzie, I. McCulloch, J. Rivnay and A. Salleo, *Chemical Reviews* 2010, 110, 3.
2. Electrostatic deposition of graphene; A. N. Sidorov, M. M. Yazdanpanah, R. Jalilian, P. J. Ouseph, R. W. Cohn and G. U. Sumanasekera, *Nanotechnology*, 2007, 18, 135301.
3. The Relationship between Nanoscale Architecture and Charge Transport in Conjugated Nanocrystals Bridged by Multichromophoric Polymers; R. Dabirian, V. Palermo, A. Liscio, E. Schwartz, M. B. J. Otten, C. E. Finlayson, E. Treossi, R. H. Friend, G. Calestani, K. Müllen, R. J. M. Nolte, A. E. Rowan and P. Samori, *Journal of the American Chemical Society* 2009, 131, 7055.
4. On the width of the recombination zone in ambipolar organic field effect transistors; M. Kemerink, D. S. H. Charrier, E. C. P. Smits, S. G. J. Mathijssen, D. M. de Leeuw and R. A. J. Janssen, *Applied Physics Letters* 2008, 93, 033312.
5. Photovoltaic Charge Generation Visualized at the Nanoscale: □ A Proof of Principle; A. Liscio, G. De Luca, F. Nolde, V. Palermo, K. Muellen and P. Samori, *Journal of the American Chemical Society* 2008, 130, 780.
6. Nanoscale Quantitative Measurement of the Potential of Charged Nanostructures by Electrostatic and Kelvin Probe Force Microscopy: Unraveling Electronic Processes in Complex Materials; A. Liscio, V. Palermo and P. Samori, *Accounts Chemical Research*, 2010, 43, 541.
7. Doping Graphene with Metal Contacts, G. Giovannetti, P. A. Khomyakov, G. Brocks, V. M. Karpan, J. van den Brink and P. J. Kelly, *Physical Review Letters* 2008, 101, 026803.
8. Local work function measurements of epitaxial graphene; T. Filleter, K. V. Emtsev, T. Seyller and R. Bennewitz, *Applied Physics Letters* 2008, 93, 133117.
9. High-Contrast Visualization of Graphene Oxide on Dye-Sensitized Glass, Quartz, and Silicon by Fluorescence Quenching; E. Treossi, M. Melucci, A. Liscio, M.

Gazzano, P. Samorì and V. Palermo, *Journal of the American Chemical Society* 2009, 131, 15576.

10. Polymer Photovoltaic Cells Based on Solution-Processable Graphene and P3HT; Q. Liu, Z. F. Liu, X. Y. Zhong, L. Y. Yang, N. Zhang, G. L. Pan, S. G. Yin, Y. Chen and J. Wei, *Advanced Functional Materials* 2009, 19, 894.

11. Fluorescence Quenching in Conjugated Polymers Blended with Reduced Graphitic Oxide; Y. B. Wang, D. Kurunthu, G. W. Scott and C. J. Bardeen, *Journal of Physical Chemistry C* 2010, 114, 4153.

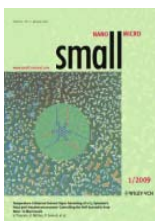
12. Percolation, statistical topography, and transport in random media; M. B. Isichenko, *Reviews of Modern Physics* 1992, 64, 961.

13. Carbon nanotubes-semiconductor networks for organic electronics: The pickup stick transistor; X. Z. Bo, C. Y. Lee, M. S. Strano, M. Goldfinger, C. Nuckolls and G. B. Blanchet, *Applied Physics Letters* 2005, 86, 182102.

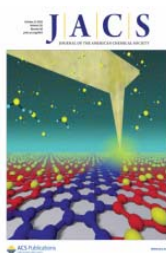
14. High-Resolution Mapping of the Electrostatic Potential in Organic Thin-Film Transistors by Phase Electrostatic Force Microscopy; P. Annibale, C. Albonetti, P. Stolar and F. Biscarini, *Journal of Physical Chemistry A* 2007, 111, 12854.

15. Transport in polycrystalline polymer thin-film transistors; R. A. Street, J. E. Northrup and A. Salleo, *Physical Review B* 2005, 71, 165202.

PUBLICATIONS:

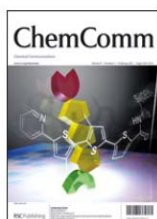


1. Temperature-enhanced Solvent Vapour Annealing of a C3 symmetric hexa-peri-hexabenzocoronene: controlling the self-assembly from nano- to macroscale; **E. Treossi**, A. Liscio, X. Feng, V. Palermo, K. Müllen, P. Samorì. *Small* Volume 5, 112, 2009. **(Cover page)**
2. Large-area processing of organic semiconductors by spray deposition and spin-coating with orthogonal solvents; **E. Treossi**, A. Liscio, X. Feng, V. Palermo, K. Müllen, P. Samorì. *Applied Physics A* Volume 95, 15, 2009.
3. The relationship between nanoscale architecture and charge transport in conjugated nanocrystals bridged by multi-chromophoric polymers; R. Dabirian, V. Palermo, A. Liscio, E. Schwartz, M.B.J. Otten, C.E. Finlayson, **E. Treossi**, R.H. Friend, G. Calestani, K. Müllen, R.J.M. Nolte, A.E. Rowan, P. Samorì. *Journal of the American Chemical Society* 131, 7055, 2009.
4. High-Contrast Visualization of Graphene Oxide on Dye-Sensitized Glass, Quartz, and Silicon by Fluorescence Quenching; **Emanuele Treossi**, Manuela Melucci, Andrea Liscio, Massimo Gazzano, Paolo Samorì, and Vincenzo Palermo. *Journal of the American Chemical Society* 131, 15576, 2009.
5. Self-Complementary Nucleoside-Thiophene Hybrid Systems: Synthesis And Supramolecular Organisation; Maria Luisa Navacchia, Laura Favaretto, **Emanuele Treossi**, Vincenzo Palermo and Giovanna Barbarella. *Macromolecular Rapid Communications* 31 (4), 351, 2010.
6. Solvent vapour annealing of organic thin films: controlling the self-assembly of functional systems across multiple length scales; Giovanna De Luca, **Emanuele Treossi**, Andrea Liscio, Jeffrey M. Mativetsky, Luigi Monsù Scolaro, Vincenzo Palermo and Paolo Samorì. *Journal of Materials Chemistry* 20 (13), 2493, 2010.



7. Local Current Mapping and Patterning of Reduced Graphene Oxide; Jeffrey M. Mativetsky, **Emanuele Treossi**, Emanuele Orgiu, Manuela Melucci, Giulio Paolo Veronese, Paolo Samori and Vincenzo Palermo. *Journal of the American Chemical Society* 132 (40), 14130 2010. **(Cover page)**

8. Facile covalent functionalization of graphene oxide using microwaves: bottom-up development of functional graphitic materials; M. Melucci, **E. Treossi**, L. Ortolani, G. Giambastiani, V. Morandi, P. Klar, C. Casiraghi, P. Samori, V. Palermo. *Journal of Materials Chemistry* 20, 9052, 2010.

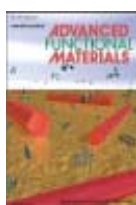


9. Multicolor, large-area fluorescence sensing through oligothiophene-self-assembled monolayers; Manuela Melucci, Massimo Zambianchi, Laura Favaretto, Vincenzo Palermo, **Emanuele Treossi**, Marco Montalti, Sara Bonacchi and Massimiliano Cavallini. *Chemical Communications* 47, 1689, 2011.

(Cover page)

10. Polymeric micelles using pseudo-amphiphilic block copolymers and their cellular uptake; Massimo Benaglia, Angelo Alberti, Enzo Spisni, Alessio Papi, **Emanuele Treossi**, Vincenzo Palermo. *Journal of Materials Chemistry* 21, 2555, 2011.

11. Charge transport in graphene-polythiophene blends as studied by Kelvin Probe Force Microscopy and transistor characterization; Andrea Liscio, Giulio Paolo Veronese, **Emanuele Treossi**, Francesco Suriano, Francesco Rossella, Vittorio Bellani, Rita Rizzoli, Paolo Samori and Vincenzo Palermo. *Journal of Materials Chemistry* 21, 2924, 2011.



12. Non-conventional processing and post-processing methods for the nanostructuring of conjugated materials for organic electronics; G. De Luca, W. Pisula, D. Credginton, **E. Treossi**, O. Fenwick, G.M.

Lazzerini, R. Dabirian, E. Orgiu, A. Liscio, V. Palermo, K. Müllen, F. Cacialli and P. Samorì. *Advanced Functional Materials* 21, 1279, 2011.

13. Graphene transistors via in-situ voltage-induced reduction of graphene-oxide under ambient conditions; J.M. Mativetsky, A. Liscio, **E. Treossi**, E. Orgiu, A. Zanelli, P. Samorì, V. Palermo.

Journal of the American Chemical Society 133, 14320, 2011.

14. Enhanced mobility in P3HT-based organic thin-film transistors upon blending with a soluble phenylene-thiophene-thiophene-phenylene small molecule. Emanuele Orgiu, Appan Merari Masillamani, Jörn-Oliver Vogel, **Emanuele Treossi**, Marcel Kastler, Florian Dötz, Vincenzo Palermo and Paolo Samorì. *Chemical Communications* 48, 1562, 2012.

15. Electrical response of GO gas sensors. C. Cantalini, L. Giancaterini, **E. Treossi**, V. Palermo, F. Perrozzi, S. Santucci, and L. Ottaviano. Accepted for publication on *Carbon Nanostructures (Graphita 2011 Conference Proceedings)*

16. Chemical production and applications of graphene based materials. **Emanuele Treossi**. Accepted for publication on *La Chimica e l'Industria*. .
(**Award of the Italian Chemical Society**)

17. Improving charge transport in poly(3-hexylthiophene) transistors via blending with an alkyl substituted phenylene-thiophene-thiophene-phenylene molecule. Andrea Liscio, Massimo Bonini, **Emanuele Treossi**, Emanuele Orgiu, Florian Dötz, Marcel Kastler, Vincenzo Palermo, and Paolo Samorì. Accepted for publication on *Journal of Polymer Science Part B: Polymer Physics*

18. Polymeric Micelles Using Pseudo-Amphiphilic Block Copolymers. Massimo Benaglia, Enzo Spisni, Angelo Alberti, Loris Giorgini, Francesco Magnoni, Alessio Papi, **Emanuele Treossi**, Vincenzo Palermo. Accepted for publication on *Macromolecular Symposia*.

19. Extreme Large area extreme-UV lithography of graphene oxide via spatially resolved photoreduction. S. Prezioso, F. Perrozzi, M. Donarelli, F. Bisti, S. Santucci, L. Palladino, M. Nardone, **E. Treossi**, V. Palermo, and L. Ottaviano. Accepted for publication on Langmuir.

PRESENTATIONS AT CONFERENCES:

Oral presentations:

1. "Controlling the self-assembly of ordered functional architectures on surfaces by Solvent Vapor Annealing." **E. Treossi**, X. Feng, A. Liscio, G. De Luca, V. Palermo, K. Müllen, P. Samorì.

IX Congresso Nazionale di Chimica Supramolecolare, Parma (Italy) 2009

2. "Chemical production and applications of graphene based materials" **E. Treossi**, A. Liscio, M. Melucci, G.P. Veronese, J.M. Mativetsky, R. Rizzoli, P. Samorì and V. Palermo.

XI Giornata della Chimica dell'Emilia-Romagna, Modena (Italy), 28 Ottobre 2011.

Posters:

1. "Self-assembly of amphiphilic discotic molecules on gold-patterned silicon oxide substrates"

E. Treossi, A. Liscio, V. Palermo, X. Feng, K. Müllen, C. Finlayson, P. Samorì.

EMRS 2008, Strasbourg (France); 26-30 May 2008.

2. "High-contrast visualization of graphene oxide on dye-sensitized substrates by fluorescence quenching" **E. Treossi**, M. Melucci, A. Liscio, M. Gazzano, P. Samorì V. Palermo.

Carbon-based Nanomaterials : from Chemistry to Applications, Institut de Physique et de Chimie des Matériaux de Strasbourg, Strasbourg (France) 13 October 2009.

3. "High-contrast visualization of graphene oxide on dye-sensitized substrates by fluorescence quenching" **E. Treossi**, M. Melucci, A. Liscio, M. Gazzano, P. Saporì, V. Palermo.

IX Giornata della Chimica dell'Emilia-Romagna, Bologna (Italy), 4 December 2009.

4. "Graphene oxide sheets functionalized with organic dyes for high contrast visualization and processing" **E. Treossi**, M. Melucci, A. Liscio, M. Gazzano, P. Klar, L. Ortolani, G. Giambastiani, V. Morandi, C. Casiraghi, P. Samorì, V. Palermo.

FUNMARCH, ISOF-CNR, Bologna (Italy); 5-7 April 2010.

5. "Unconventional fabrication of organic nanofibers and nanocrystals by temperature-enhanced solvent vapour annealing" **E. Treossi**, A. Liscio, X. Feng, G. De Luca, M. Bonini, K. Müllen, P. Samorì, V. Palermo. FUNMARCH, ISOF-CNR, Bologna (Italy); 5-7 April 2010.

6. "Local Current Mapping and Patterning of Reduced Graphene Oxide"

E. Treossi, J. M. Mativetsky, E. Orgiu, M. Melucci, G. P. Veronese, P. Samorì, V. Palermo.

X Giornata della Chimica dell'Emilia-Romagna, Parma (Italy), 26 Novembre 2010.

7. "Graphene oxide-quaterthiophene composites obtained by microwave-assisted synthesis"

E. Treossi, A. Liscio, M. Melucci, G. Giambastiani, P. Klar, C. Casiraghi, L. Ortolani, V. Morandi, P. Samorì and V. Palermo.

GraphITA, Graphene workshop, Gran Sasso National Laboratories (Italy) 2011.

8. "Covalent and supramolecular functionalization of graphene for electronics applications"

E. Treossi, A. Liscio, M. Melucci, G.P. Veronese, J.M. Mativetsky, R. Rizzoli, P. Samorì, V. Palermo.

Quantum Phenomena in Graphene, other Low-dimensional materials, and Optical Lattices, Erice (Italy) 2011.

AWARDS:

Award of the Italian Chemical Society for research work during Ph.D.

XI Giornata della Chimica Dell'Emilia Romagna.